The Effect of Residual Thermal Stresses on the Viscoelastic Behavior of Adhesively Bonded Joints

by

James Norman Cooper

Thesis submitted to the Faculty of the
Virginia Polytechnic Institute and State University
in partial fulfillment of the requirements for the degree of
Master of Science
in
Engineering Mechanics

APPROVED:

Wallace Grant, Chairman

Hal F. Brinson

David A. Dillard

September 22, 1987

Blacksburg, Virginia

The Effect of Residual Thermal Stresses on the Viscoelastic Behavior of Adhesively Bonded Joints

by

James Norman Cooper

J. Wallace Grant, Chairman

Engineering Mechanics

(ABSTRACT)

Present stress analysis of adhesively bonded joints suffers from inadequate adhesive material characterization. The lack of correlation between bulk adhesive properties and the corresponding *in-situ* behavior has led to numerous adhesive test geometries. The current study was an attempt to predict the nonlinear viscoelastic response of an adhesive *in-situ* using properties obtained from a pure shear test geometry. Four candidate adhesive test geometries were studied both analytically and experimentally in terms of accurate shear property determination and realistic adhesive bond simulation. The thick adherend joint was chosen as the experimental reference of actual viscoelastic response *in-situ*; the Arcan specimen provided a pure shear stress state for material viscoelastic characterization. Results of finite element analysis and extensive experimental evidence suggest that residual thermal stresses alter the *in-situ* adhesive properties compared to the bulk adhesive. Furthermore, preliminary results indicate that the free volume nonlinear viscoelastic theory accounts for the effect of residual strains on the *in-situ* adhesive mechanical response.

Acknowledgements

The author would like to express gratitude to the 3M Company for their support of this work in the form of adhesive and primer supplies. Thanks are also due to Mr. Chan Ko for his instruction on anodization and especially to Mr. Daniel Reed for his unending patience and diligent machine work.

The true motivation for seeing this effort through to completion was supplied by several individuals. Dr. Daniel Post's maxim, "Experiment is the truth, theory must follow", instilled a strong desire to unravel one key to understanding adhesive behavior in an adhesive bond. Ms. Paula Black, as well as students associated with the Adhesion Center, provided emotional and intellectual support.

Table of Contents

List of Illustrations

List of Tables

I

Introduction

Historically, the aerospace industry has fostered the development of lightweight yet efficient structural designs. With the advent of high speed computers and the development of advanced materials, the structural engineer now has the ability to confidently design efficient structures which meet the critical demands of safety, reliability, and cost effectiveness. The increased demand on further performance gains over existing designs will continue to push materials technology and design strategies to new levels of complexity.

During World War II, the British company, deHavilland Aircraft, introduced structural adhesives into their airframe designs. The first true structural adhesive, Redux, paved the way for future adhesive applications. In fact, the Redux sytem first demonstrated the principle of toughening a thermosetting resin with a high-molecular weight linear polymer. The modern structural adhesive, a blend of epoxy with elastomer tougheners, is a direct descendent of the Redux heritage.

While the initial bonding requirements in aircraft were metal-to-metal bonds, or metal-to-wood in the deHavilland Mesquito, the utilization of advanced composites has rapidly expanded aircraft adhesive applications. The Fokker aircraft company has two small commuter aircraft that employ

adhesive bonding exclusively for metal to metal and metal to composite bonds. In service for over 28 years, the large volume Boeing 707 atests to the durability of nitrile rubber-phenolic resin adhesive film in aircraft applications. Many current advanced fighter aicraft have composite bonded to metal in the form of step lap adhesive joints.

Despite the advantages of adhesive bonding over conventional methods of fastening, aircraft designers are reluctant to use adhesive bonding in the design of their primary structural components. The complexity of the stress and failure analysis of the thin adhesive layer, and the lack of testing-methodology for mechanical property characterization, raise serious doubts about the reliabilty of bonded structures. The power and versatility of the finite element method as a design and analysis tool could offset the impaired confidence in adhesive bonding.

Many investigators have applied finite element analysis to adhesively bonded joints. The main thrust of the application of this numerical analysis has been on quantifying the stress distributions in adhesive specimens. Further application of the finite element method to fracture mechanics and large deformation analyses of adhesive bonds has also been performed. New constitutive models, accounting for various aspects of adhesive nonlinear behavior, have also been incorporated into finite element programs. Although much activity is directed toward stress analysis and adhesive fracture mechanics of adhesively bonded joints using the finite element method, experimental validation of the numerical codes in predicting adhesive deformation in an actual joint has yet to appear in the literature.

Perhaps the single most important deficiency in the stress analysis of adhesively bonded joints is the lack of material data for adhesives. Unfortunately, there is little or no information on the correlation between bulk adhesive properties and the corresponding properties of the adhesive *in-situ*. Generally, it is recognized that the presence of the adherends during cure, and the ensuing conditions under which the adhesive cures, alters the mechanical properties of the adhesive in the bond compared to the isolated film or bulk polymer. According to Alfrey [1], behavior of the adhesive *in-situ* should resemble the behavior in bulk form if equivalent assumptions regarding composition,

history, material parameters, specimen thickness, residual stress distribution, and environment can be accurately assessed. The concept of a weak boundary layer separating a bulk adhesive and the metal substrate is a plausible explanation for differences in mechanical behavior of the adhesive *in-situ* and in bulk form. In general, the properties of the adhesive depend entirely on the thermodynamic state at the time of cure.

Unlike metals and ceramics, the elastic moduli of polymeric solids is very structure sensitive [2]. Specifically, the modulus of a polymer increases with: (1) thermodynamic stability of the main chain bonds, (2) percent crystallinity, and (3) packing density of the chains. Excess free volume, defined as the difference between the equilibrium and actual glassy free volumes, is thought to be important in understanding the relationship between adhesive properties and their thermodynamic state. Due to the mismatch in the coefficients of thermal expansion between the adhesive and adherend, thermal stresses are induced in the adhesive at the time of cure. The ensuing state of residual stress in the adhesive may affect the excess free volume, and ultimately, the adhesive properties.

Many researchers have compiled detailed information on the mechanical and physical properties of a wide range of bulk polymers [3]. Recently, the identification of the adhesive as a separate material in a bonded joint has focused attention on characterizing the bulk properties of adhesives. Peretz and Weitsman [4] used unscrimmed neat FM-73 adhesive samples to characterize the behavior of the adhesive in terms of Schapery's nonlinear viscoelastic model [5]. Knauss et al. [6] determined the linear viscoelastic shear creep compliance of the same material using a creep torsiometer. Lefebvre and Brinson [7] studied the relaxation and cyclic creep response of neat unscrimmed specimens of FM-73 and FM-300.

Because it is not clear that neat resin adhesive properties reflect the *in-situ* properties, Dolev and Ishai [8] investigated the relationship between bulk and *in-situ* adhesive mechanical and strength properties. They postulated two important premises: (1) the basic mechanical behavior of an *in-situ* bonded adhesive layer is similar to its corresponding bulk adhesive reference , and (2) the failure

of a properly surface-treated bonded joint is cohesive and initiates within the adhesive layer. Extensive practical experience in the aerospace industry indicates that the adhesive film does typically fail cohesively under various load and test conditions [9]. As a consequence, the mechanical properties of the adhesive *in-situ* are important if realistic stress analysis of adhesively bonded joints is to be realized. In reference to the first premise, the authors concluded that the mechanical properties of the *in-situ* adhesive and the bulk material are in fair correlation in the elastic and yield-plateau ranges. In addition, the authors asserted that the thickness of the adhesive layer has a small effect on its yield strength and elastic moduli for thicknesses of 0.004 in. and greater.

Other recent investigations tend to contradict the assertion that the neat resin and *in-situ* properties of the adhesive correlate. Stringer [10] found that the apparent shear modulus of the *in-situ* adhesive depends strongly on the bondline thickness in torsional butt-joint specimens with a linearly varying shear stress. However, his data reflects large scatter due to the practical limitations of measuring the adhesive bondline thickness to a large degree of accuracy. Furthermore, Stringer concludes that as the bondline thickness increases the plastic strain to failure of the *in-situ* adhesive decreases. Because the shear stress varied linearly with radius, this observation may not reflect adhesive plasticity in a pure shear state.

A well-conceived investigation by Knollman and Hartog [11] identified that a gradient in shear modulus exists in the interfacial accomodation zone, or interfacial region, of an epoxy bonded to aluminum. The determination of a shear modulus gradient near the material interface was made by ultrasonic waves propagating on successively exposed layers of FM-73 throughout the bondline region. The experimental results indicate that the shear modulus of the adhesive increases fairly linearly through the interfacial region. Furthermore, at approximately 0.008 in. adhesive thickness the modulus tends toward a constant value. These results were invariant to the surface treatment of the aluminum and the adhesive cure cycle. Thus, the presence of a weak boundary layer in the adhesive is a valid argument for the lack of correlation between the bulk and *in-situ* adhesive mechanical properties.

The variation in adhesive shear modulus in the interfacial accomodation zone may be due to the variation of residual stresses in the curing adhesive. Hahn [12] developed a sensitive measurement technique to determine the stress in a curing adhesive by immersing a costantan wire in an initially liquid adhesive. Resistance measurements of the embedded wire at different heights in the adhesive indicated a varying residual stress state in the adhesive. The variation in residual stress, and residual strain, implies that the free volume of the adhesive varies throughout the bond.

Due to the sensitivity of the adhesive to its cure conditions, *in-situ* mechanical properties may reflect the test specimen and not the adhesive properties in an actual joint. There are numerous adhesive test geometries which yield qualitative information about adhesives; Portelli [13] presents a comprehensive review of the many adhesive test specimens in use. To characterize the mechanical properties of the adhesive *in-situ*, a test specimen should produce a constant state of stress in the adhesive. Futhermore, the residual state of stress in the adhesive should not affect the mechanical property determination.

The goal of this study was to predict the nonlinear viscoelastic response of an actual adhesive in a bond configuration. Because adhesive bonds typically transmit loads through shear stresses, the main emphasis was on identifying a pure shear adhesive geometry for viscoelastic shear characterization. In Chapter 2, two existing adhesive specimens, the single lap and thick adherend lap joints; were analyzed using an existing finite element program. Furthermore, experimental tests were conducted on the thick adherend lap joint using a Krieger extensometer. Although neither test geometry studied is suitable for viscoelastic property determination, the thick adherend joint was chosen to be the experimental comparison for nonlinear viscoelastic finite element predictions due to its similarity to an actual adhesive joint.

The need for a pure shear adhesive test led to studies of the cone-and-plate and Arcan specimens in Chapter 3. Finite element results disputed the predicted constant shear stress state in the cone-and-plate test geometry. Subsequent analysis of the Arcan specimen indicated a uniform shear stress state in the adhesive; hence, it was chosen as the viscoelastic shear specimen for adhesive

characterization. Experimental tests of both specimens were conducted as further comparisons of *in-situ* behavior to that of the bulk adhesive.

In Chapter 4, results of the previous two chapters were applied to the nonlinear viscoelastic response of an adhesive joint. The Arcan specimen demostrated that free volume changes due to residual thermal stresses make *in-situ* linear viscoelastic shear characterization impossible. Nonetheless, experimental viscoelastic measurements of thick adherend joints indicated strong adhesive nonlinearities. Finite element analysis using available linear viscoelastic properties of a adhesive indicated that the residual thermal stress state in the adhesive layer directly influences the adhesive mechanical response.

II

Existing adhesive tests

Single lap Joint

The single lap joint is the most widely used adhesive specimen because of its simplicity and cost. In addition, the single lap joint is a common overlap design of bonded joints and its serves as a qualitative test of adhesives and surface treatments. According to ASTM D1002-72, the single lap joint consists of two 0.064 inch thick metal adherends that form a 0.5 inch adhesive overlap. In most applications, glass beads are placed in the adhesive layer to regulate and ensure an even bondline thickness. The relatively thin adherends and the load eccentricity about the bond centerline create a complex state of stress in the test adhesive.

Although not generally noted in the literature, Volkersen [14] provided the first stress analysis of the single lap joint. His analysis, referred to as the shear lag analysis, was limited to stresses arising from differential displacements in the overlap region. Later, Goland and Reissner [15] used variational principles to account for the adherend bending. Although their analysis did not account for axial

strains in the adhesive, the solution obtained still serves as comparison to finite element analyses. Portelli [13] provides a review of both the Volkersen and the Goland and Reissner analyses. Botha et al. [16] give a more comprehensive review of both the analytical and finite element stress analyses of the single lap joint specimen.

Finite element analysis

The complex state of stress present in the adhesive layer makes the single lap joint a poor choice for mechanical characterization of the adhesive properties. A linear elastic stress analysis of a titanium/epoxy single lap joint was performed using the existing finite element program VISTA [17]. Under the assumption that plane strain conditions prevail, eight node isoparametric quadrilateral elements were used to model the specimen. The adhesive layer consisted of five elements through the thickness and twenty elements along the bondline. The element length was adjusted to provide a finer mesh at the joint ends where the stress gradients are higher. Figure 1 shows the model geometry along with pertinent material properties.

From the finite element results, the geometric properties of the single lap joint configuration lead to undesirable stresses in the adhesive layer. According the deformed mesh plot of Figure 2, the eccentricity of the load produces bending moments in the thin adherends. For most adhesive systems, a single lap joint loaded to failure will invariably plastically deform the adherends. The large rotations of the adherends necessitate the use of geometric nonlinear strains in a finite element analyses. The normalized stress distribution along the adhesive centerline with respect to the applied stress is plotted in Figure 3. Note that at the ends of the joint overlap, peel stresses dominate. The large peel stresses at the end of the joint typically result in adhesive failure.

Because of the dominant peel stresses and a small axial stress component, the single lap joint makes a poor specimen for measuring adhesive shear properties. Also, the thin adherends and the asso-

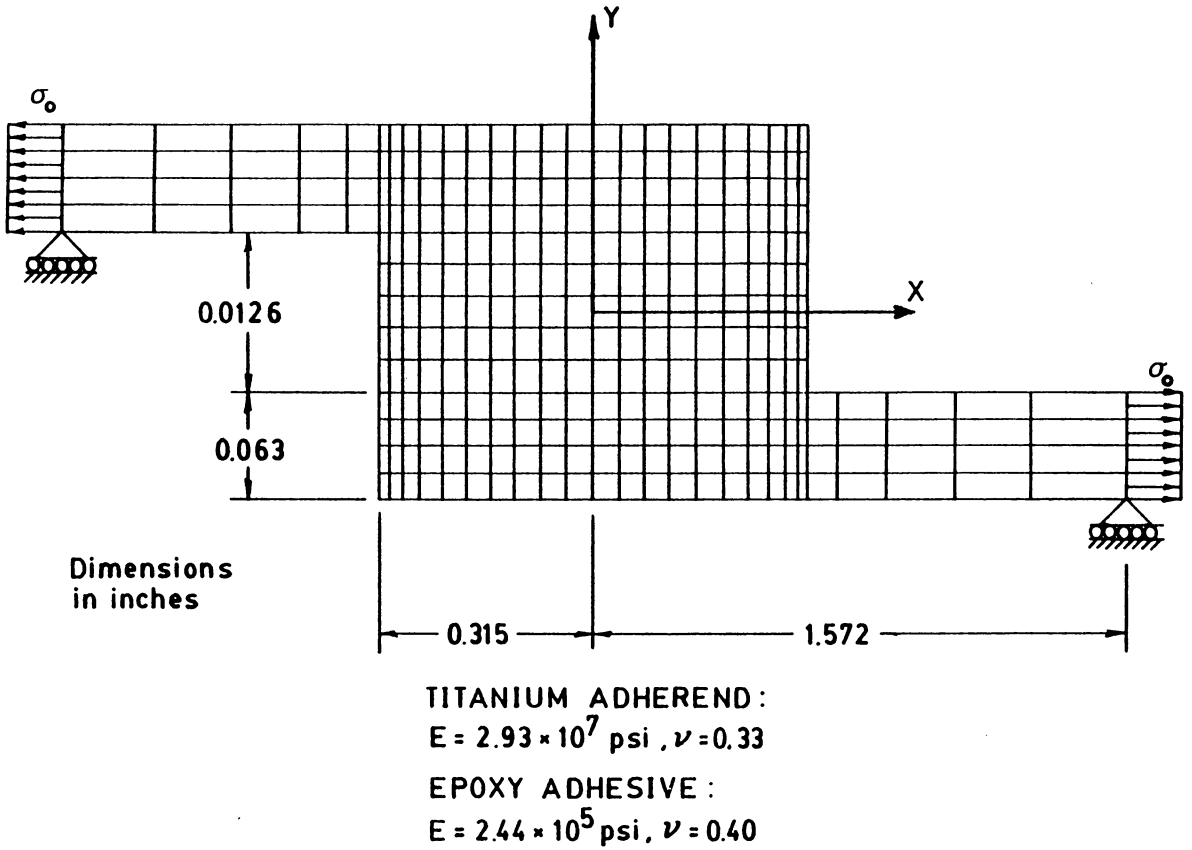

Figure 1. Finite element model of single lap joint under mechanical loading: dimensions and material properties are shown for the model.

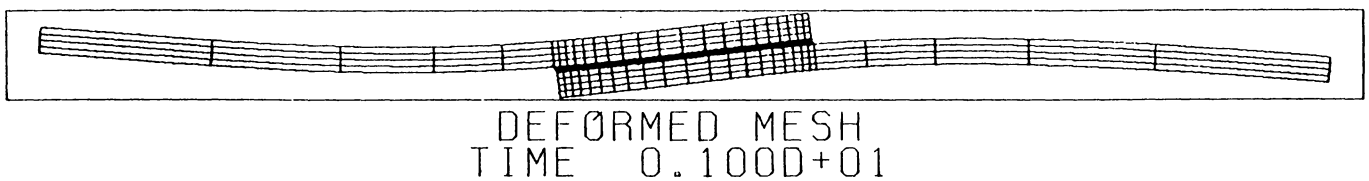

Figure 2. Deformed finite element mesh of single lap joint: note large bending rotations in adherend.

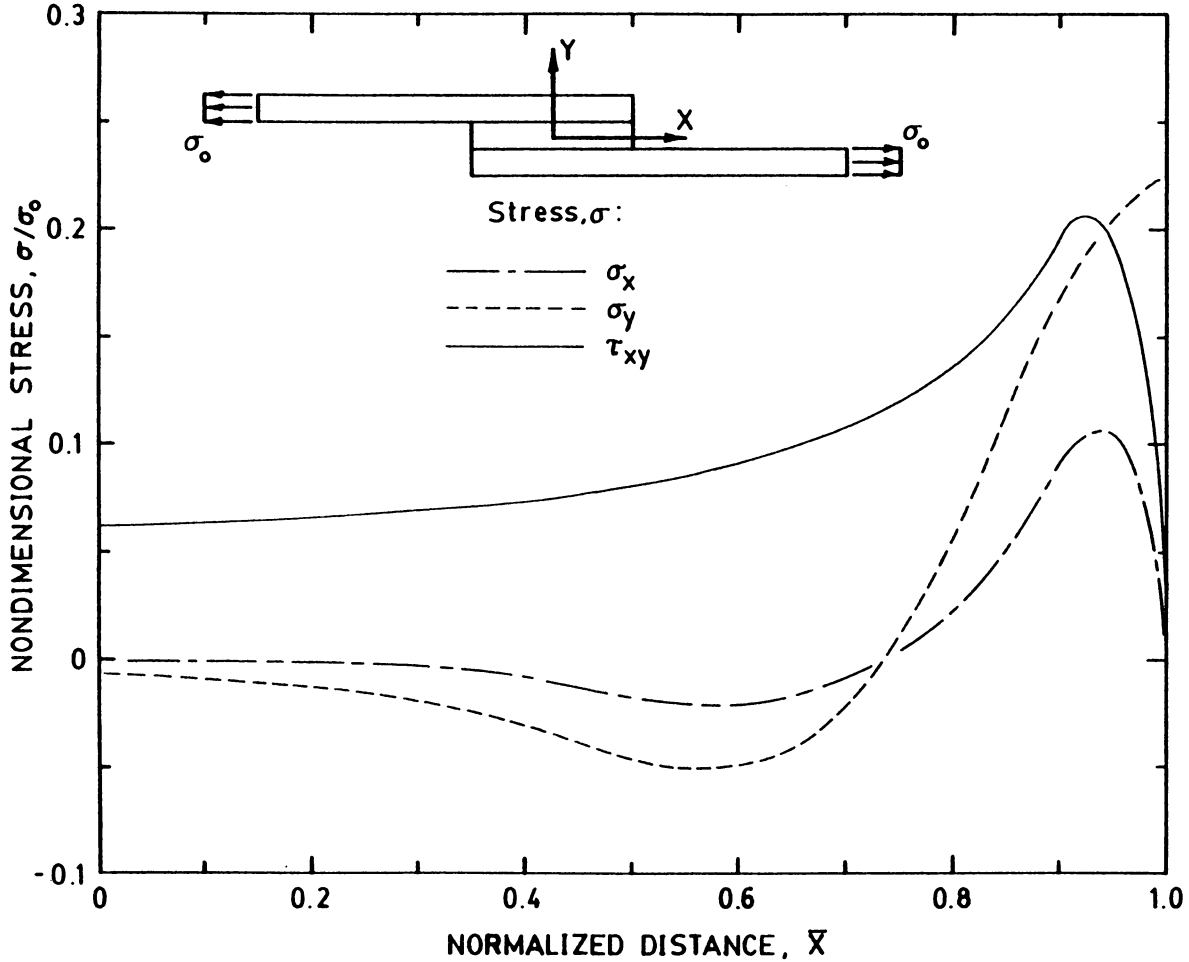

Figure 3. Normalized stress distribution in single lap joint: stresses normalized with respect to applied load.

ciated large bending rotations makes any measurement of the relative displacements of the adherends across the bondline difficult. Despite these problems, adhesive manufacturers and researchers continue to use the single lap joint as a shear test of structural adhesives.

Embedded strain gage

The problem of accurately measuring adhesive deformation in the single lap joint was approached by Tuttle et al. [18]. In an effort to correlate bulk adhesive properties with the *in-situ* adhesive properties, they embedded strain gages in the adhesive layer of titanium/epoxy single lap joints. They reported good agreement with the comparison of finite element results using neat resin properties and experimental measurements of the axial strain in the adhesive. However, several concerns arise over measuring adhesive strain using an embedded strain gage.

The application of embedded strain gages in adhesive bonds raises two important questions: first, does the strain gage influence the stress and strain distribution in the vicinity of the gage, and secondly, does the strain gage accurately measure axial strain in the adhesive layer. The main reason for questioning the strain gage measurement is that the strain gage acts as a rigid inclusion in the softer adhesive material. In addition, the axial strain in the adhesive is probably influenced more by the stiffer adherends than by the properties of the adhesive. To gain insight into these questions, a finite element analysis was conducted on a single lap joint with an embedded strain gage. The finite element model was of the adhesive and adherends was identical to the previous model (Fig. 1). The strain gage was included in the model as depicted in Figure 4. For comparison, the strain gage was located both in the middle of the bond and at the end of the bond.

The properties chosen for the strain gage were thought to be representative of a gage consisting of a polyimide backing and a constantan grid. For simplicity, it was assumed that the strain gage is isotropic and linear elastic. From the linear elastic finite element results, the presence of the strain

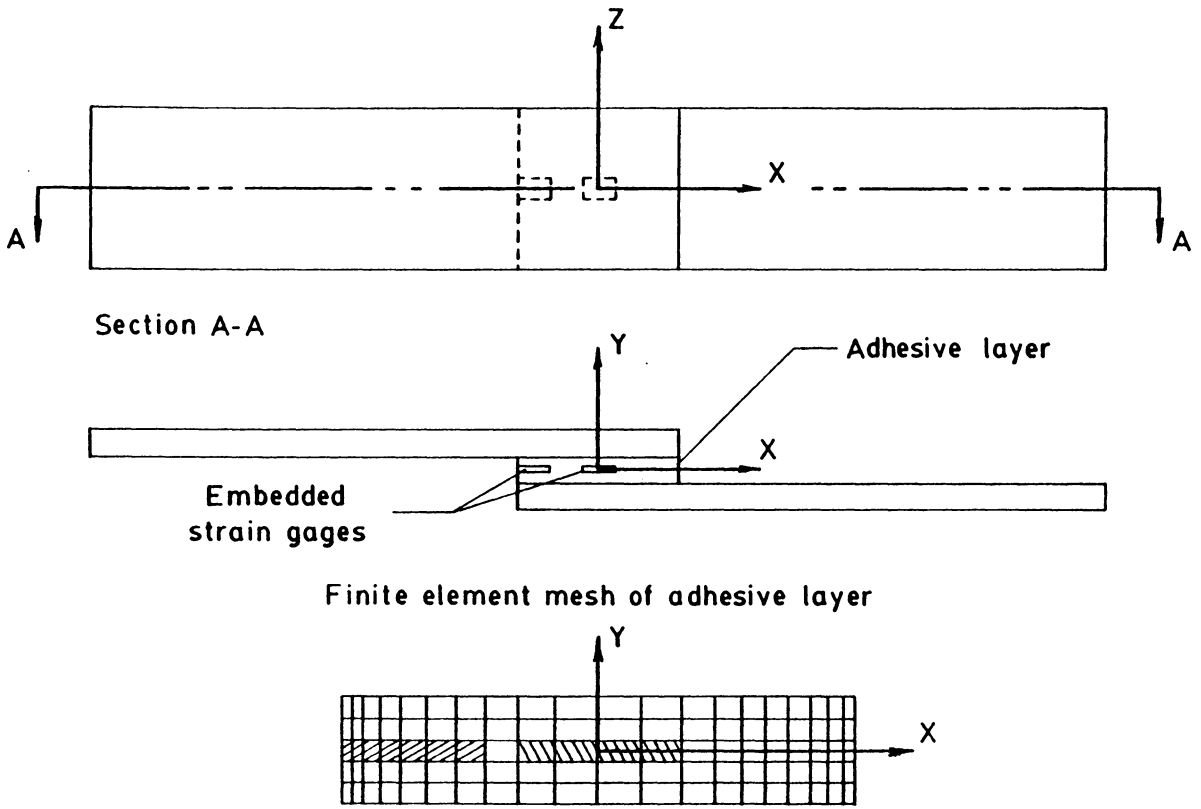

Figure 4. Embedded strain gages in the single lap joint: gages present in the adhesive layer at two bondline locations.

gage produces stress concentrations in the adhesive. Figure 5 shows the axial stress distribution with the strain gage present normalized to the stress distribution without a gage in the adhesive. From the plot, the presence of the strain gage at the end of the bond produces significant stress concentrations compared to the strain gage located at the adhesive middle.

Because the strain gage measures axial strian and not stress in the adhesive, comparisons of the axial strain profile are presented in Figure 6. For both strain gage locations studied, the presence of the stiffer gage in the adhesive does influence the strain distribution in the vicinity of the gage. However, in the actual strain measurement, a strain gage averages the material strain of the gage effective length. Thus, the effect of the strain perturbation due to the strain gage itself on the accuracy of the axial strain measurement would be difficult to assess using finite element results.

From the nature of the single lap joint geometry, the axial strain in the adhesive is influenced more by the relative stiffness of the adherend than by the stiffness of the adhesive. Dimensionally, the adherend is much thicker than the adhesive layer; thus, the adherend would dominate the axial strain distribution in the adhesive overlap region due to the nature of the applied load. The influence of the adherend stiffness on the adhesive strain distribution was studied by varying the adhesive/adherend modulus ratio in the finite element analysis. Figure 7 shows the axial strain distribution at the adhesive centerline for a joint with a centrally located strain gage for various modulus ratios. Although the modulus ratio varies by two orders of magnitude, the strain distribution in the strain gage shows only a slight variation in magnitude.

Although the embedded strain gage will indeed respond to axial strain in the adhesive, it is clear that the actual properties of the adhesive do not determine the measured strain. In fact, the axial strain distribution in the adhesive is governed more by the adherend stiffness due to the geometry of the specimen and the nature of the loading. The perturbation of the axial stress and strain distribution in the adhesive is due to the gage acting as a stiff inclusion in the softer adhesive. Obviously, if the stiffness of the strain gage was roughly the same as the adhesive, the perturbations would be nonexistent.

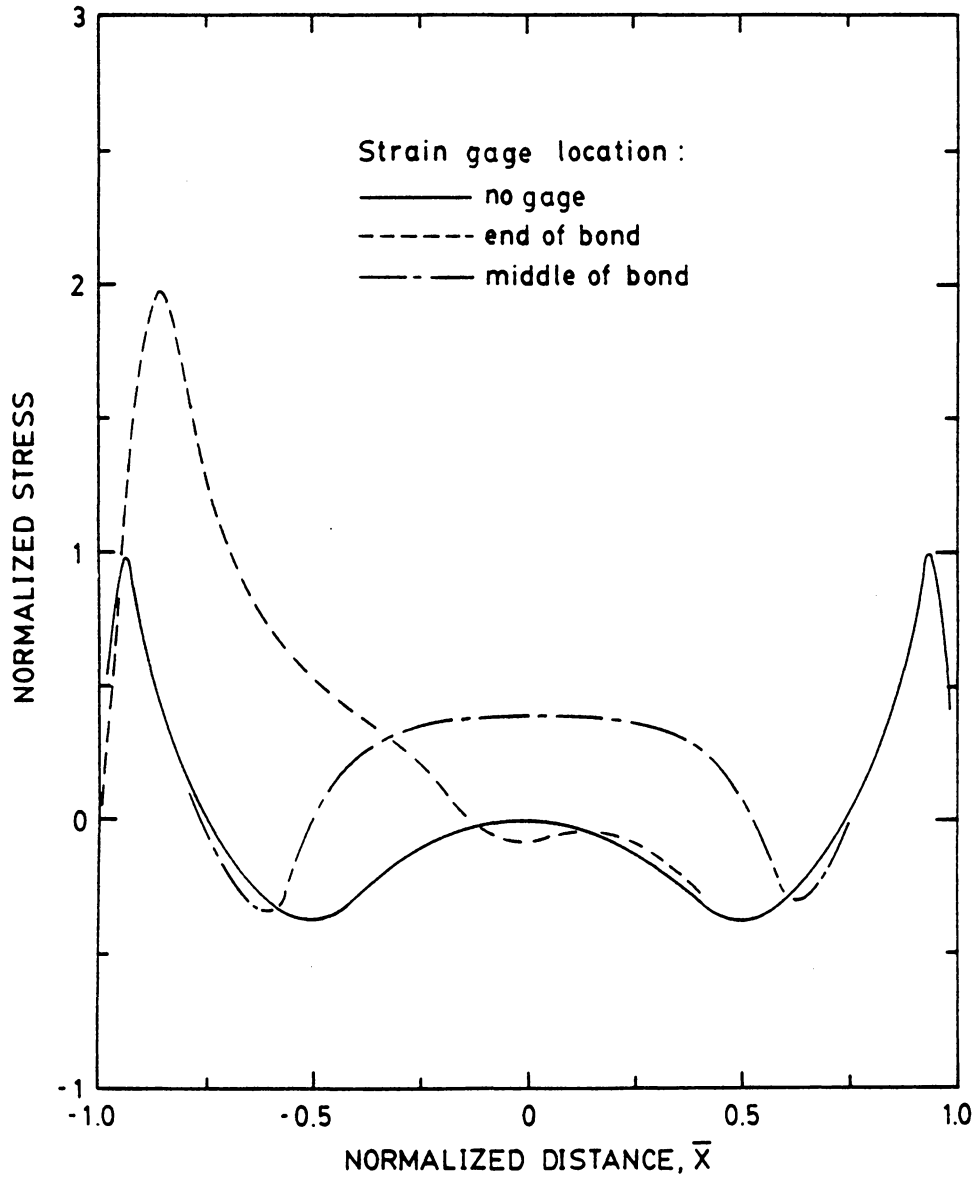

Figure 5. Axial stress distribution along adhesive centerline for embedded strain gage: stress distribution for both strain gage locations normalized to the stress distribution without a strain gage present in the adhesive.

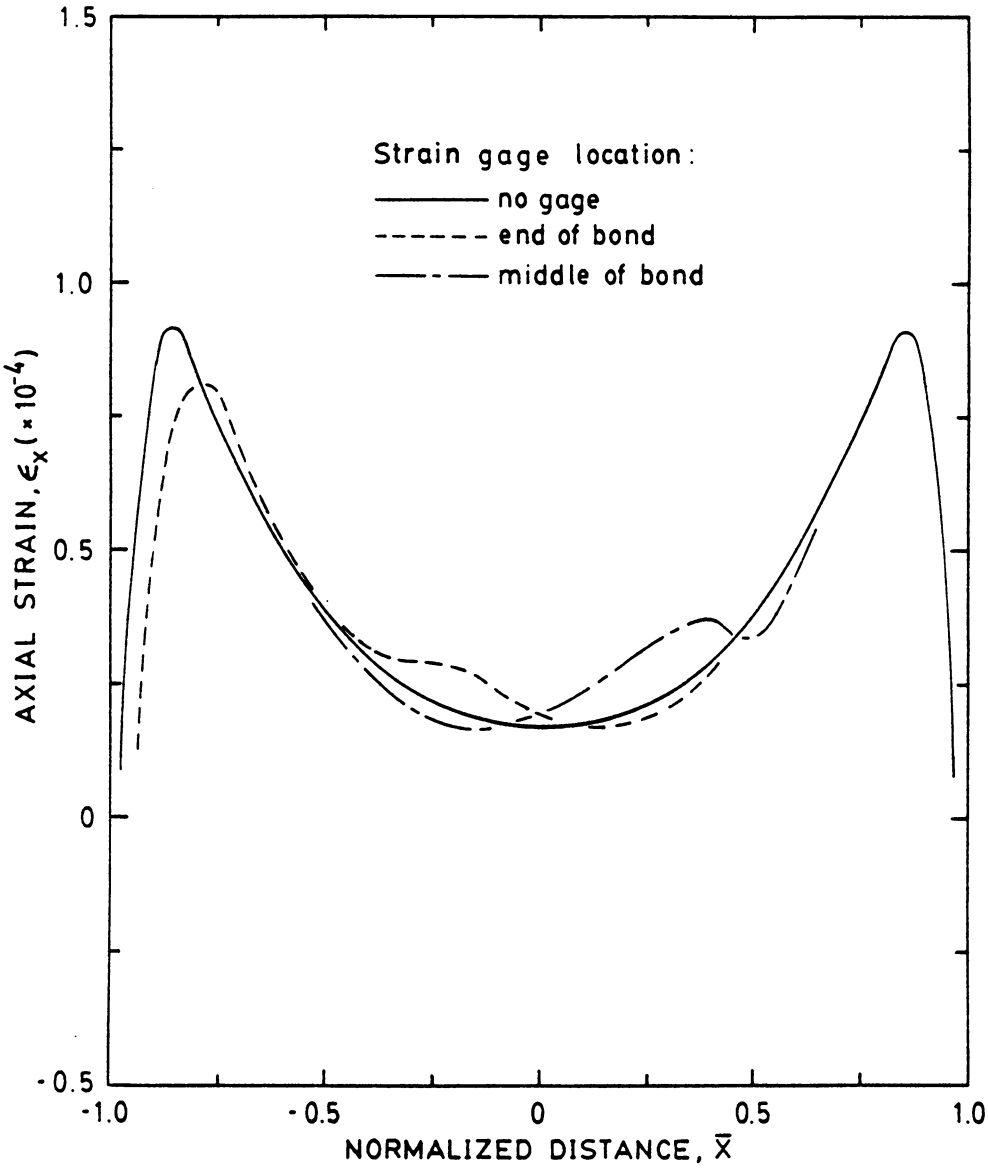

Figure 6. Axial strain distribution along adhesive centerline for embedded strain gage: comparison of the strain field for gages present in the adhesive with no gages present.

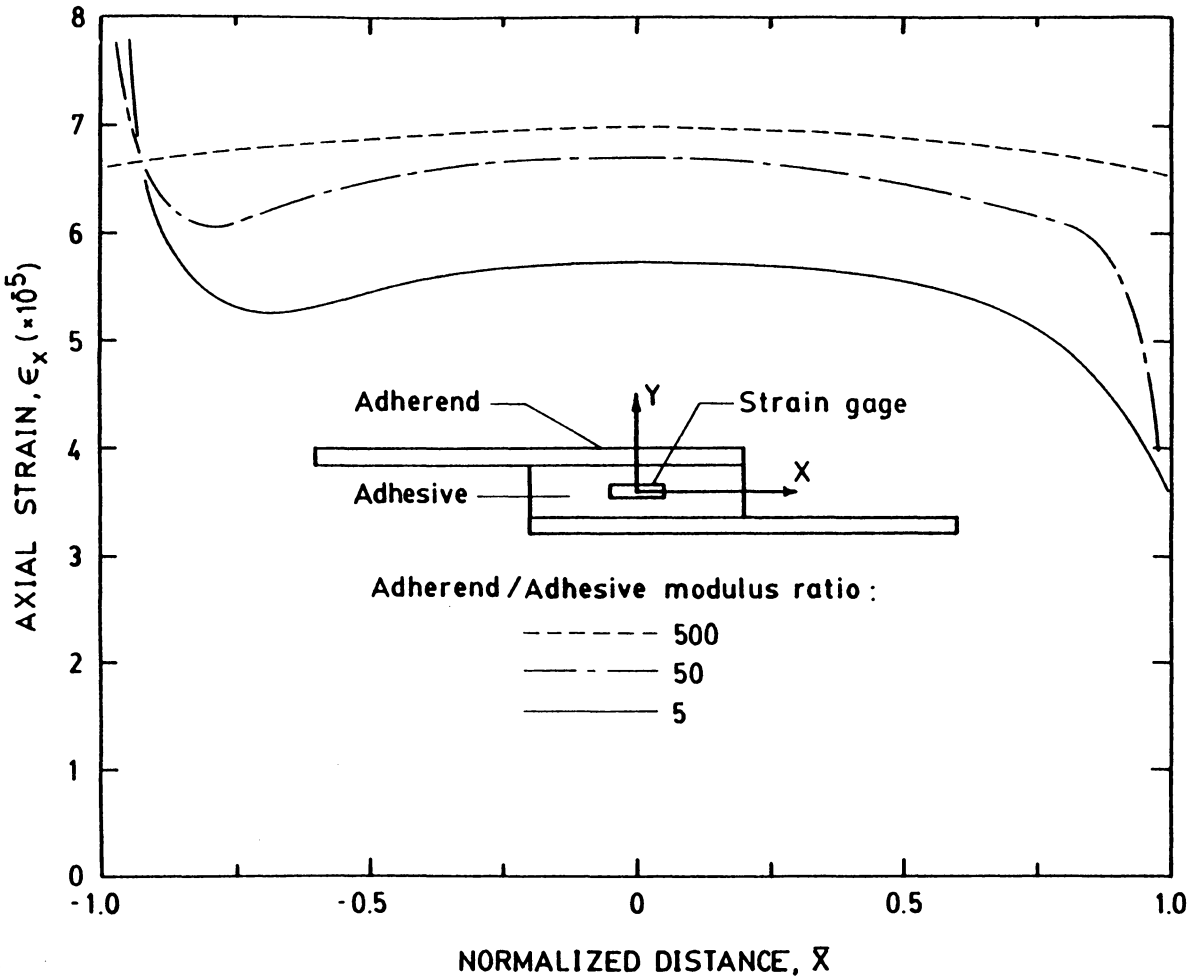

Figure 7. Effect of adherend/adhesive modulus ratio on strain measurement: axial strain distribution for a centrally embedded strain gage in the adhesive.

Thermal stresses

Because of the mismatch in thermal coefficients of expansion between the adhesive and adherend, residual thermal stresses will occur in any bonded joint that undergoes elevated temperature curing. Depending on the joint configuration, these thermal stresses may influence the ultimate performance of the joint. Despite the presence of thermal stresses in adhesively bonded joints, little attention is given to both predicting their presence in the adhesive and their affect on adhesive durability.

The analysis of thermal stresses is complicated by the viscoelastic nature of the polymeric adhesive. At the time of cure, polymerization converts the adhesive into a highly crosslinked amorphous polymer. At this time, the adhesive is free of thermal stresses. As the bond cools, however, thermal stresses develop in the adhesive due to the difference in thermal expansion between the adhesive and stiffer adherend. As the cooling progresses, the thermal stresses increase proportionally to the difference between the current and stress free temperatures. At the same time as the thermal stresses are increasing, viscous mechanisms in the adhesive are relieving the building thermal stresses. At some point following thermal equilibrium, the viscous dissipation ceases and the rigidity of the polymer chains and crosslinks insure that the thermal stresses remain locked into the adhesive.

The residual state of stress due to the cure conditions of a titanium/epoxy single lap joint was studied using VISTA under the following conditions: (1) both the titanium and epoxy are isotropic, linear elastic materials with no property dependence on temperature, (2) the stress free state is defined at the cure temperature of 250 $^{\circ}C$, and (3) the joint was cooled slowly so that thermal gradients were not present in the bonded joint assembly. The finite element mesh used was identical to the mesh employed in the study of adhesive stresses due to mechanical loading (Fig. 1). Values of the coefficients of thermal expansion are listed in Table 1.

From the finite element results, several important features of the thermal stresses in the adhesive are apparent. The axial stress distribution, σ_x, and the peel stress distribution, σ_y , appear in Figure

8. The other relevant stress component, τ_{xy} , is negligible. According to Figure 8, the elevated cure temperature and property mismatch results in a large axial stress state in the adhesive. In comparison to the peel stress, σ_y, the axial stress component, σ_x, dominates the stress state in the adhesive. Note that σ_y is small in comparison to σ_x except for the presence of a large peel stress at the joint ends.

Because the strain free reference state of the adhesive was defined at the cure temperature, the axial strains are compressive in relation to the cure state. However, the constraint of the stiffer adherends prevents the adhesive from contracting fully with respect to a bulk or neat resin specimen undergoing the same cure cycle. Hence, the actual strain state in the *in-situ* adhesive is actually tensile with respect to the bulk adhesive reference. Figure 9 shows the residual axial strain distribution along the adhesive centerline for the two reference states described above. The tensile strain state was calculated simply by adding the thermal strain component, $\alpha\Delta T$, to the compressive mechanical strain determined by the finite element analysis.

From the previous analysis of the adhesive stresses due to mechanical loading, axial stresses and strains due to thermal loading are more severe in the adhesive than mechanically induced axial stresses at low loads. Because the thermal axial strain distribution is fairly uniform in the center of the adhesive, an embedded strain gage would respond to the thermal strains present in the adhesive similar to the work done by Hahn [12] using embedded wires in an adhesive layer. Mismatches in mechanical properties between the strain gage and adhesive would affect the local strain field in the gage vicinity; however, the embedded strain gage may serve as a tool in quantifying residual strains in adhesively bonded joints. Obviously, the stiffer adherend dominates the axial strain behavior in the adhesive for both the mechanical and thermal loading. For this reason, the embedded strain gage may serve only to define the strain free reference temperature of the adhesive.

Finite element analyses revealed several problems associated with using the single lap joint configuration in measuring adhesive properties. First, the multiple state of stress in the adhesive due to mechanical loading seriously questions the measurement of shear properties. Secondly, the use of

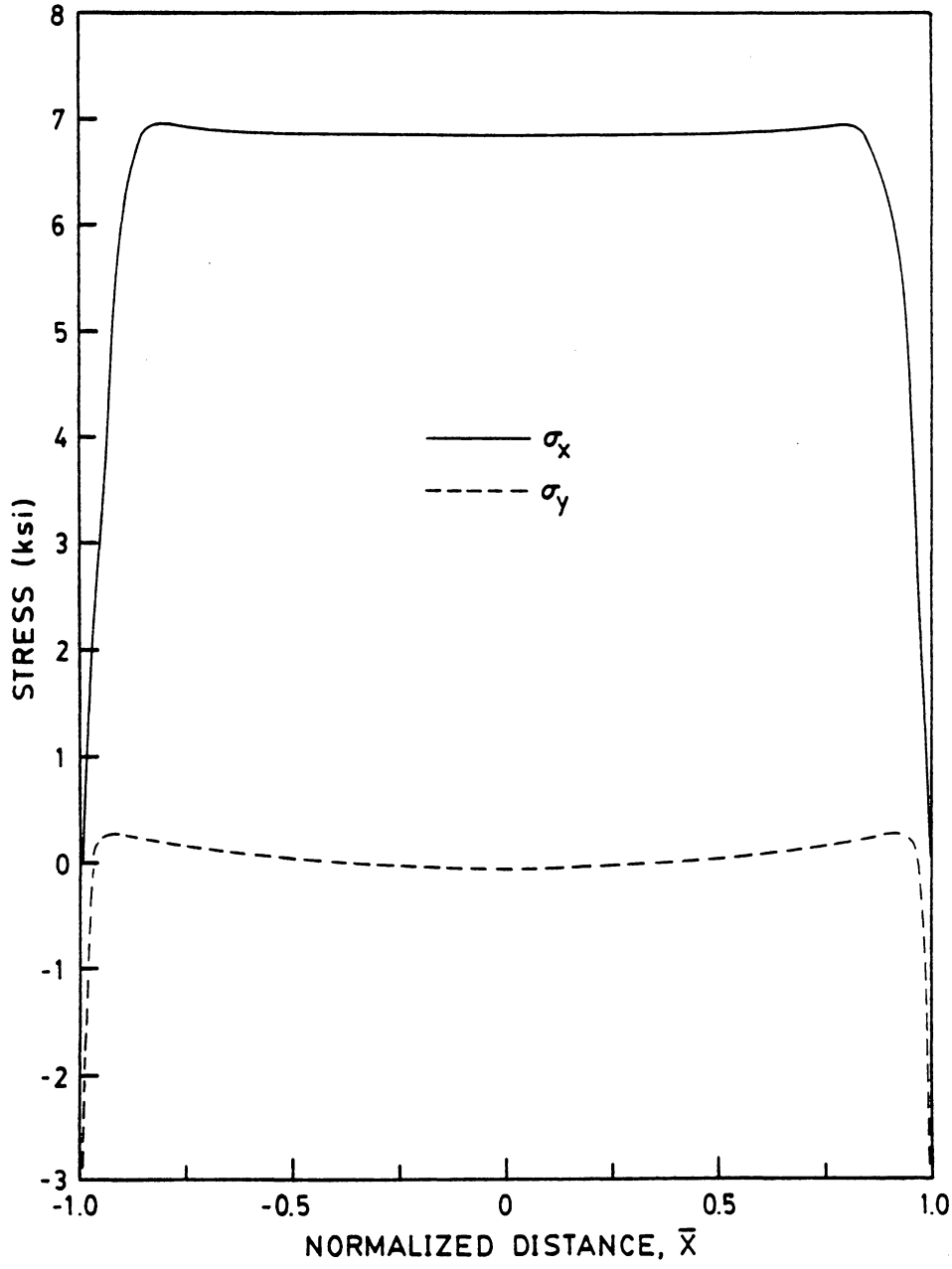

Figure 8. Residual thermal axial and peel stress distribution in single lap joint adhesive layer.

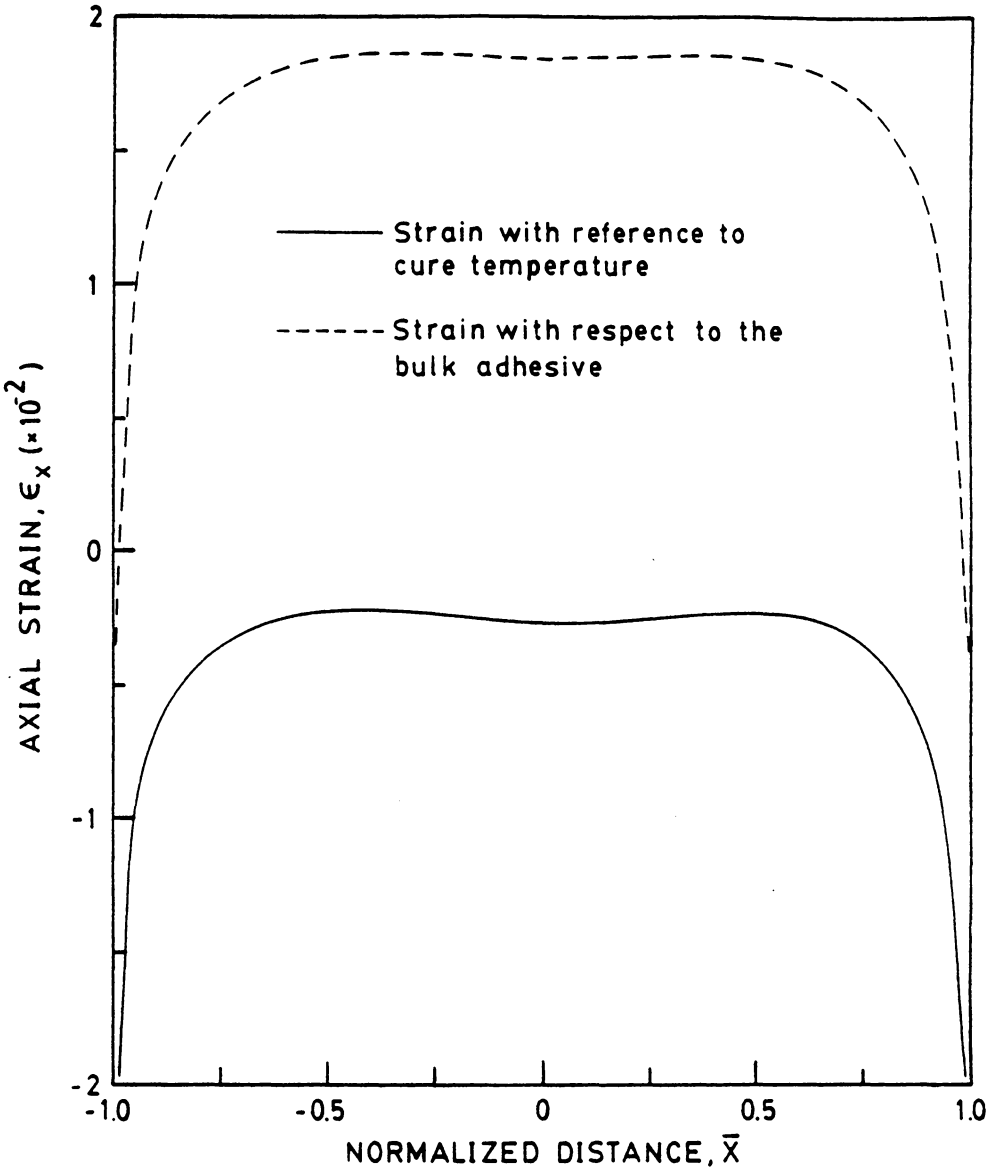

Figure 9. Residual thermal axial strain distribution in single lap joint adhesive layer.

embedded strain gages lacks validity in collaborating axial strain mesurements with adhesive mechanical properties. Lastly, the residual thermal stresses present in the adhesive following cure further complicate material property determination.

Thick adherend joint

The geometry of the thick adherend joint is an evolution of the single lap specimen. In the thick adherend specimen, thicker adherends replace the the thin adherends of the single lap configuration inorder to reduce bending and stretching of the adherends. In this manner, stress concentrations are reduced in the thick adherend joint. Although several investigators appear to have independently developed the thick adherend specimen, Frazier [19] was the first to publish results using this specimen.

The thick adherend specimen is a vast improvement over the single lap specimen for two reasons. First, the thick adherend lap joint is made by bonding two plates of metal under pressure in a hydraulic press. This procedure is equivalent to assembly procedures of laminated structures in industry. Contrastingly, single lap specimens are customarily assembled under clamp pressure with glass beads serving to regulate the bondline thickness. Secondly, the stress distribution in the test adhesive of the thick adherend joint approaches a constant shear state although stress concentrations occur at the ends of the adhesive bondline.

Finite element analysis

The stress distribution in the adhesive layer was determined using the finite element method. For simplicity , it was assumed that both the adherends and adhesive are isotropic, linear elastic mate-

rials and that plane strain conditions prevail. Figure 10 shows the deformed mesh obtained using the finite element program VISTA. The adhesive layer was modelled with five elements across the thickness and twenty elements along the overlap length. Eight node isoparametric quadrilateral elements were used throughout the model. The entire model consisted of 448 elements.

The multiple stress state along the adhesive centerline is shown in Figure 11. From the finite element analysis, the thicker adherends improve the axial and peel stress concentrations at the bond ends compared to the single lap joint. Furthermore, a near uniform state of shear stress exists in the middle of the joint away from the edges. Because the thick adherend geometry does provide a more uniform shear stress distribution in the adhesive, realistic assessment of adhesive shear behavior is possible. According to Hart-Smith [20], the most important property of an adhesive in determining its relative usefulness compared to other adhesives is the area under its shear stress-strain curve to failure. The area under the shear stress-strain curve is aptly called the adhesive toughness and is readily obtained from experimental measurements using the thick adherend specimen.

Several investigators have reported adhesive stress-strain data using thick adherend lap joints. Frazier [21] modified an inductance coil tension extensometer to a "zero gage length" thick adherend shear extensometer. Perhaps the most elaborate extensometer to date is the Krieger extensometer [22]. Designed for hostile environments, the Krieger extensometer senses relative deformations in the adherends using an LVDT. In practice, the adhesive shear stress-strain curve is obtained from a plot on an X-Y plotter of load versus relative displacement in the adherend across the adhesive bondline. A more detailed discussion of this measurement procedure follows.

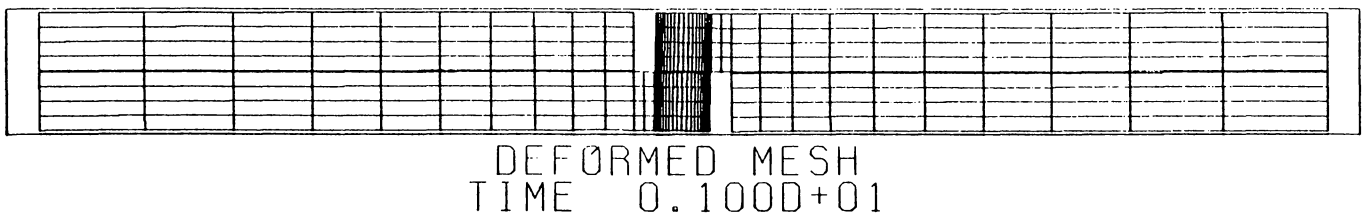

Figure 10. Deformed finite element mesh of thick adherend joint.

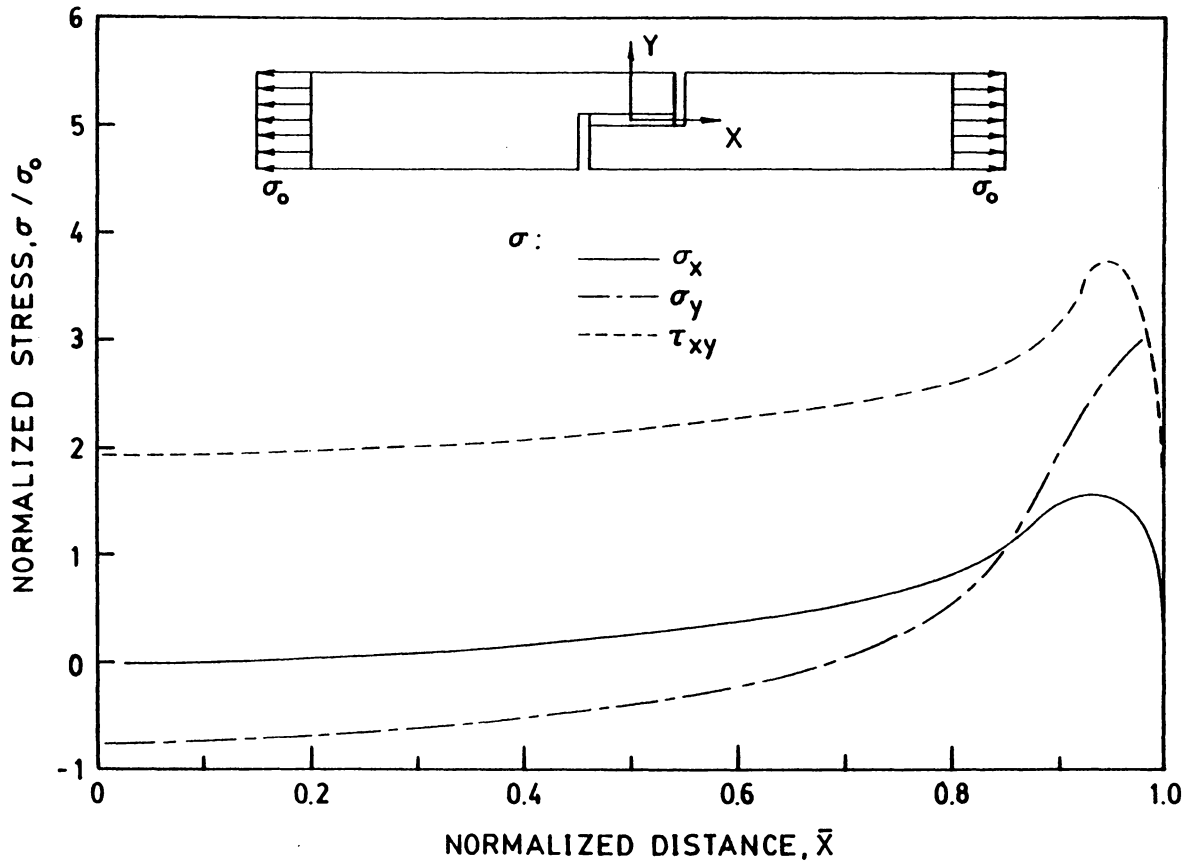

Figure 11. Normalized stress distribution along adhesive centerline in thick adherend joint: stresses normalized with respect to the applied stress.

Krieger extensometer

The Krieger extensometer consists primarily of two rigid frames, an 60 hz LVDT and core, and two spring steel arms. The two rigid frames are connected via the two flexible spring steel arms, which allow translation of one frame relative to the other frame. The LVDT itself is mounted on one frame while the core is threaded to the other frame. The translational motion of the free frame relative to the fixed frame results in translational motion of the LVDT core. The extensometer rests on the surface of the adherends via three steel points; two points are part of the fixed frame whereas the third point is an extension of the independent frame.

With the gage mounted on the adherend surface, the displacement of the independent point relative to the two fixed points is a measure of the adhesive shear deformation. After compensating for the deflections in the adherend, this relative displacement measurement becomes an adhesive strain measurement. For more detailed information on the adhesive strain measurement technique, and the design of the Krieger extensometer, see the report by Krieger [23].

The engineering shear strain in the adhesive may be determined from simple geometry. Consider a homogeneous shear deformation in the adhesive between the two rigid adherends as depicted in Figure 12. From the engineering definition, the shear strain, γ , is given by

$$\gamma = \arctan \frac{\delta_a}{t_a} \qquad [1]$$

where δ_a is the relative displacement across the bondline and t_a is the adhesive thickness. The adhesive thickness is determined by averaging optical measurements at several locations along the bondline. From measurements of aluminum adherend displacements using a dummy joint, i.e. a thick adherend joint with the same dimensions but no bondline, Krieger determined that the adherend deformation is a function of the applied load, extensometer point gap, and bondline thickness such that

$$\delta_c = 9.328 \times 10^{-8} P \frac{\delta_p - t_a}{\delta_p} \quad [2]$$

where P is the applied load in lbs., δ_p is the extensometer point gap in inches. The true adhesive deformation is related to the extensometer deformation measurement by the relation

$$\delta_a = \delta_t - \delta_c \quad [3]$$

where δ_t is the extensometer deformation measurement (total deformation in the adherend).

The application of the Krieger extensometer to adhesive shear stress-strain property measurement was studied both experimentally and analytically in terms of accuracy. Thick adherend lap joint specimens were fabricated using 3M Company's AF 163-2U adhesive in the following manner. First, two 3/4" inch aluminum 2024-T4 plates were surface treated according to Boeing Company Process Specification BAC-5555 which is listed in Appendix A. After the plates were anodized, a 3M primer EC-3960 was sprayed on the anodized surfaces using an automotive spray gun with stirring capability. The constant stirring of the primer was necessary to obtain a consistent primer coating. The primer itself is an epoxy resin which both protects the freshly anodized surface of the aluminum and acts as an adhesion promoter. The plates were baked at 121 °C for one hour. The assembly of the bonded plates consisted of two steps. First, two adhesive sheets were carefully applied to one of the primed surfaces. Roller pressure was applied to the adhesive to eliminate any visible air entrapments. Following application of the adhesive, the plates were assembled to form a sandwich. At this stage, the sandwich was placed in a hydraulic press at 40 psi. The adhesive cure temperature was set for 121 °C for a period of one hour. After cure and subsequent cooldown of the adhesively bonded plates, the lap joint specimens were machined from the plates according to the dimensions in Figure 13.

Experimental test results indicated two of the Krieger extensometers salient features. The extensometer is capable of determining the load versus relative displacement of the thick adherend joint with careful application of the gage on the joint surface. Figure 14 shows the results of a

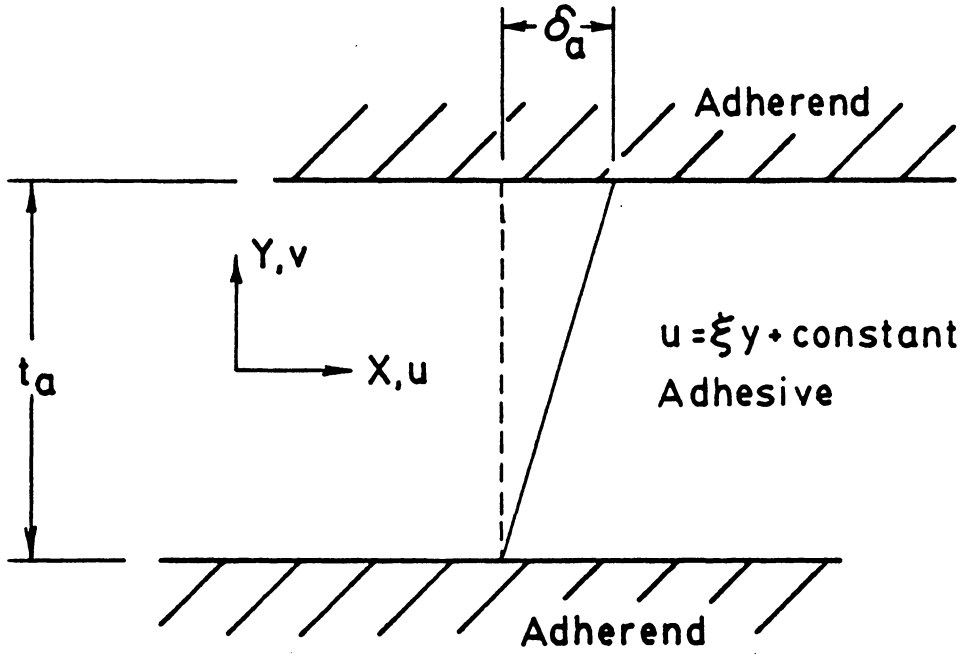

Figure 12. Idealized shear deformation field in an adhesive layer: deformation occurs between two rigid adherends.

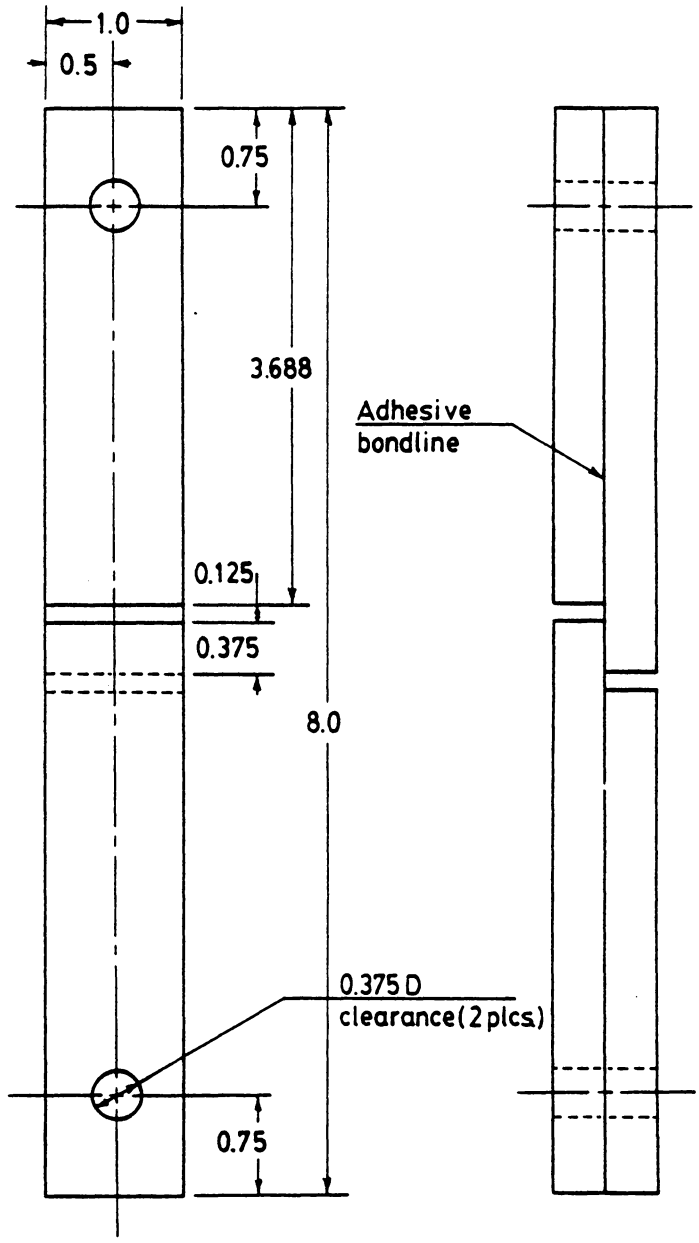

Figure 13. Dimensions of the thick adherend lap joint specimens: joints machined from bonded plates.

typical measurement made with the gage. Not shown in the figure, however, is the noise problem associated with the 60 hz LVDT. Because the frequency of the LVDT excitation voltage is the same as all electrical signals present in the test room, the signal from the extensometer contains excessive noise. The noise was eliminated to some degree by placing capacitors in parallel with the output signal. However, this creates a RC circuit with an unknown time constant that will affect the response of the plotter to the extensometer signal. Also, the noise is minimized when the LVDT core is zeroed; however, the noise increases with core diplacement from the zero point. Due to the noise problems, one of the extensometer pair was modified to accomodate an MTS axial strain extensometer instead of the 60 hz LVDT as the displacement signal transducer.

A complete shear stress-strain curve to failure was obtained for the AF 163-2U adhesive using both the modified and regular Krieger extensometer. For the data reduction of the load versus extensometer output, the shear stress is defined as the average stress in the adhesive. Thus, the shear stress is simply the applied load, P, divided by the overlap area, A

$$\tau = \frac{P}{A} \qquad [4]$$

Figure 15 shows the shear stress strain behavior using the modified extensometer as calculated using the shear stress definition (Eq. 4) and the shear strain definition (Eq. 1). Furthermore, the results of a simultaneous measurement of both the modified and regular Krieger extensometers on the same joint are shown in Figure 16. Note that both extensometers were calibrated prior to the test. According to the experimental results, a large discrepancy exists between the two extensometer measurements.

The difference in extensometer measurements raises questions about the measurement technique in general. As mentioned previously, capacitors were employed to reduce noise in the regular Krieger extensometer. The time constant associated with the capacitors may be large enough to cause the deformation signal to lag the load signal. This would explain the difference in ultimate stress and strain; however, the linear region of the two curves contradict this assertion. Although

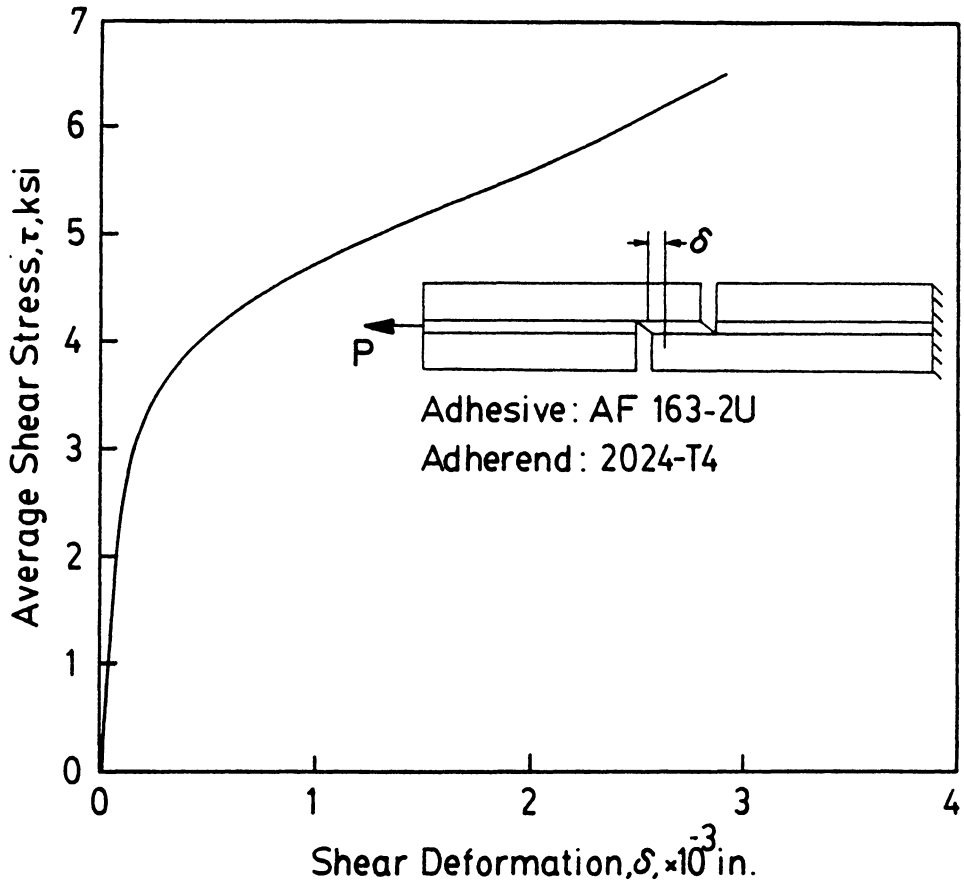

Figure 14. Preliminary measurement of the adhesive deformation in the thick adherend joint: average shear stress versus adhesive deformation determined using the Krieger extensometer.

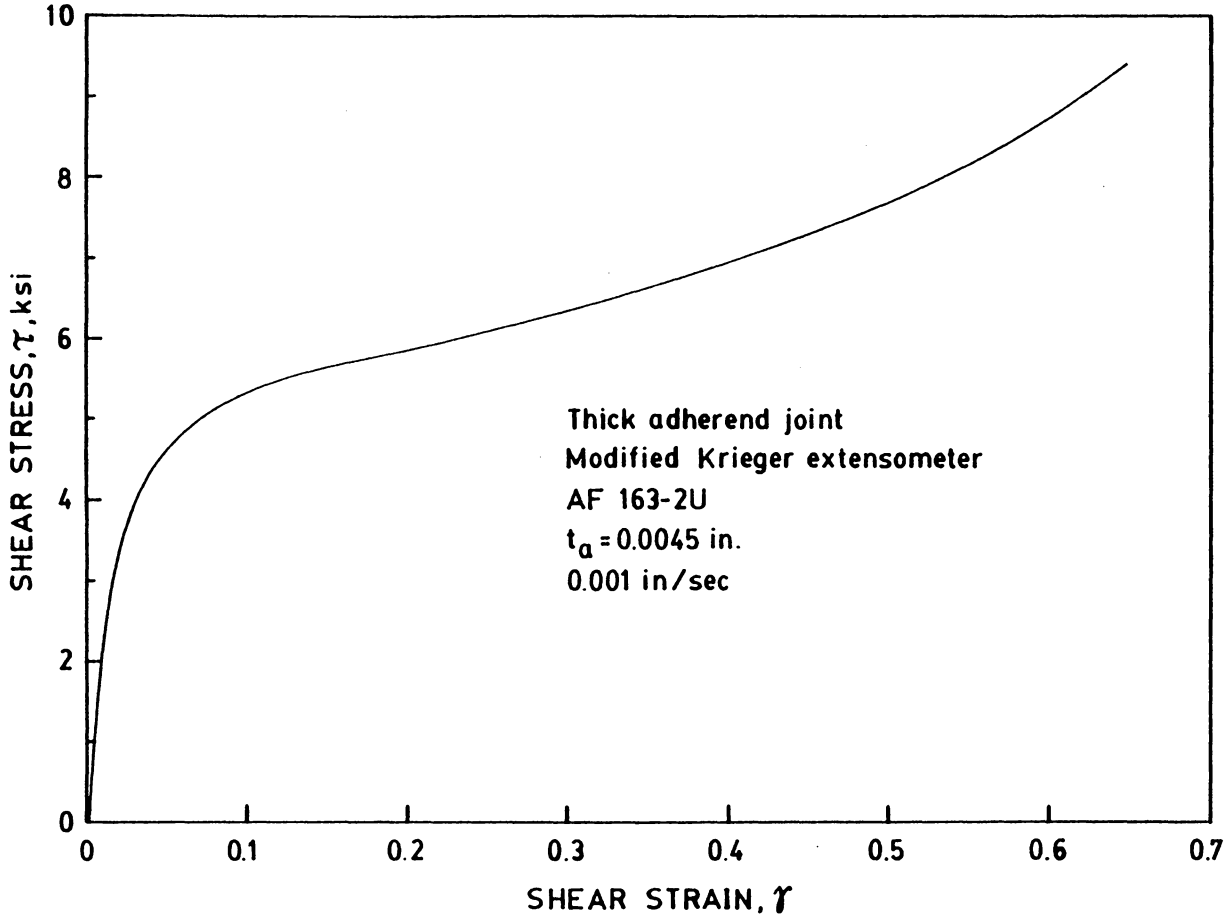

Figure 15. Shear stress-strain curve to failure of AF 163-2U in thick adherend joint.

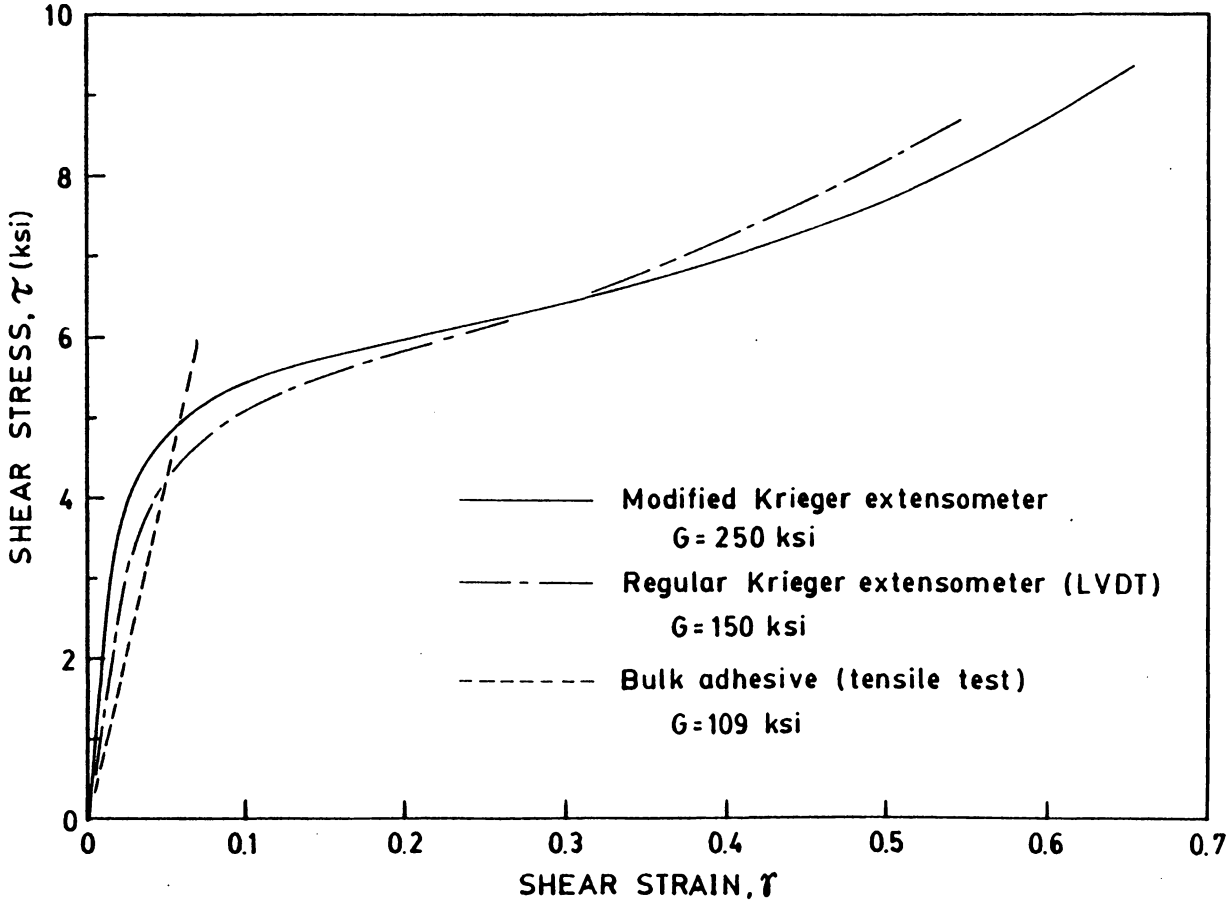

Figure 16. Comparison of simultaneous extensometer measurements on thick adherend joint: results of modified and regular Krieger extensometers on the shear stress-strain measurement with comparison with bulk adhesive modulus.

Krieger never mentions the drawbacks of using 60 hz LVDT's, he does analyze the various types of errors associated with the mechanical aspect of the adherend deformation measurement [22]. An obvious cause of the disparity between the simultaneous measurements could be misalignment of the load axis due to machining errors. However, the dimensional tolerances used to machine the specimens were close enough to eliminate such problems.

The accuracy of the Krieger extensometer measurement technique was studied using a finite element analysis. There were two main questions addressed: (1) does the measurement of the adhesive deformation at an arbitrary point in the adherend relate to the actual adhesive properties and (2) is the measurement subject to large errors due to extensometer placement along the bondline and with respect to the bond centerline.

The analysis of the measurement technique was based on the same finite element mesh employed to determine the stress distribution in the adhesive due to mechanical loading. With the adhesive properties known as input into the finite element analysis, the adhesive deformation was found at several points along the bondline. Using these deformations, and the definitions of shear stress (Eq. 4) and shear strain (Eq. 1), the apparent adhesive modulus was calculated at the various localities. The results of these calculations are given in Table 2. From the finite element analysis, the measurement of the adhesive shear deformation at the 1/4 point ($\bar{x} = 0.5$) of the overlap is well within experimental error of the actual shear modulus. The results indicate that the measurement is sensitive to the position of the extensometer points along the bondline.

The Krieger extensometer measures deformations at two points in the adherend removed from the bondline. Hence, it is possible that this creates errors in the strain measurement due to the position of the extensometer with reference to the adhesive centerline. The u_x diplacement distribution is nonlinear in the adherend due to the presence of bending moments. Figure 17 illustrates this nonlinearity and the effect of the extensometer position relative to the adhesive centerline. According to the finite element results, the extensometer measurement is only slightly prone to error due to offset of the gage about the joint centerline.

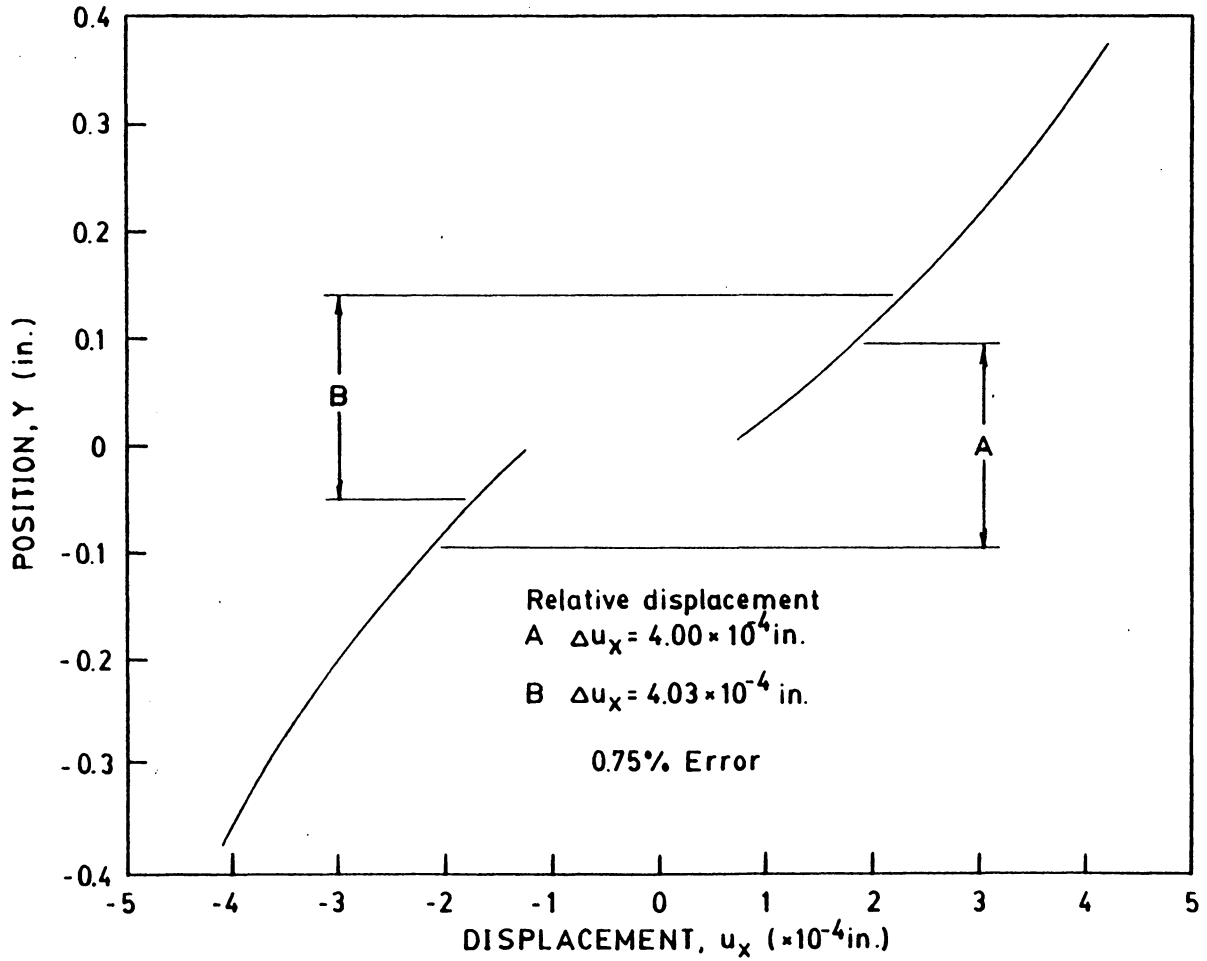

Figure 17. Nonlinear displacement in thick adherend joint at an arbitrary location in adherend: effect of the point location on the deformation measurement technique using the Krieger extensometer.

Nonlinear strains

One important characteristic of adhesives is their ability to allow large strains as depicted in Figures 13-15. The use of linear strain definitions is thus highly questionable when analyzing adhesive deformations. For this reason, geometrically nonlinear behavior is often incorporated into finite element analysis of adhesively bonded joints [17,24]. Post et al. [25] determined the deformations in a thick adherend joint using Moire interferometry. The results of their work indicate that geometric definitions of shear strain suffice for an adhesive undergoing deformation between rigid adherends. The large deformations associated with the shearing of the constrained adhesive also involve extensional strain as will be demonstrated using a simple deformation field and the Lagrangian nonlinear strain tensor.

The Lagrangian nonlinear strain tensor is given by

$$L_{ij} = \frac{1}{2} \times [\frac{\partial u_i}{\partial a_j} + \frac{\partial u_j}{\partial a_i} + \frac{\partial u_r}{\partial a_i} \times \frac{\partial u_r}{\partial a_j}] \qquad [5]$$

For the adhesive in the thick adherend joint, plane strain conditions dominate; hence, the three nonlinear strain components are

$$\varepsilon_x = \frac{1}{2} \times [2\frac{\partial u}{\partial x} + \frac{\partial u}{\partial x}^2 + \frac{\partial v}{\partial x}^2 + \frac{\partial w}{\partial x}^2] \qquad [6a]$$

$$\varepsilon_y = \frac{1}{2} \times [2\frac{\partial v}{\partial y} + \frac{\partial u}{\partial y}^2 + \frac{\partial v}{\partial y}^2 + \frac{\partial w}{\partial y}^2] \qquad [6b]$$

$$\varepsilon_{xy} = \frac{1}{2} \times [\frac{\partial u}{\partial y} + \frac{\partial v}{\partial x} + \frac{\partial u}{\partial x} \times \frac{\partial u}{\partial y} + \frac{\partial v}{\partial x} \times \frac{\partial v}{\partial y} + \frac{\partial w}{\partial x} \times \frac{\partial w}{\partial y}] \qquad [6c]$$

Using the assumed adhesive deformation illustrated in Figure 12, the deformation components are

$$u = \xi y$$

$$y = constant$$

$$w = 0$$

Thus, the Lagrangian nonlinear strain tensor becomes

$$[L_{ij}] = \begin{bmatrix} 0 & 1/2\xi & 0 \\ 1/2\xi & 1/2\xi^2 & 0 \\ 0 & 0 & 0 \end{bmatrix}$$

The slope, ξ, is related to the adhesive deformation and the bondline thickness as

$$\xi = \frac{\delta_a}{t_a} \qquad [7]$$

According to the Lagrangian nonlinear strain tensor and the magnitude of ξ due to the large adhesive deformation, shear deformation in a rigidly constrained layer results in an additional strain component, ε_y.

Often, the engineering strains are more convenient than the tensorial strain components. Again using the Lagrangian definition , introduce the nonlinear engineering strains

$$\varepsilon_x^L = \sqrt{1 + 2\frac{\partial u}{\partial x} + \frac{\partial u}{\partial x}^2 + \frac{\partial v}{\partial x}^2 + \frac{\partial w}{\partial x}^2} - 1 \qquad [8a]$$

$$\varepsilon_y^L = \sqrt{1 + 2\frac{\partial v}{\partial y} + \frac{\partial u}{\partial y}^2 + \frac{\partial v}{\partial y}^2 + \frac{\partial w}{\partial y}^2} - 1 \qquad [8b]$$

$$\gamma_{xy}^L = \frac{\frac{\partial u}{\partial y} + \frac{\partial v}{\partial x} + (\frac{\partial u}{\partial x})(\frac{\partial u}{\partial y}) + (\frac{\partial v}{\partial x})(\frac{\partial v}{\partial y}) + (\frac{\partial w}{\partial x})(\frac{\partial w}{\partial y})}{(1 + \varepsilon_x^L)(1 + \varepsilon_y^L)} \qquad [8c]$$

Using the previous deformation field, the engineering nonlinear strain components become

$$\varepsilon_x^L = 0$$

$$\varepsilon_y^L = \sqrt{1 + \xi^2} - 1$$

$$\gamma_{xy}^L = \arcsin \frac{\xi}{\sqrt{1 + \xi^2}}$$

Using geometry, the shear strain is expressed as

$$\gamma_{xy} = \arctan \xi \qquad [9]$$

which is identical to the shear strain defined by Eq. 8c for the given deformation field.

Table 3 shows the importance of the large shear deformations on the nonlinear strain field. Note that the values of the adhesive deformation, δ_a, are values taken from mesaurements of the thick adherend lap joint. The presence of the nonlinear strain component , ε_y^L , due to the large deformations implies that a state of pure shear cannot exist in any adhesive specimen even at moderate deflections. Because the thick adherend joint has a multiple state of stress throughout the adhesive, the presence of the nonlinear extensional strain may be of secondary importance in interpreting shear stess-strain curves to failure.

Discussion

The thick adherend joint specimen is a vast improvement over the single lap joint specimen in terms of obtaining adhesive shear property data. The thick adherend joint approaches a constant shear state away from the ends of the bond based on linear elastic adhesive behavior. Furthermore, the thick adherend joint is a more realistic test geometry due to the fact that the bond is formed under

pressure without the presence of beads in the adhesive. Consequently, useful engineering properties are readily obtainable from the thick adherend lap joint.

The Krieger extensometer is a useful tool in evaluating adhesive shear stress-strain properties. Because the stress distribution in the adhesive layer is a complex state of varying dilatational and deviatoric stresses, the practical uses of the extensometer measurement are limited to elastic and possibly plastic adhesive property determination. Furthermore, practical application of the Krieger extensometer has demonstrated some of the problems associated with the device and the measurement technique.

Table 1. Elastic properties used in linear elastic finite element analyses

Material	E (psi)	ν	α (*in/in/°F*)
Titanium	2.93×10^{7}	0.33	12.0×10^{-6}
Aluminum	1.00×10^{7}	0.32	12.9×10^{-6}
Epoxy	2.43×10^{7}	0.40	11.9×10^{-5}
Strain gage	3.00×10^{6}	0.32	N/A

Table 2. Effect of placement on the Krieger extensometer measurement.

$\bar{x}$	δ_a ($\times 10^4 in$)	γ	G (psi)	% Error
0.17	2.128	0.0244	65781	8.6
0.24	2.087	0.0240	67074	6.8
0.32	2.004	0.0235	68451	4.9
0.42	2.007	0.0231	69696	3.2
0.54	1.971	0.0226	71021	1.3

Table 3. Effect of large shear deformation on induced extensional strain

δ_a (in)	$\log_{10}\delta_a$ (in)	ε_y^L	$\log_{10}\varepsilon_y^L$
1.861×10^{-5}	-4.73	8.551×10^{-6}	-5.07
5.759×10^{-5}	-4.24	8.188×10^{-5}	-4.09
1.324×10^{-4}	-3.88	4.327×10^{-4}	-3.36
2.548×10^{-4}	-3.59	1.602×10^{-3}	-2.79
5.396×10^{-4}	-3.27	7.164×10^{-3}	-2.15
9.813×10^{-4}	-3.01	2.350×10^{-2}	-1.63
1.613×10^{-3}	-2.79	6.230×10^{-2}	-1.20
2.164×10^{-3}	-2.66	1.096×10^{-1}	-0.96
2.697×10^{-3}	-2.57	1.658×10^{-1}	-0.78
3.404×10^{-3}	-2.47	2.539×10^{-1}	-0.59

III

Improved Shear test geometries

The advantages and disadvantages of both the single lap and thick adherend lap joint specimens in determining adhesive properties were discussed in the previous chapter. The motivation for pure shear specimens has fostered the development of several improved shear test geometries for adhesive characterization. At this time, the standard adhesive shear test is the napkin ring test as defined by ASTM E229-70. However, the shear stress distribution in the napkin ring varies linearly with radius. Furthermore, alignment of the two adherend halves is a major drawback of this test.

Cone-and-Plate shear test

The cone-and-plate shear stress adhesive test was introduced by Grant and Cooper [26]. Based principally on the cone and plate viscometer, the cone-and-plate specimen was intended as an improvement to the napkin ring test. The geometry of this test is depicted in Figure 18; the specimen consists of an adhesive layer between two solid cylindrical adherends. One of the adherends has a

flat plate at the bonded end while the other adherend has a convex conical end. When the conical end contacts the flat plate, the adhesive bond becomes a disk with a conical indentation. The test geometry was analyzed from an equilibrium point of view to determine the possible state of stress in the adhesive.

In spherical coordinates, the coordinate system most suited to the adhesive geometry, the equations of equilibrium neglecting body forces are

$$\frac{\partial \tau_{rr}}{\partial r} + \frac{1}{r \sin\theta}\frac{\partial \tau_{r\varphi}}{\partial \varphi} + \frac{1}{r}\frac{\partial \tau_{r\theta}}{\partial \theta} + \frac{2\tau_{rr} - \tau_{\varphi\varphi} - \tau_{\theta\theta} + \tau_{r\theta}\cot\varphi}{r} = 0 \qquad [10a]$$

$$\frac{\partial \tau_{r\theta}}{\partial r} + \frac{1}{r \sin\theta}\frac{\partial \tau_{\varphi\theta}}{\partial \varphi} + \frac{1}{r}\frac{\partial \tau_{\theta\theta}}{\partial \theta} + \frac{3\tau_{r\theta} + (\tau_{\theta\theta} - \tau_{\varphi\varphi})\cot\theta}{r} \qquad [10b]$$

$$\frac{\partial \tau_{r\varphi}}{\partial r} + \frac{1}{r \sin\theta}\frac{\partial \tau_{\varphi\varphi}}{\partial \varphi} + \frac{1}{r}\frac{\partial \tau_{\theta\varphi}}{\partial \theta} + \frac{3\tau_{r\varphi} + 2\tau_{\varphi\theta}\cot\theta}{r} = 0 \qquad [10c]$$

The stress distribution in the adhesive was obtained without recourse to a complete elasticity solution. To achieve the solution, various assumptions were proposed regarding the presence of the stress components in the adhesive. If the specimen is loaded in pure torsion as shown in Fig. 18, then the normal stresses τ_{rr} , $\tau_{\theta\theta}$, and $\tau_{\varphi\varphi}$ would be zero. Similarly, a pure torsional load would produce only a shear stress in the $\theta\varphi$ direction; hence, $\tau_{r\theta} = \tau_{r\varphi} = 0$. With these assumptions, the equilibrium equations reduce to

$$\frac{\partial \tau_{\theta\varphi}}{\partial \theta} + 2(\cot\theta)\tau_{\theta\varphi} = 0 \qquad [11]$$

$$\frac{\partial \tau_{\theta\varphi}}{\partial \varphi} = 0 \qquad [12]$$

Since $\tau_{\theta\varphi}$ is not a function of φ which indicates symmetry about the torsional axis, then Eq. 11 becomes

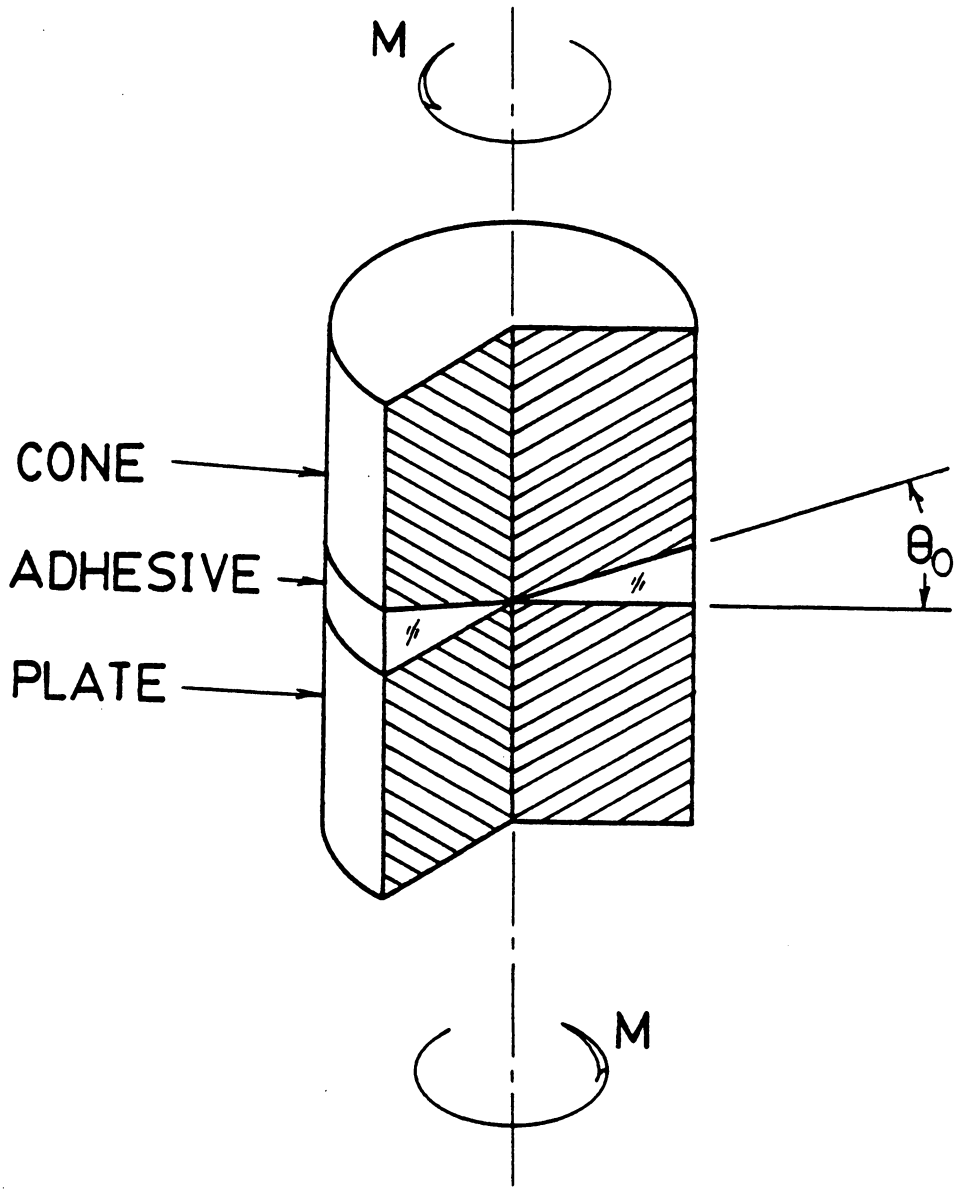

Figure 18. Cone-and-plate geometry: internal view of the adhesive test volume.

$$\frac{d\tau_{\theta\varphi}}{\tau_{\theta\varphi}} = -2(\cot\theta)d\theta \qquad [13]$$

This equation is integrated to obtain

$$\tau_{\theta\varphi} = \frac{C}{\sin^2\theta} \qquad [14]$$

where C is a constant of integration. Thus, for small values of the cone angle θ_o, the variation in shear stress $\tau_{\theta\varphi}$ becomes small. Assuming that $\tau_{\theta\varphi}$ is constant for small cone angular openings θ_o, integration of the shear stress component over the adhesive area is equivalent to the applied moment such that

$$M = \frac{2}{3}\pi r_o^3 \tau_{\theta\varphi} \qquad [15]$$

where r_o is the outside radius of the specimen. The shear strain was found by geometry to be

$$\gamma = \frac{\Phi}{\tan\theta_o} \qquad [16]$$

where Φ is the relative twist across the adhesive at $r = r_o$ (or the outer periphery). As a consequence of the assumptions leading to Eq. 14, the cone and plate geometry would produce a constant state of shear stress in the adhesive. This constant shear stress state would be a significant improvement over existing adhesive test geometries. In addition, the fact that the cone makes contact with the plate would ensure uniformity in specimen fabrication. However, the geometry of the cone in contact with the plate creates a complex state of residual stresses in the test adhesive.

Finite element analysis

The residual thermal stresses in the cone and plate geometry were analyzed using the finite element program VISTA. Due to symmetry about the central axis, the problem is two dimensional in nature. For simplicity of analysis, both the adhesive and adherend were modelled as isotropic, linear elastic materials. Further, it was assumed that the elastic properties of the two materials were invariant to temperature changes. 240 eight noded quadrilateral isoparametric elements were used throughout the model. To model the cone geometry, elements lying on the cone interface were distorted. The distortion of these elements did not cause integration problems in the program. Figure 19 shows the deformed mesh in the bond region; furthermore, this figure depicts the modelling of the cone geometry.

The results of the finite element analysis indicates that the small adhesive volume at the cone apex experiences a compressive stress state while the outer periphery is in a tensile stress state. Figure 20 shows the σ_r stress distribution at various locations in the adhesive. Similarly, Figure 21 shows the σ_z stress distribution in the adhesive. Furthermore, the conical geometry produces residual shear stresses τ_{rz} as shown in Figure 22. Thus a complex residual thermal stress state consisting of undesirable shear stresses as well as a varying tensile stress field exists in the cone and plate adhesive specimen.

The stresses present in the adhesive due to mechanical loading were also analyzed to check the validity of Eq. 14. Because a torsional load is applied to the specimen, it was necessary to use the three dimensional capabilities of the finite element program ABAQUS. Figures 23 and 24 show two views of the three dimensional mesh which consisted of 256 20 node reduced integration brick elements. The isoparametric reduced integration elements were employed in the analysis to reduce approximation errors since the mesh is course (two elements) in the radial direction. Zienkiewicz [27] provides a detailed justification that reduced integration elements eliminate errors due to ap-

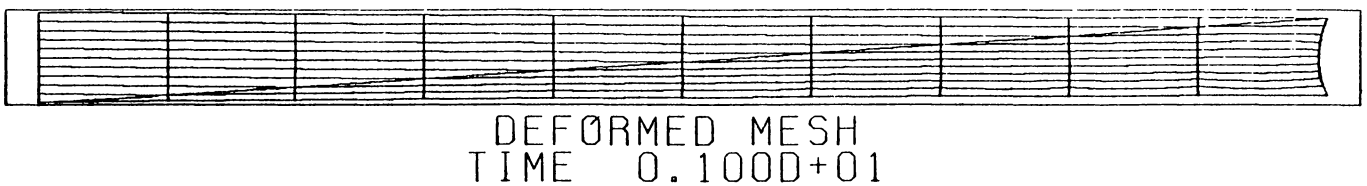

Figure 19. Deformed finite element mesh of the cone-and-plate region: deformed adhesive due to thermal loads.

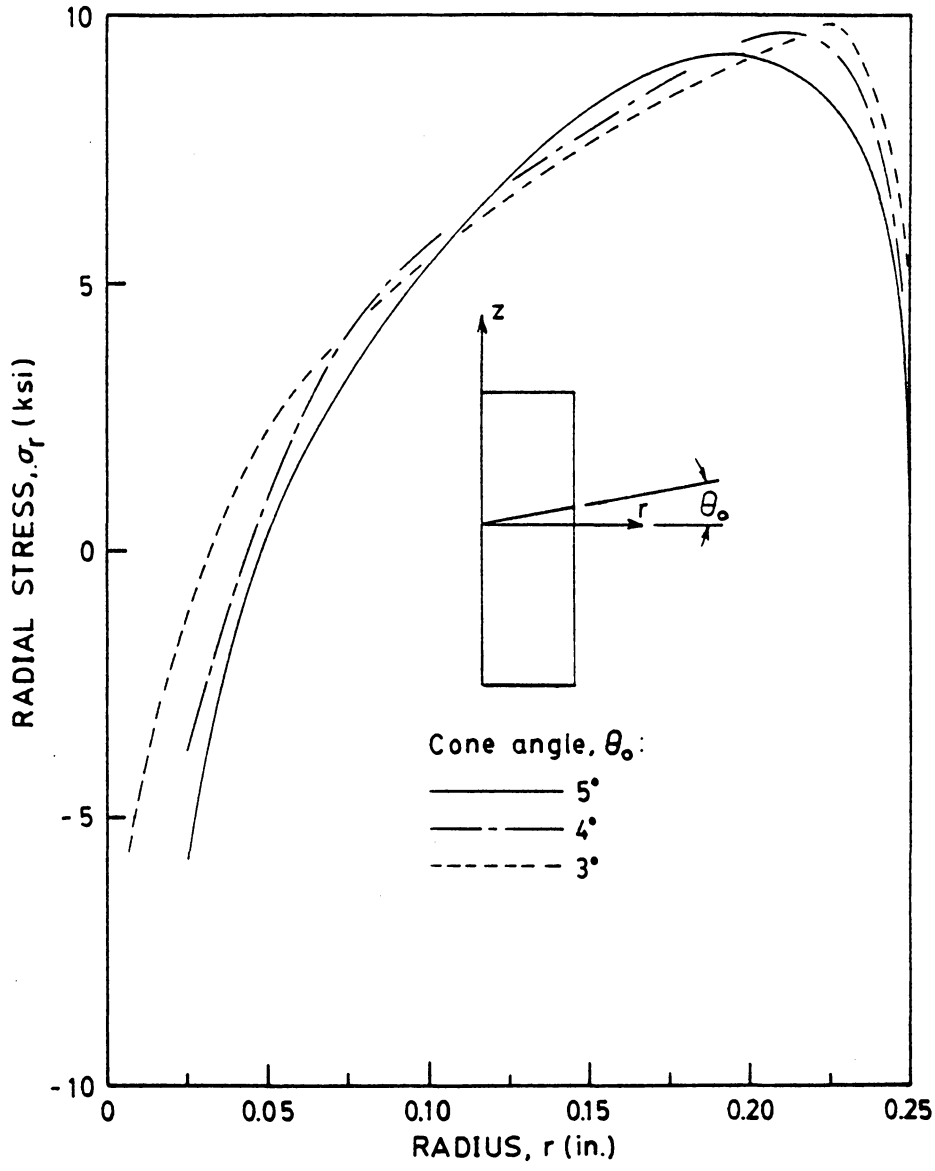

Figure 20. **Residual thermal radial stress distribution in cone-and-plate adhesive volume: various cone angular openings.**

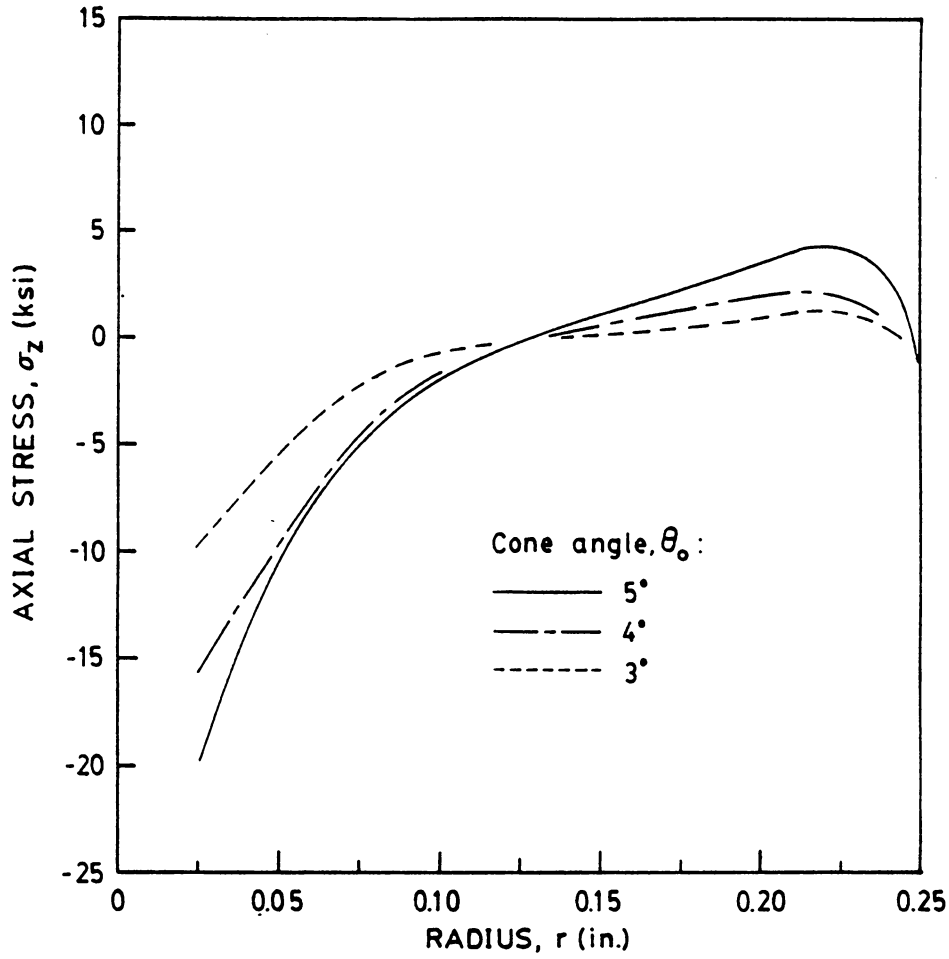

Figure 21. Residual thermal axial stress distribution in cone-and-plate adhesive volume: various cone angular openings.

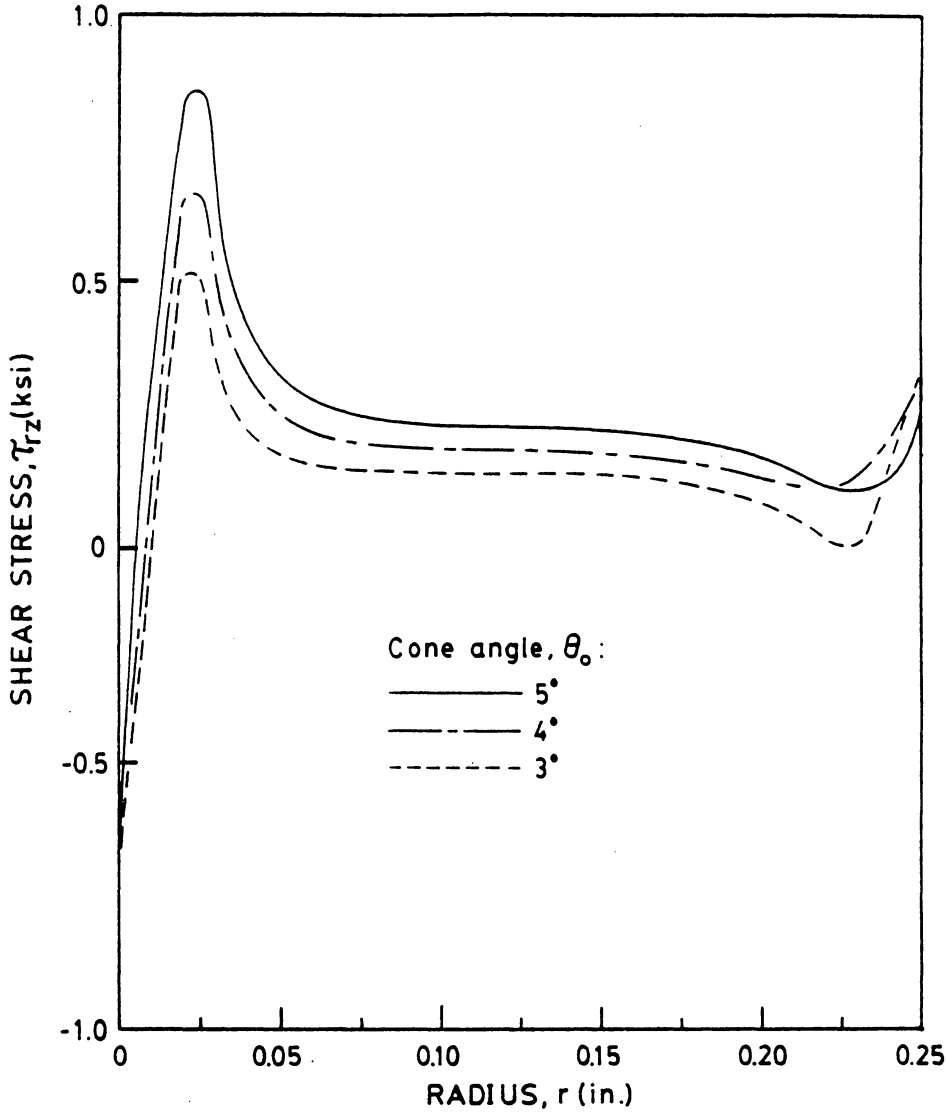

Figure 22. Residual thermal shear stress distribution in cone-and-plate adhesive volume: various cone angular openings.

proximation of the geometry. Also, the nature of the geometry, specifically the small size of the adhesive volume, causes aspect ratio problems in full integration elements.

The stress distribution in the adhesive is not as uniform as predited by Eq. 14. The shear stress distribution, normalized with respect to the predicted value, for various adherend/ adhesive modulus ratios are shown in Figure 25. From the finite element analysis, it was determined that the shear stress $\tau_{\theta\omega}$ is indeed the only stress component present in the adhesive due to mechanical loading. From the symmetry of the specimen about the torsional axis, it becomes apparent that the shear stress must be zero at the center of the specimen ($r = 0$). The fact that the stress distribution is relatively invariant to the modulus ratio atests to the dependence of the stress distribution on the geometry alone. Furthermore, the finite element analysis indicates that the shear stress approaches the predicted value away from the conical apex.

The observation that the shear stress quickly approaches the predicted value away from the center of the specimen led to the belief that removal of the center of the specimen would result in a constant shear stress state in the adhesive. To check this hypothesis, the finite element mesh was modified by the removal of the central elements as shown in Figure 26. The resulting shear stress distribution along the adhesive interface is shown in Figure 27. Note that the stress distribution for two flat adherend surfaces was also obtained using a further modification of the mesh;comparisons of the two stresses appear together in Figure 27. Although the mesh consisted of only one element in the radial direction, a constant state of shear stress may be obtainable in the cone and plate geometry without resulting to the dimensions associated with the napkin ring test. These preliminary results justify further analysis of a modified cone-and-plate shear test specimen.

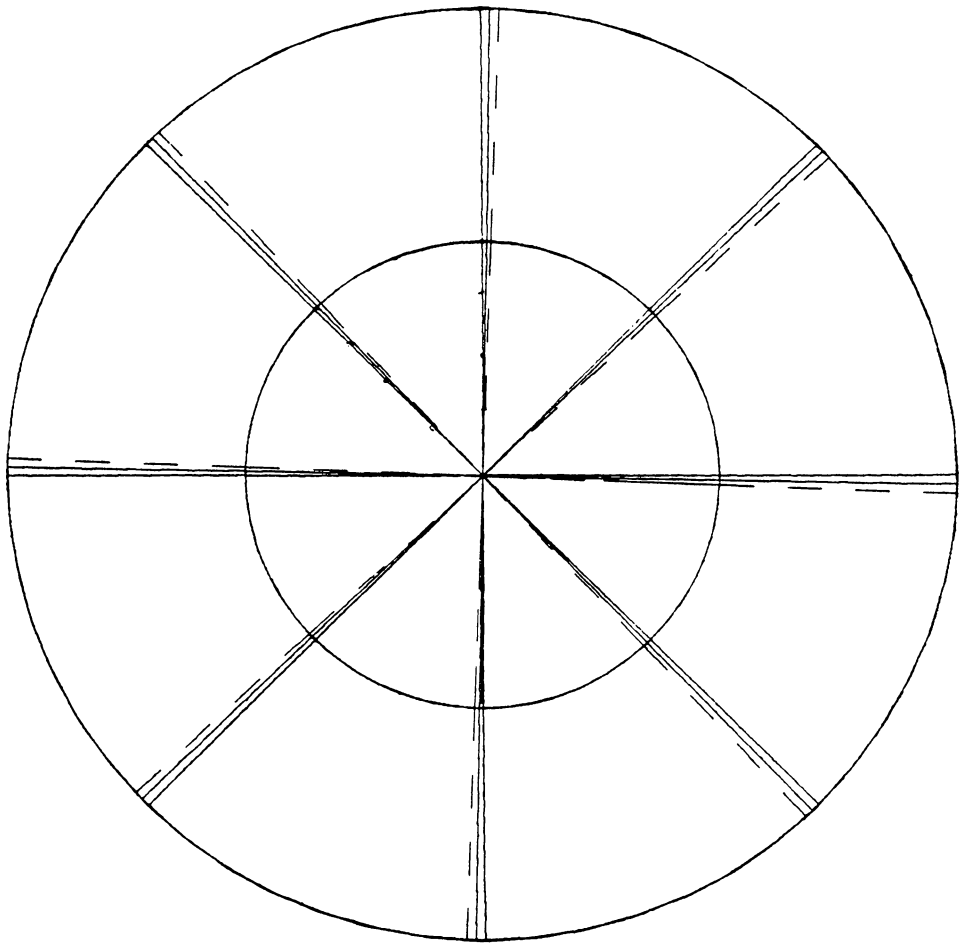

Figure 23. Top view of deformed and original mesh of cone-and-plate specimen.

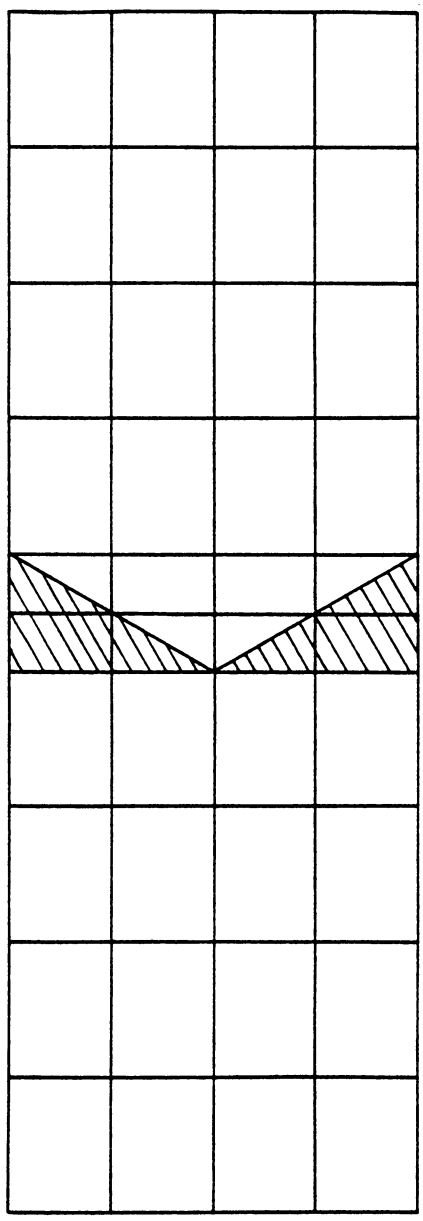

Figure 24. Finite element mesh on a plane parallel to the central axis (y = 0).

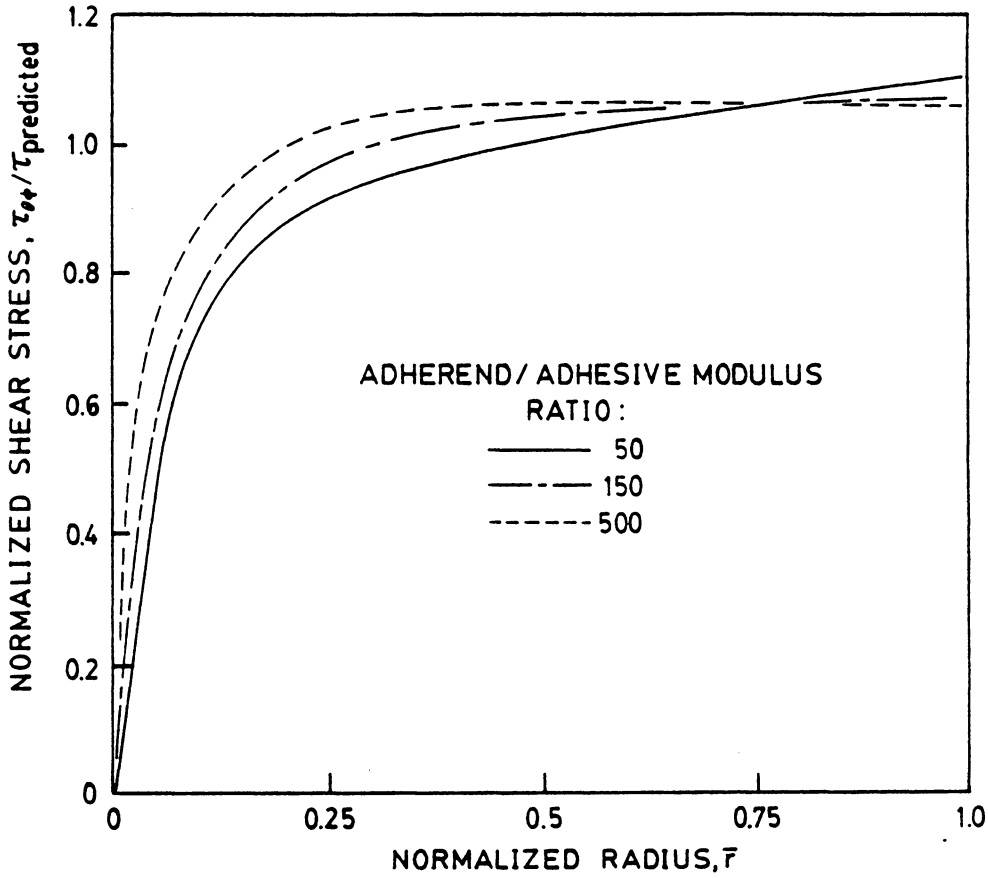

Figure 25. Shear stress distribution in cone-and-plate adhesive specimen: normalized shear stress with respect to the predicted value for several adherend adhesive modulus ratios.

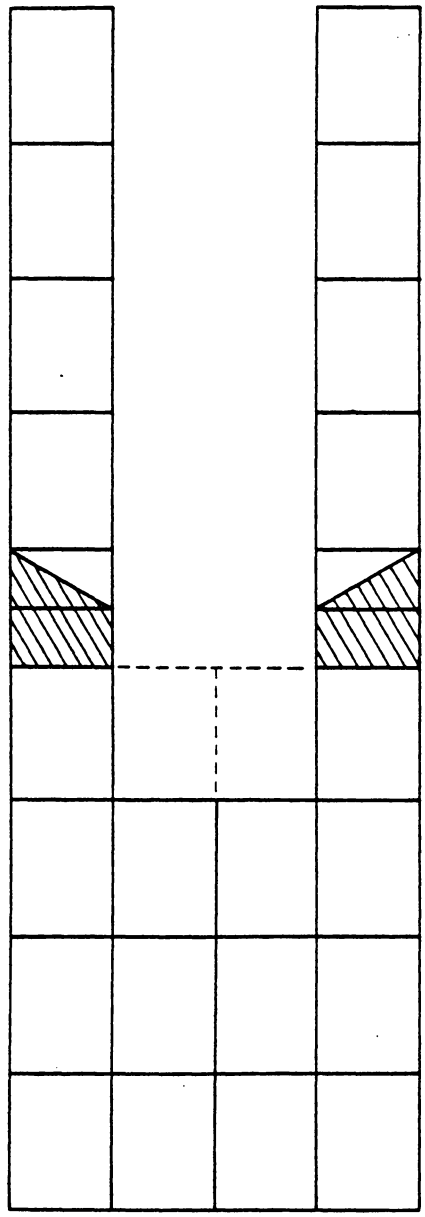

Figure 26. Modified finite element mesh of cone-and-plate with central elements removed: two hole depths.

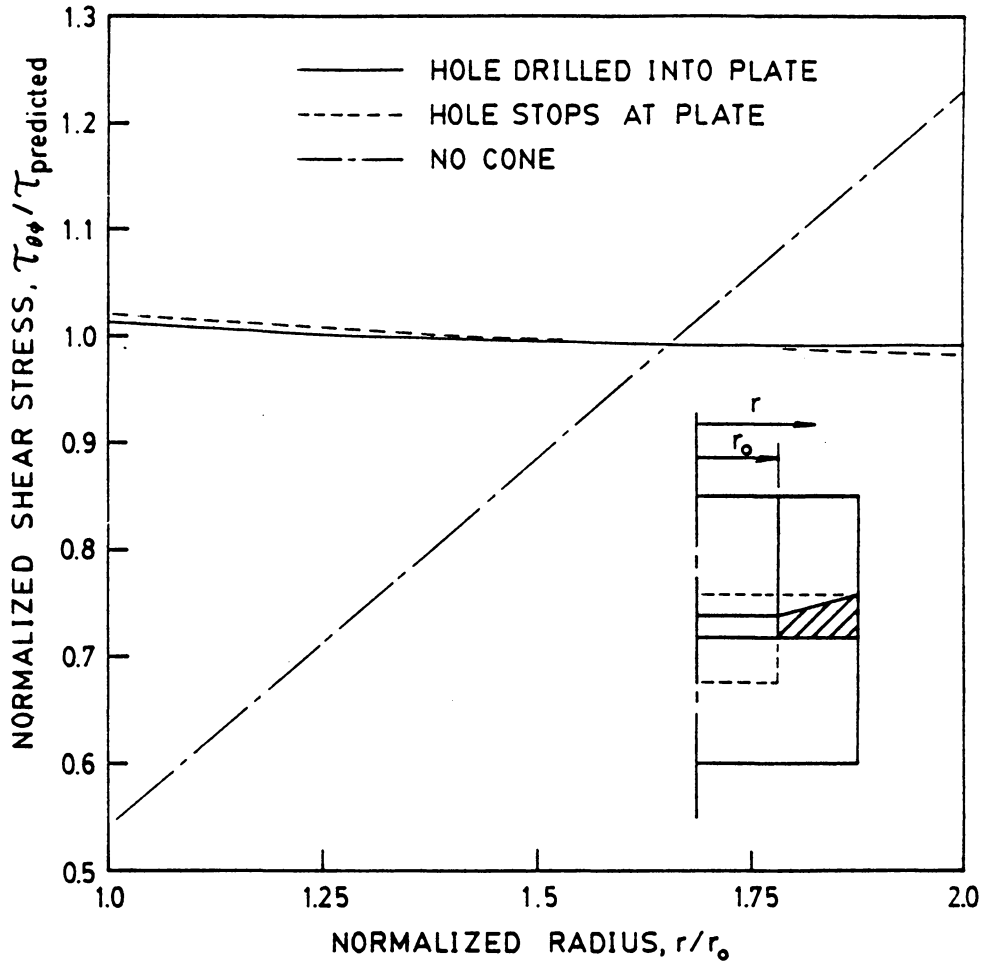

Figure 27. Shear stress distribution in modified cone-and-plate adhesive specimen: stress normalized to predicted value with comparison to napkin ring type test.

Experimental results

Tests were conducted to check the feasibilty of the cone-and-plate specimen in determining accurate adhesive properties. The tests consisted of applying a torsional load to the bonded specimen to adhesive failure. Although the finite element results disputed the predicted constant shear stress state in the adhesive, the test results demostrated several of the advantages of the cone and plate geometry.

As with the thick adherend lap joints, cone-and-plate specimens were fabricated using 3M Company's AF 163-2U adhesive. Half inch diameter aluminum 2024 - T4 adherends were machined to cone angles of 1-5 degrees. The adherends were surface treated according to BAC-5555, as noted previously, followed by the application and cure of 3M Company's EC-3960 primer sealer. Circular disks of the film adhesive were cut using a brass cork cutter.

The bonding process took place in a split mold consisting of two identical plates of aluminum with parallel circular grooves (Figure 28). The circular grooves held the adherends in place during adhesive cure; furthermore, the grooves reduced axial misalignment of the adherends. Each mold half was coated thoroughly with a mold release agent. Constant pressure was applied to both ends of the adherends and the mold plates with bolts during the one hour cure at 121 $^{\circ}C$. The molding procedure resulted in good axial alignment of the specimen. Subsequent visual inspection of the failed adhesive revealed little or no void content.

Torsional tests were conducted on the specimens in an Instron load frame with torsional capability. The relative angular twist in the adherends was measured using two methods. The first method consisted of two matched gears, one being an anti-backlash gear, an RVDT (rotational variable differential transformer), and brackets to mount the gears and RVDT on the specimen as depicted in Figure 29. The alternate measurement apparatus consisted of an MTS axial strain extensometer mounted on a special fixture similar to the extensometer fixture used by Dolev and Ishai [8]. The

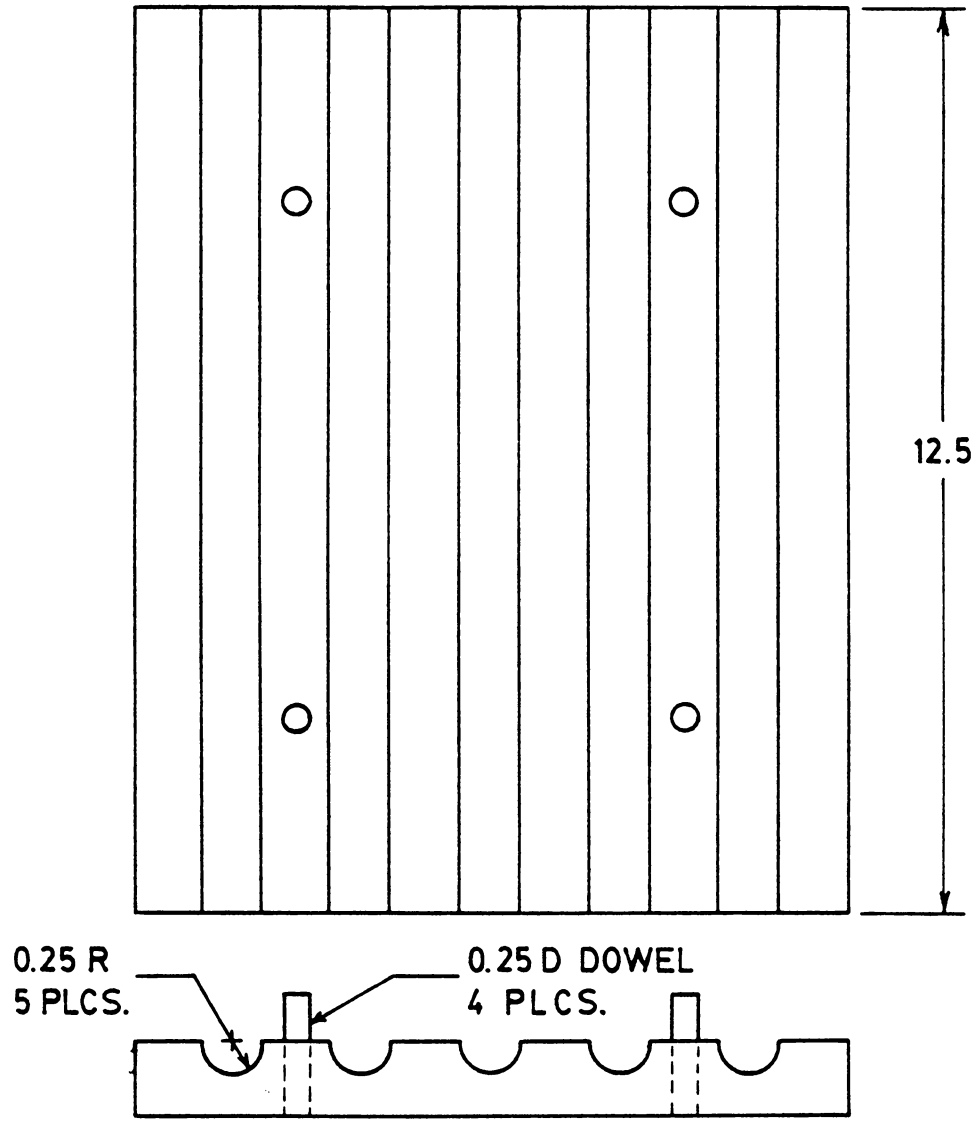

Figure 28. Split mold half showing internal detail of the parallel grooves.

gear and RVDT system permits direct measurement of the relative angular displacement whereas the extensometer reading must be converted into an angular measure using simple trigonometry. Simultaneous use of both measurement devices on a single specimen compared favorably. However, it is important to note that the gear and RVDT system is capable of measuring angular displacement to failure.

For the tests, torque versus RVDT or extensometer output was recorded on a X-Y plotter. After correcting for the angular twist of the aluminum adherends with the strength of materials solution for the torsion of a circular rod, the adhesive shear strain was calculated using Eq. 16; the shear stress was calculated using eq. 15. Figure 30 represents a typical stress-strain curve. The measured shear stress-strain curve is compared to the shear modulus calculated from tensile test results of a neat resin sample of the same adhesive.

The test results demonstrated two important features of adhesive shear testing. First, properly prepared specimens in terms of surface treatment and cure conditions result in cohesive and not adhesive failure. Secondly, multiple tests of the same cone angle specimen result in large scatter of the measured data. The raw data curves of the torque versus RVDT ouput for a 3 ° cone angle appear together in Figure 31. Note that the apparent adhesive modulus for similar specimens has a great deal of experimental variance.

One possible explanation for data scatter is the misalignment of the torsional axis of the Instron machine. The adherends used were six inches long; hence, small misalignment errors would create substantial extraneous stresses in the relatively soft adhesive. To eliminate the possibility of misalignment problems, a special torsional load device was constructed. The apparatus is shown in Figure 32. The device was designed to fit in a conventional axial load frame and produce a state of pure torsion in a cylindrical test specimen. The device consists of four part groups: (1) the upper and lower control arms, (2) four spring steel pivot arms, (3) two torque arms, and (4) two specimen clamps. The upper and lower control arms attach directly to the load frame (MTS) via two threaded steel rods. The control arms are rigid and actuator displacement of the lower control arm

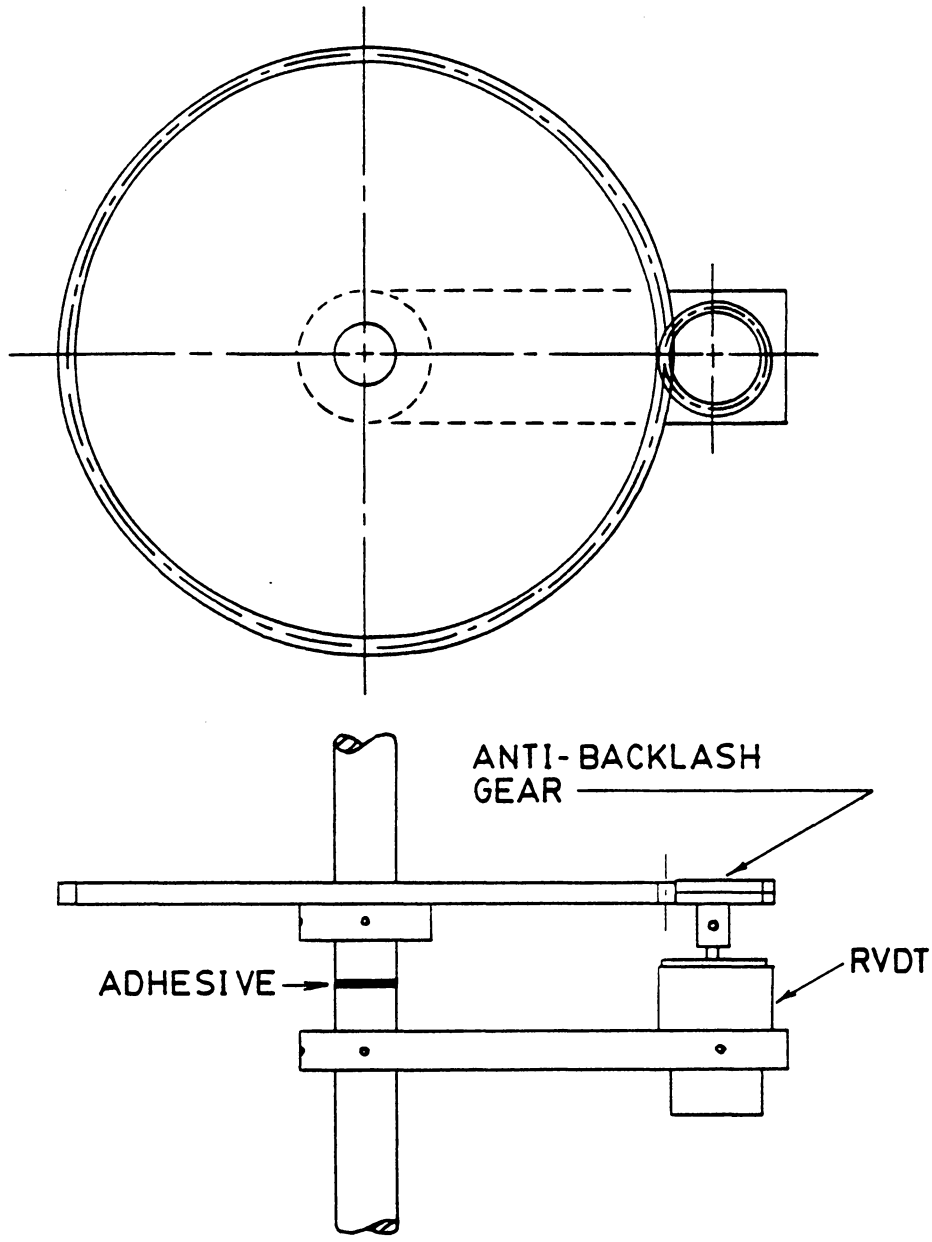

Figure 29. RVDT fixture and associated gearing used to measure relative twist.

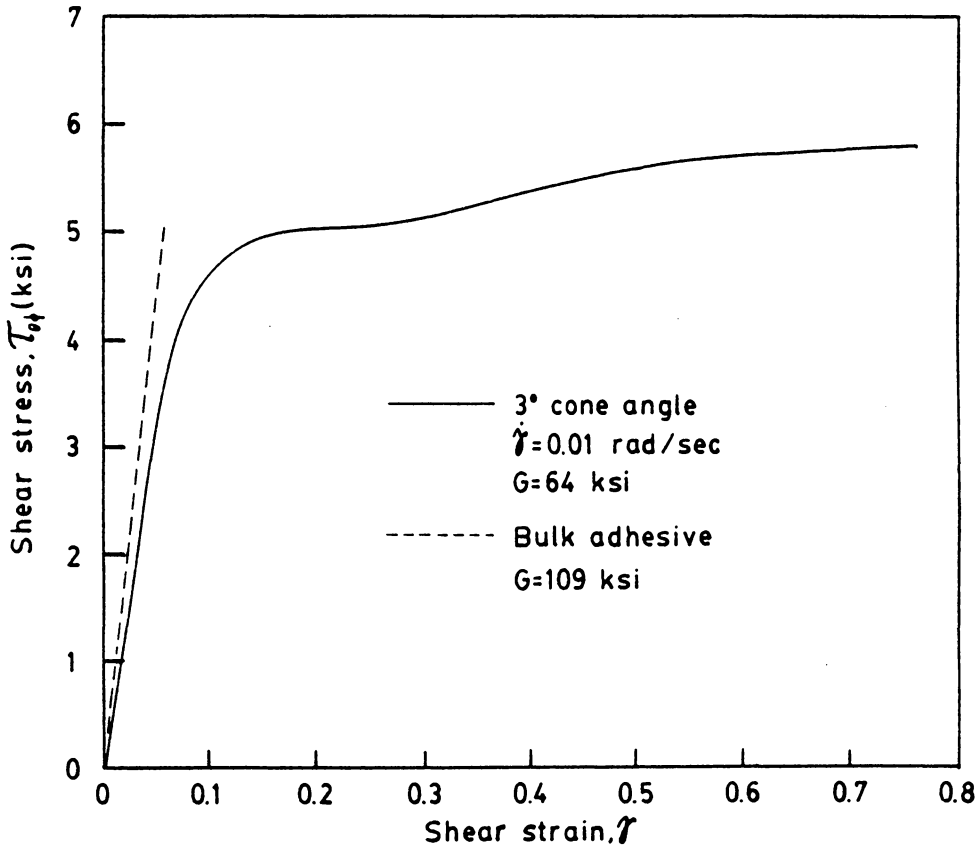

Figure 30. Typical shear stress-strain curve for AF 163-2U in cone-and-plate specimen: shear behavior to failure compared to bulk modulus.

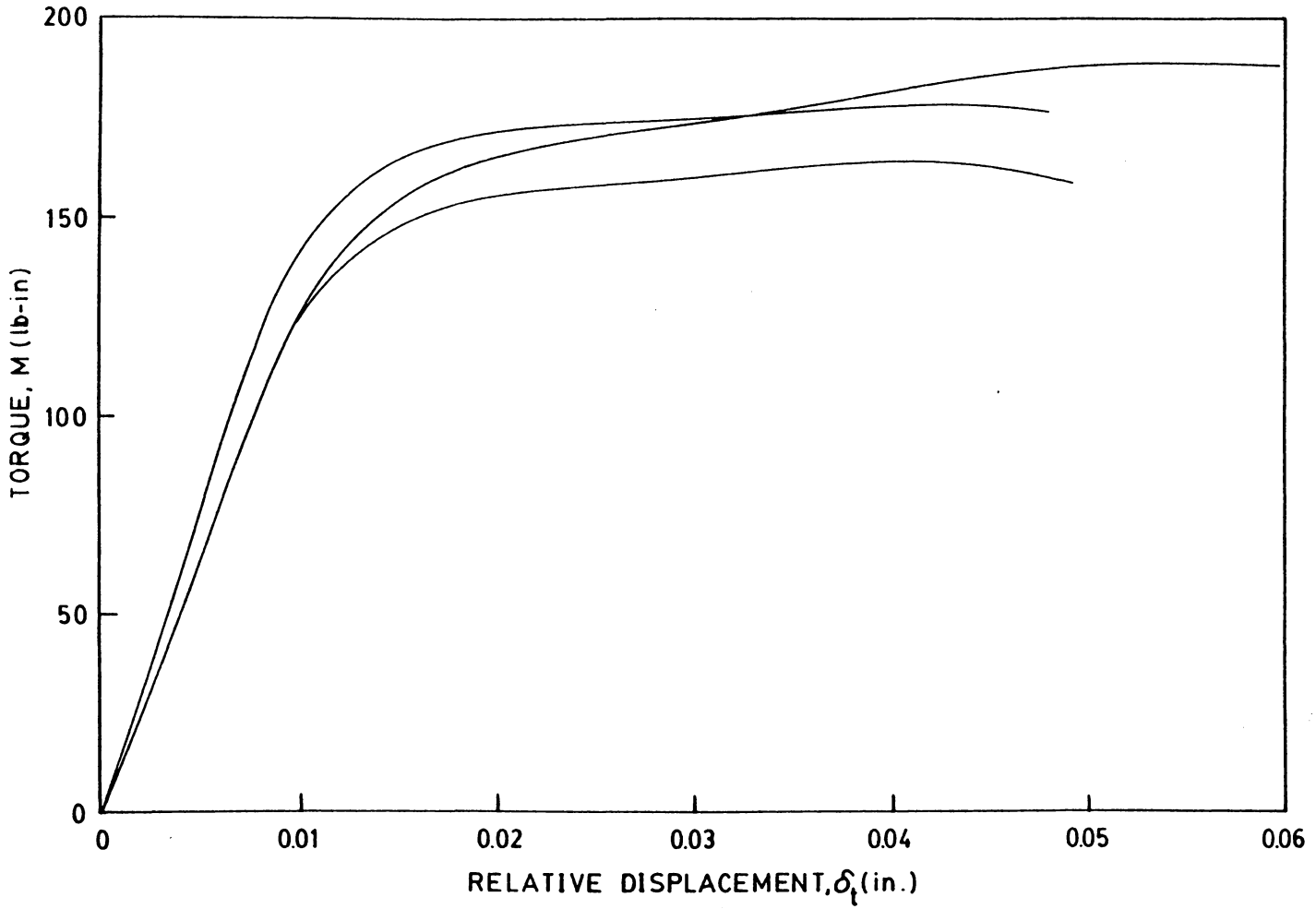

Figure 31. Torque versus relative deformation for several cone-and-plate specimens: 3° cone angle specimens.

produces a torsional load on the adhesive specimen. When the lower control arm translates, the four steel spring arms flex and allow the torque arms to rotate about the torsional axis. Each torque arm has a provision for a specimen clamp. The specimen clamp consists of two steel blocks with an identical circular channel in each block half. The clamping surface of each block half was grit blasted to eliminate specimen slippage. Clamping pressure was applied to the adhesive specimen using four bolts which force the clamp halves together.

The design permits torsional loads up to 500 lb-in without specimen slippage in the clamps. In the design of this type of loading apparatus for adhesive testing there are two important considerations. First, alignment of the specimen along the torsional axis is important to alleviate extraneous loads. Alignment of the fixture as an assembly is also critical in producing only a torsional load. Secondly, the steel spring arms impose a limit on the relative twist allowed between torque arms depending on the length of the steel spring arms. The amount of relative twist available in the loading device depends on the adherend length of the specimen.

Preliminary tests of the cone and plate specimen in the torsional loading apparatus indicated the need for further improvements of the device. Specimens tested under static loading often failed at low shear strains as measured by the extensometer fixture arrangement. With the parts of the load fixture carefully aligned, curves similar to the ones shown in Fig. 31 were obtained. Thus, the data scatter in the torque versus relative displacement measurement was not necessarily due to alignment problems in either the Instron or the special load apparatus.

Arcan adhesive shear specimen

The lack of a constant state of shear stress in the cone-and-plate geometry necessitated study of another adhesive test geometry for shear characterization. The Arcan, or stiff adherend, adhesive

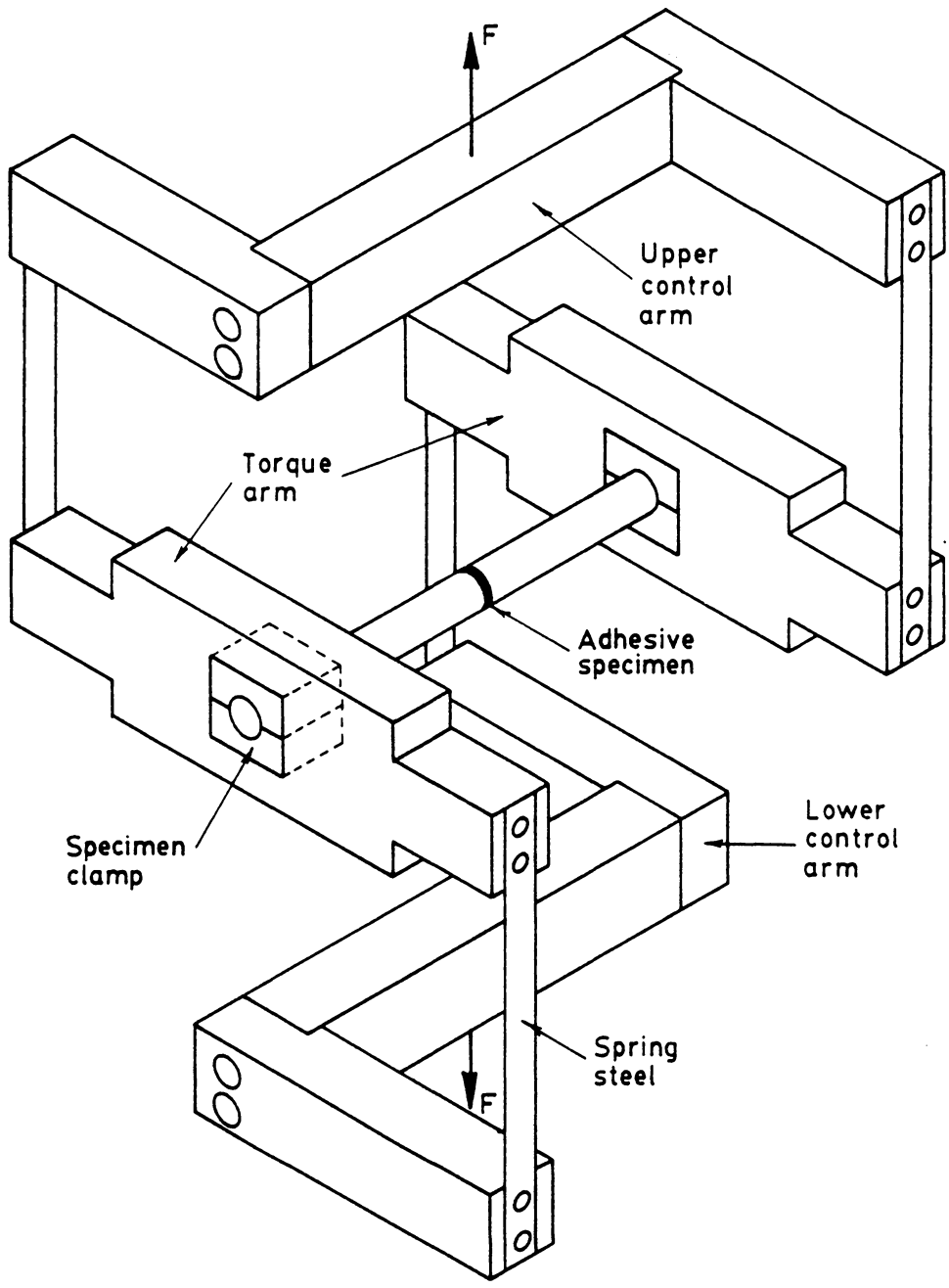

Figure 32. Torsional load apparatus designed to produce a pure moment on a cylindrical specimen.

test was developed originally by Arcan [28] as a mode II fracture specimen. Recently, Arcan and Wietsman [29] presented a modified version of the fracture test fixture and specimen as an adhesive shear test. The present design of the specimen and load frame is extremely versatile in both adhesive shear property measurements and mixed mode fracture studies of adhesive bonds. It is interesting to note that some controversy surrounds the parallel development of the Arcan and Isopescu specimens [30].

Arcan and Weitsman contend that the stiff adherend specimen produces a nearly uniform state of shear stress in the adhesive layer. They performed linear elastic finite element stress analysis of the specimen [29]. Their results indicate that a constant shear stress state free of tensile stresses exists at a small distance from the free edge of the specimen. Furthermore, a shear stress-strain curve of a 3M Company adhesive was reported.

Finite element analysis

A similar finite element analysis was performed to verify the results presented by Arcan and Weitsman. The stiff adherend specimen and load frame was modelled as shown in Figure 33 using the finite element program VISTA. The model consisted of 400 eight node quadrilateral isoparametric elements. The adhesive layer contained five elements across the thickness and twenty elements along the bondline length; mesh refinement at the adges was incorporated as shown in the enlarged region of the mesh in Figure 34.

The linear elastic finite element results confirmed that a uniform state of shear stress does exist in the adhesive away from the edges. Figure 35 shows the three stress components along the centerline of the adhesive layer. Note that although tensile stresses are present at the edge region, the magnitude of these stresses are insignificant compared to the dominant shear stress component. Thus, the stiff adherend specimen produces the most uniform shear stress state of any specimen to date.

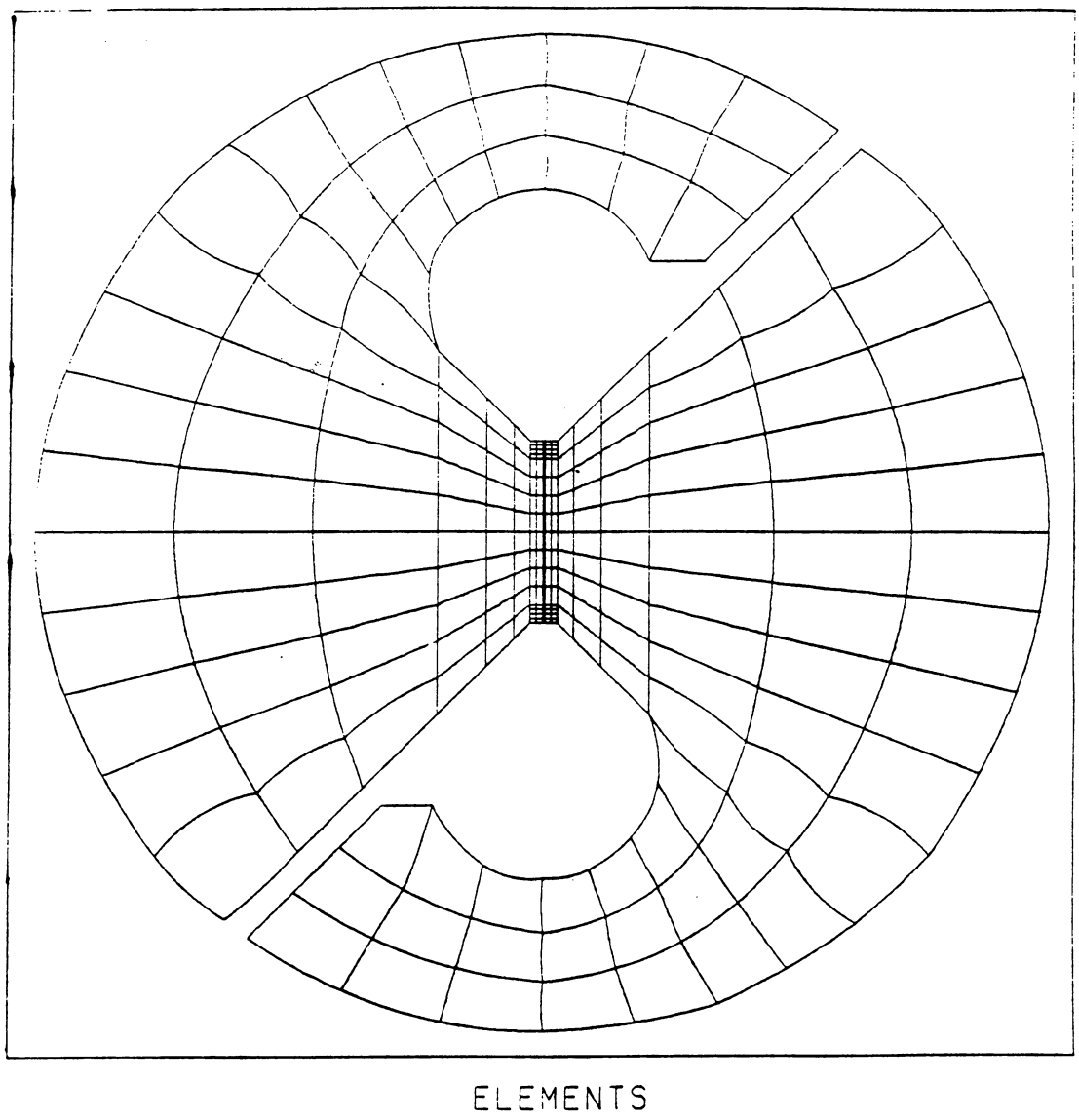

Figure 33. Finite element mesh of Arcan specimen and load fixture.

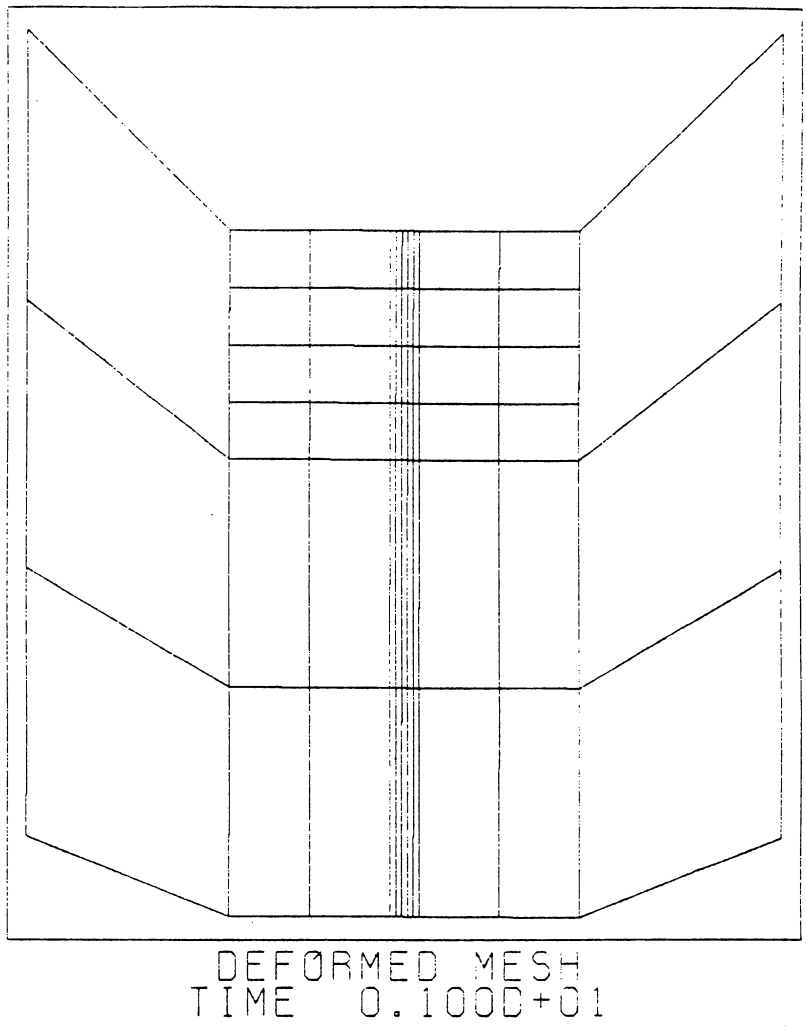

Figure 34. Enlarged view of the mesh showing refinement at adhesive ends in Arcan specimen.

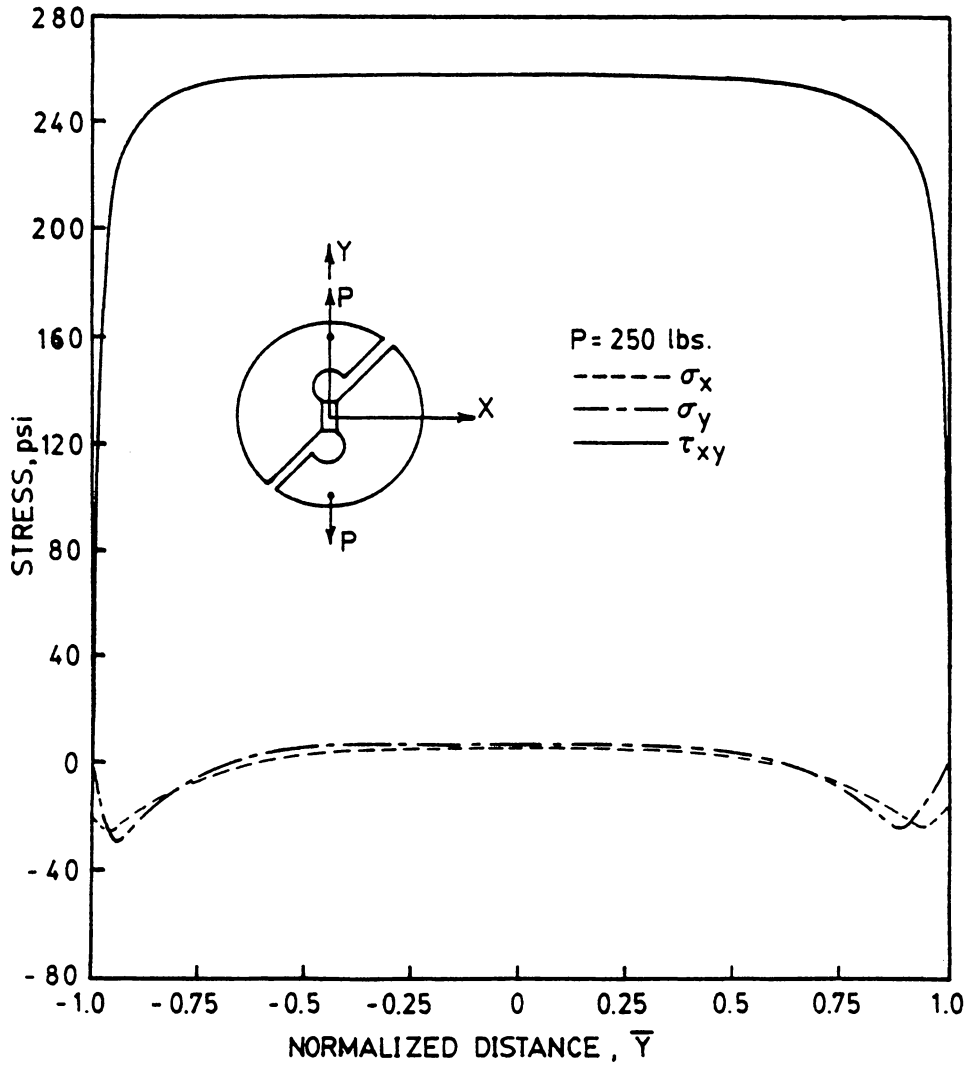

Figure 35. Adhesive centerline stress distribution in the Arcan specimen.

Further finite element anaylsis was conducted to investigate the relative magnitude of residual thermal stresses. Because the specimen (adherend and adhesive) is symmetric about three mutually perpendicular planes, it was only necessary to model one quarter of the specimen as shown in Figure 36. The properties of the adhesive and adherend were the same as those used previously for the residual stress analysis of the cone-and-plate specimen. Under the assumption of linear elastic behavior, the adhesive has a state of stress shown in Figure 37. There are no thermal shear stresses present in the adhesive due to the symmetry; however, the magnitude of the residual tensile stresses are higher than the tensile stresses due to mechanical loading. This is due entirely to the size of the adherends compared to the thin adhesive layer. For an isotropic material, no coupling exists between shear and dilatational behavior; thus, the presence of the tensile residual stresses should not influence elastic shear behavior of the adhesive.

Experimental results

Static tests were conducted using the Arcan specimen and load frame in an MTS load frame. The machine drawings of the device and specimen mold appear in Figures 38-41. The specimens and load frame were machined from aluminum 2024-T4 while the mold was constructed of mild steel. Five different adhesive layer thicknesses were made in matched pairs of 0.003, 0.007, 0.011, 0.015, and 0.019 inches.

The specimens were again fabricated using AF 163-2U. The bonding surfaces of the adherends were surface treated and primed as detailed earlier for both the thick adherend and cone and plate specimens. Each mold consisted of two mold plates and four 3/8 inch dowel pins. With the adhesive in place between the adherends, the specimen lay flat between the two parallel mold plates. The four dowel pins maintained alignment of the adherends during adhesive cure. Bolt pressure kept the mold plates firmly against the adherend surfaces during the one hour cure in a convection oven. Because the aluminum adherends have a higher coefficient of thermal expansion than the

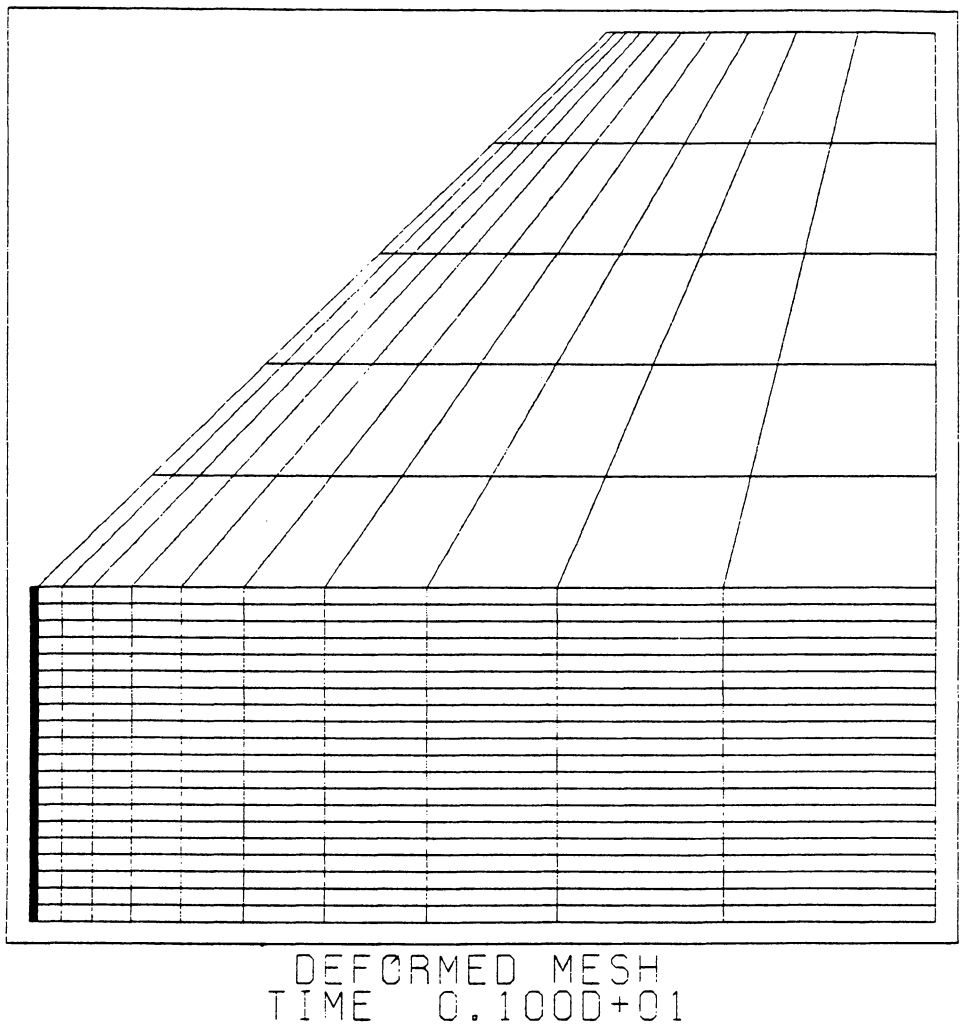

Figure 36. Quarter model of Arcan specimen used to find residual thermal stress state.

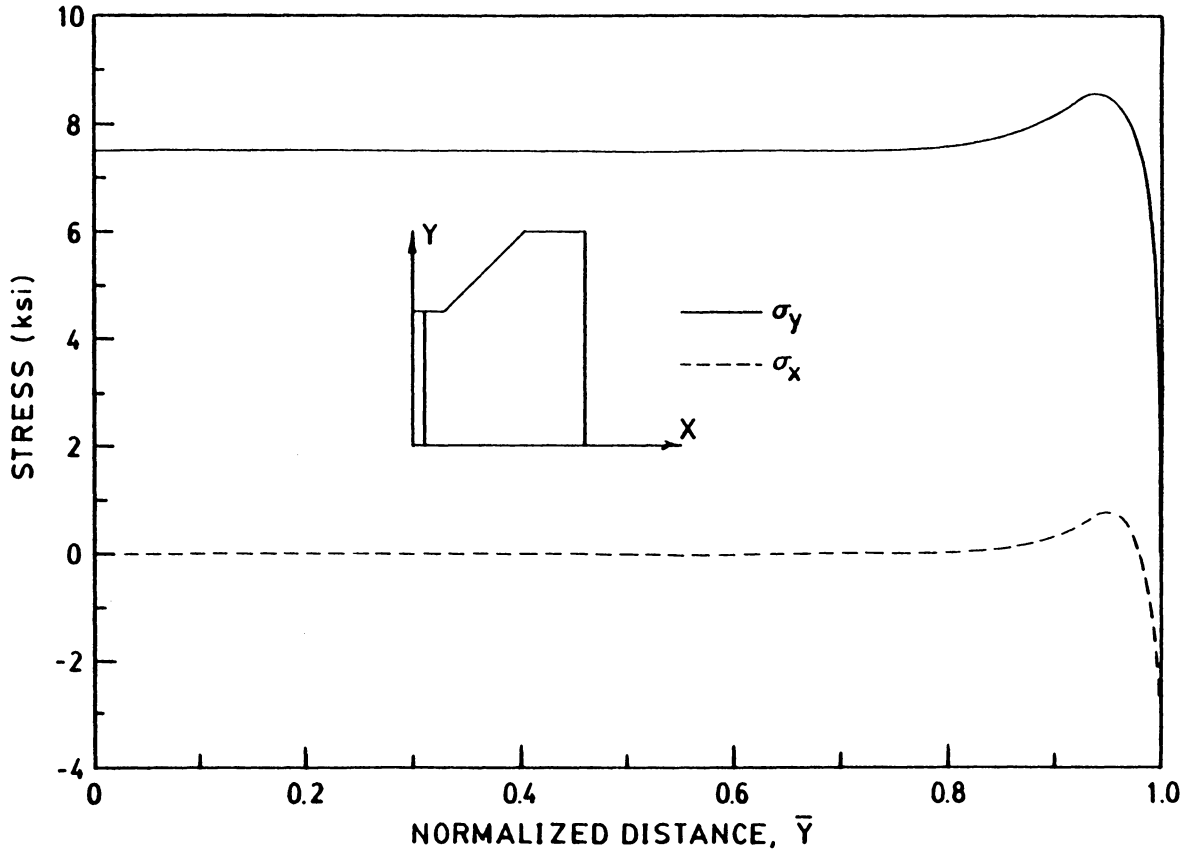

Figure 37. Residual thermal stress state in Arcan specimen along adhesive centerline.

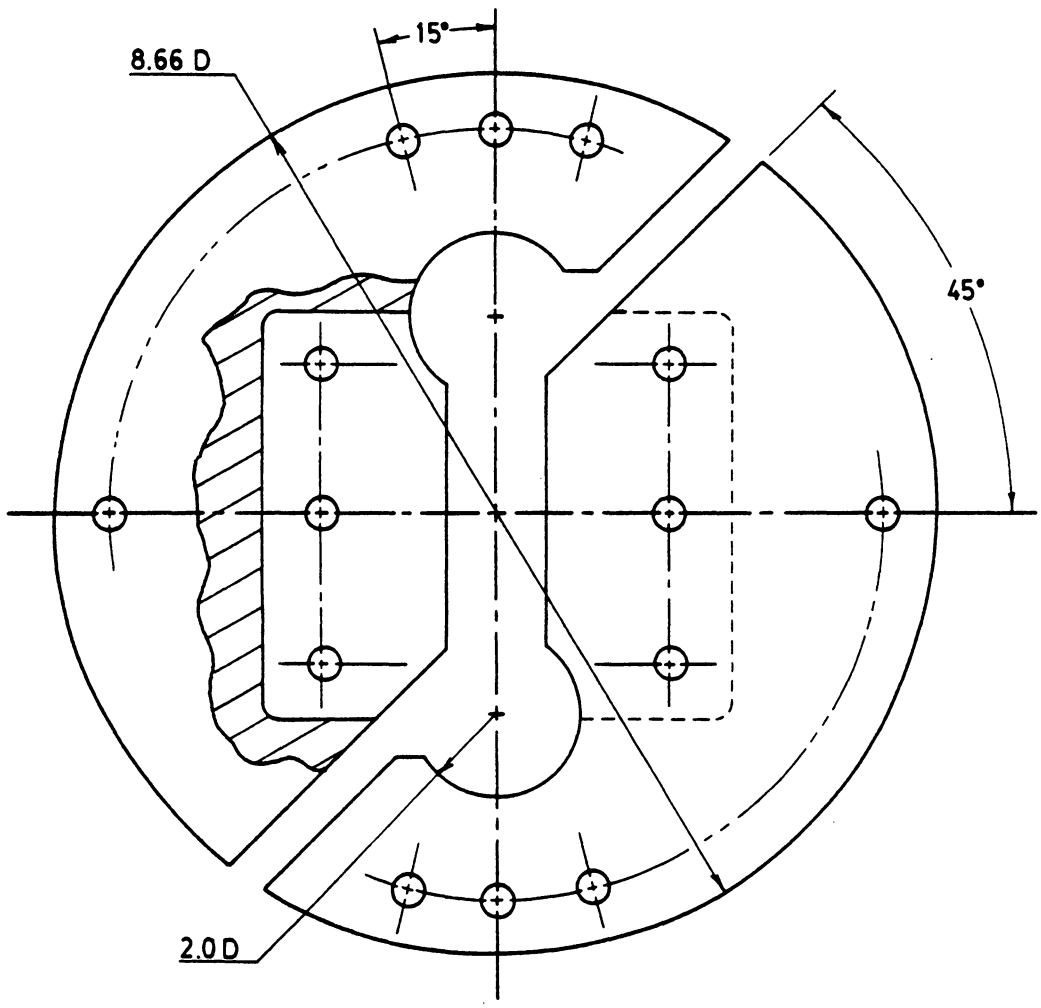

Figure 38. Front view of the load fixture used to grip Arcan specimen during testing.

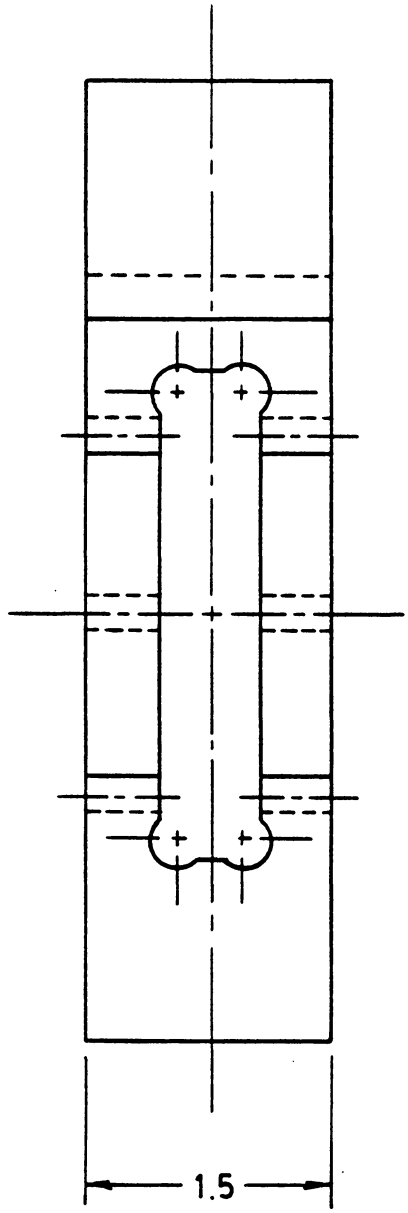

Figure 39. Side view of Arcan load fixture: note specimen groove.

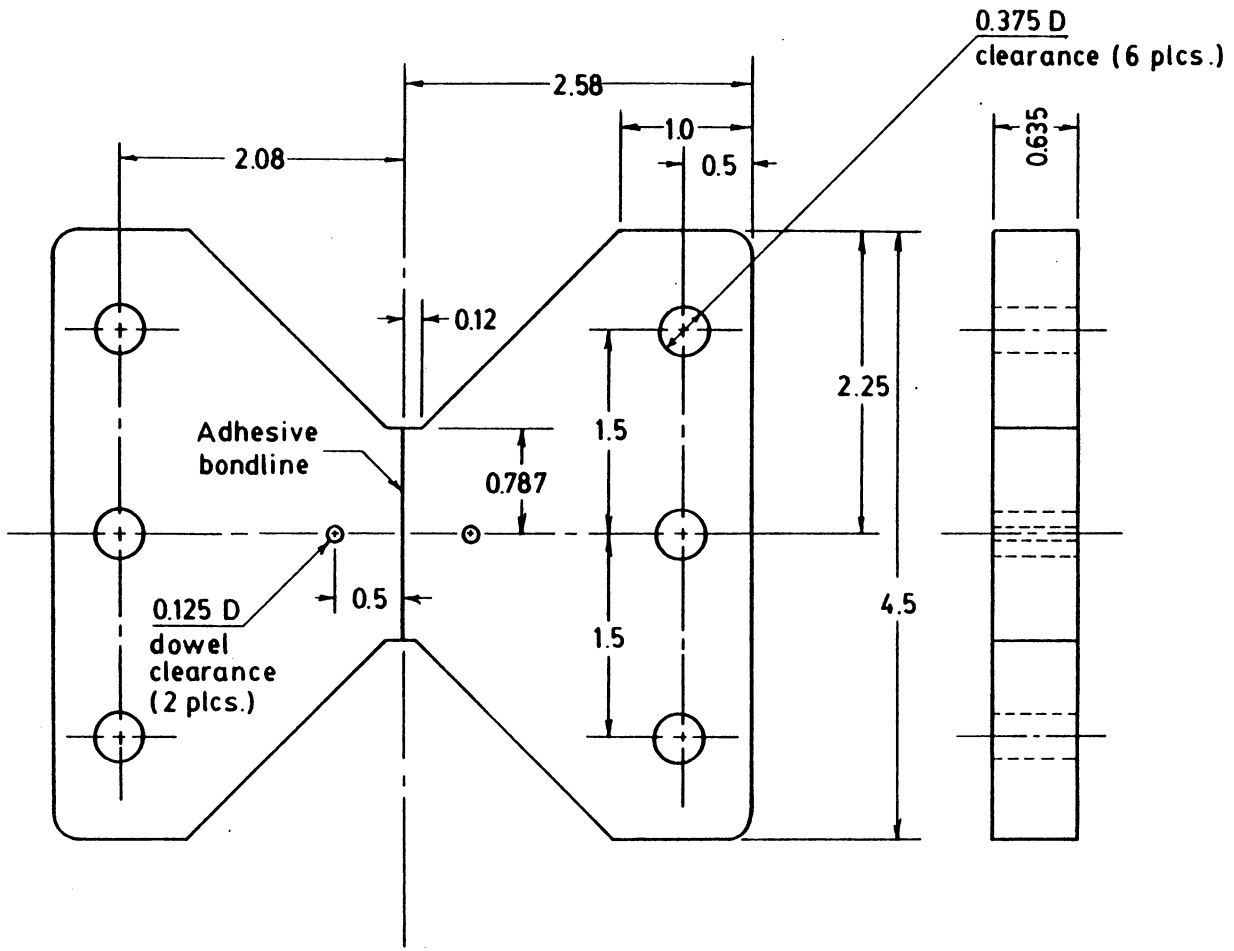

Figure 40. Arcan specimen with provisions for extensometer fixture: dowel clearances.

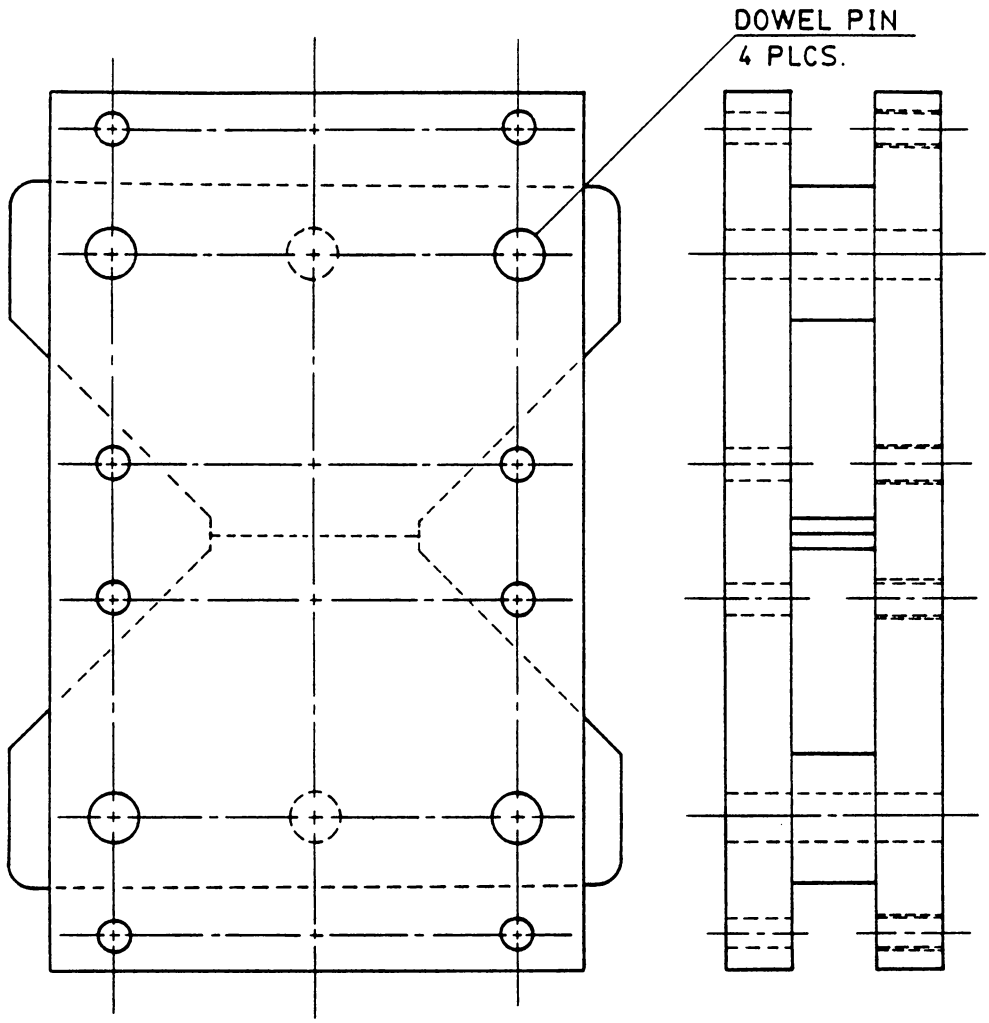

Figure 41. Arcan specimen held in place during cure by the two mold half plates.

steel mold plates, the mold arrangement creates pressure in the curing adhesive due to the mechanical constraint imposed by the stiffer steel plates and dowel pins.

The specimens were tested in a MTS load frame under load control. The deformation was measured in the adherends using a fixture attached to the adherends via dowel pins as shown in Figure 42. Load versus extensometer output was recorded on an X-Y plotter. The resulting curves showed an abberation in the extensometer signal. Initially, the extensometer signal went negative until at some low value of load the signal reversed and went positive as expected. The problem was due to bending deformations in the adherends. Figure 43 shows that a bending moment exists in the adherends at any slice location due to eccenticity of the applied load. These bending moments go to zero at the adhesive centerline.

The presence of the measurement anomaly required compensation of the adherend deflection signal. A calibration specimen was machined according to the dimensions of the actual bonded specimen (Fig. 40). Figure 44 shows the deformation in the aluminum adherend due to the bending moment as a function of load. With this calibration curve, the static testing of the adhesive specimens was resumed.

The shear moduli for the various adhesive bondline thicknesses were determined. The adhesive specimens were loaded to 2000 lb in load control at several load rates. For the specimen geometry, the adhesive overlap area is exactly one square inch; hence, the shear stress is exactly the applied load in psi. For each of the adhesive specimens tested, the total deformation was obtained at the maximum load of 2000 lbs. Using the calibration curve, the adhesive deformation, δ_a ,was calculated by subtracting the calibration curve value from the total measured deformation. The shear strain was computed using Eq. 4. Figure 45 shows the shear moduli measured for the various bondline thicknesses. As indicated in the figure, a great deal of scatter is present in the data. Despite the large scatter, the data indicates that the adhesive shear modulus increases with increasing bondline thickness which agrees with the results of Knollman and Hartog [11].

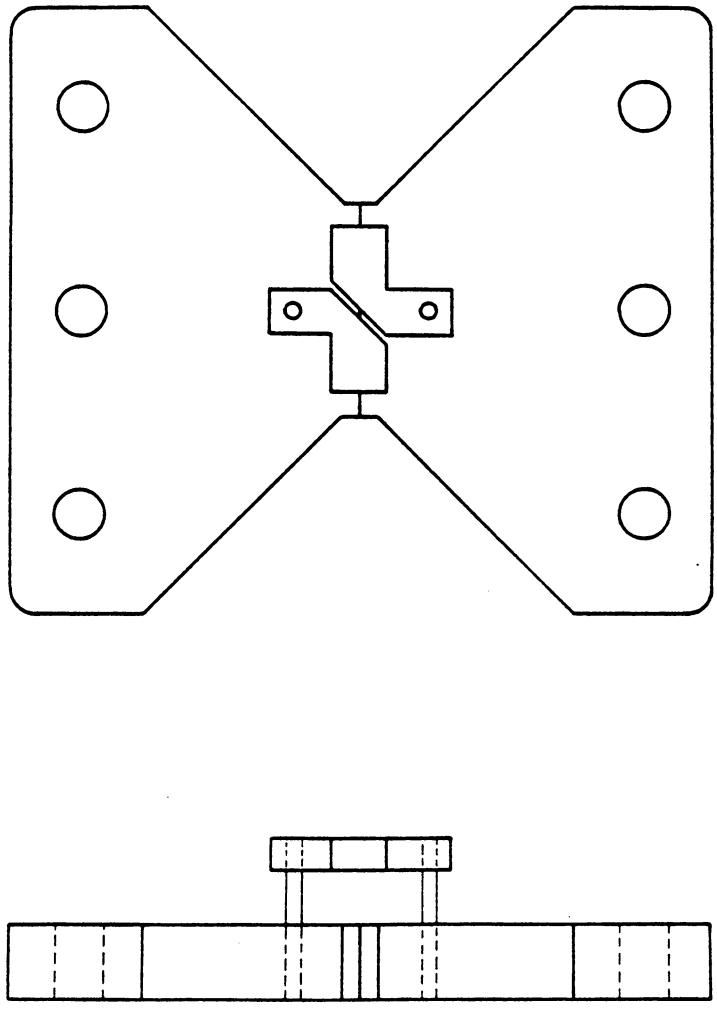

Figure 42. Extensometer fixture mounted on Arcan specimen via dowel pins.

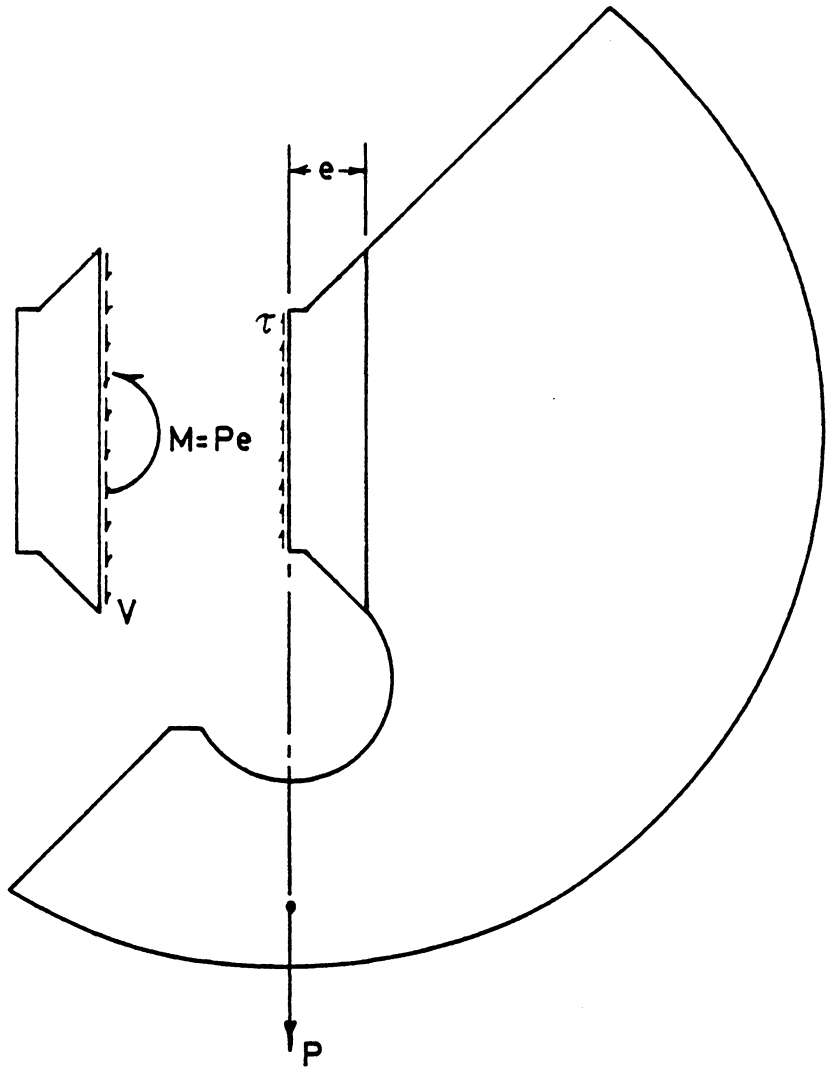

Figure 43. Bending moment produced in Arcan specimen due to load eccentricity.

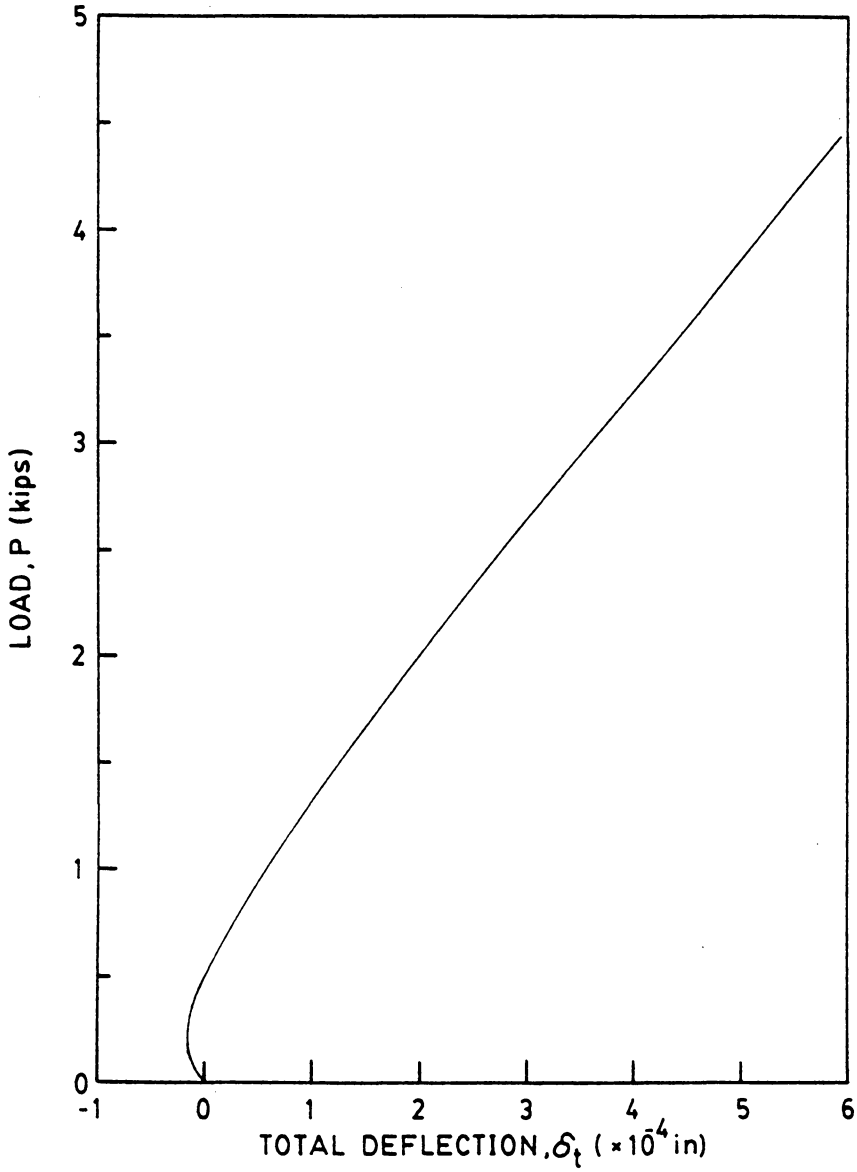

Figure 44. Calibration curve of the bending deflection in dummy Arcan specimen: deflection as a function of the applied load.

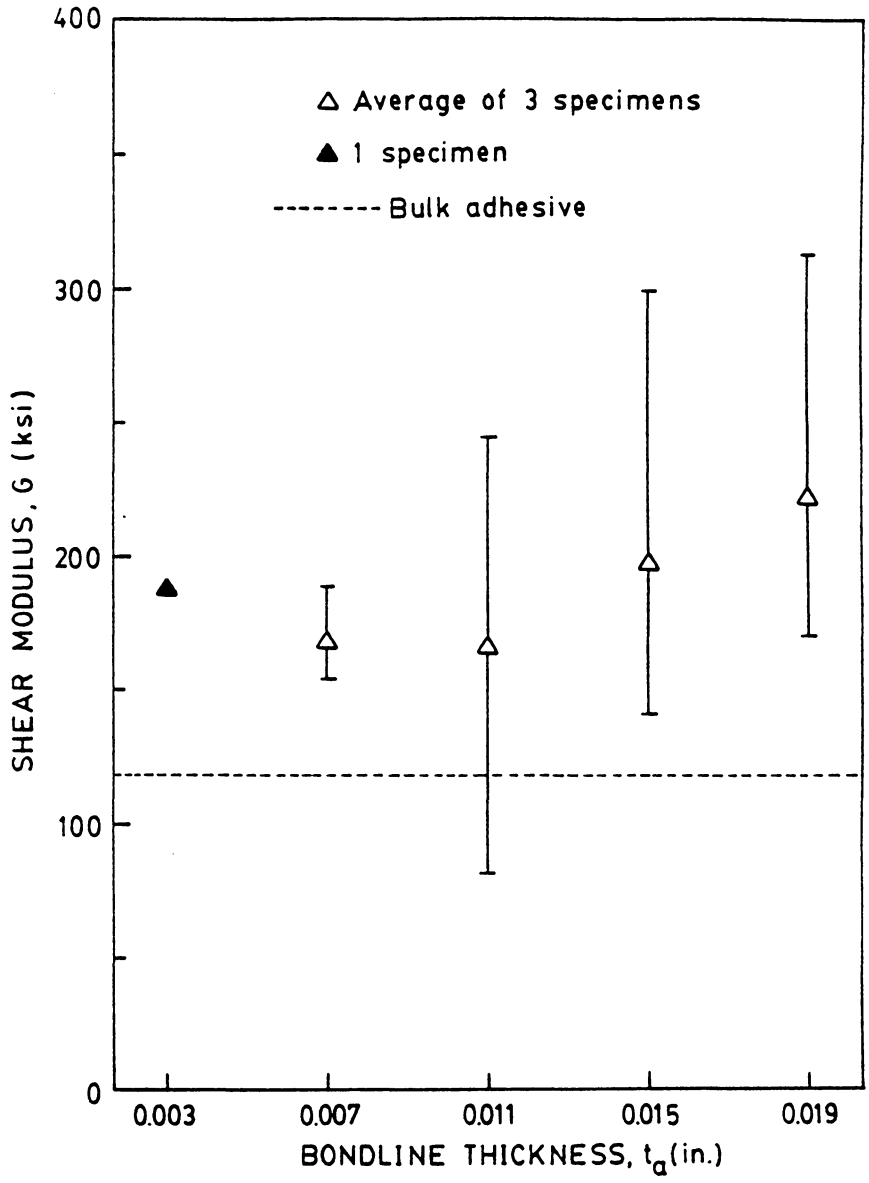

Figure 45. Measured elastic shear moduli as a function of the bondline thickness: comparison to the bulk shear modulus.

Several of the specimens were loaded under stroke control to failure to investigate the effect of bondline thickness on overall stress-strain behavior. Figure 46 shows the comparative behavior of several representative bondline thicknesses. As the bondline thickness increases, the strain to failure increases, which disagrees with the conclusions of Stringer [10].

Error analysis

The amount of scatter in the shear modulus values warranted analysis of the measurement uncertainty. Uncertainty propagation due to systematic errors was determined in the least squares sense. By definition, the shear modulus is

$$G = \frac{\tau}{\gamma} \qquad [16]$$

Using the small shear strain definition, the shear modulus becomes

$$G = \frac{\tau t_a}{\delta_a} \qquad [17]$$

The uncertainty in the shear modulus value becomes a function of the uncertainties of the measured load, deflection, and bondline thickness; hence,

$$\frac{u_G}{G} = \sqrt{(\frac{u_\tau}{\tau})^2 + (\frac{u_{t_a}}{t_a})^2 + (\frac{u_{\delta_a}}{\delta_a})^2} \qquad [18]$$

For the load and deflection measurements obtained from MTS components , it is reasonable to assume an uncertainty of ± 2% in these signals. The adhesive bondline thickness, t_a , is subject to tolerance errors introduced by the machining process. For each of the bondline thicknesses, a tolerance of 0.0005 in is reasonable. Thus, the error in the bondline thickness will be greater at smaller bondline thicknesses.

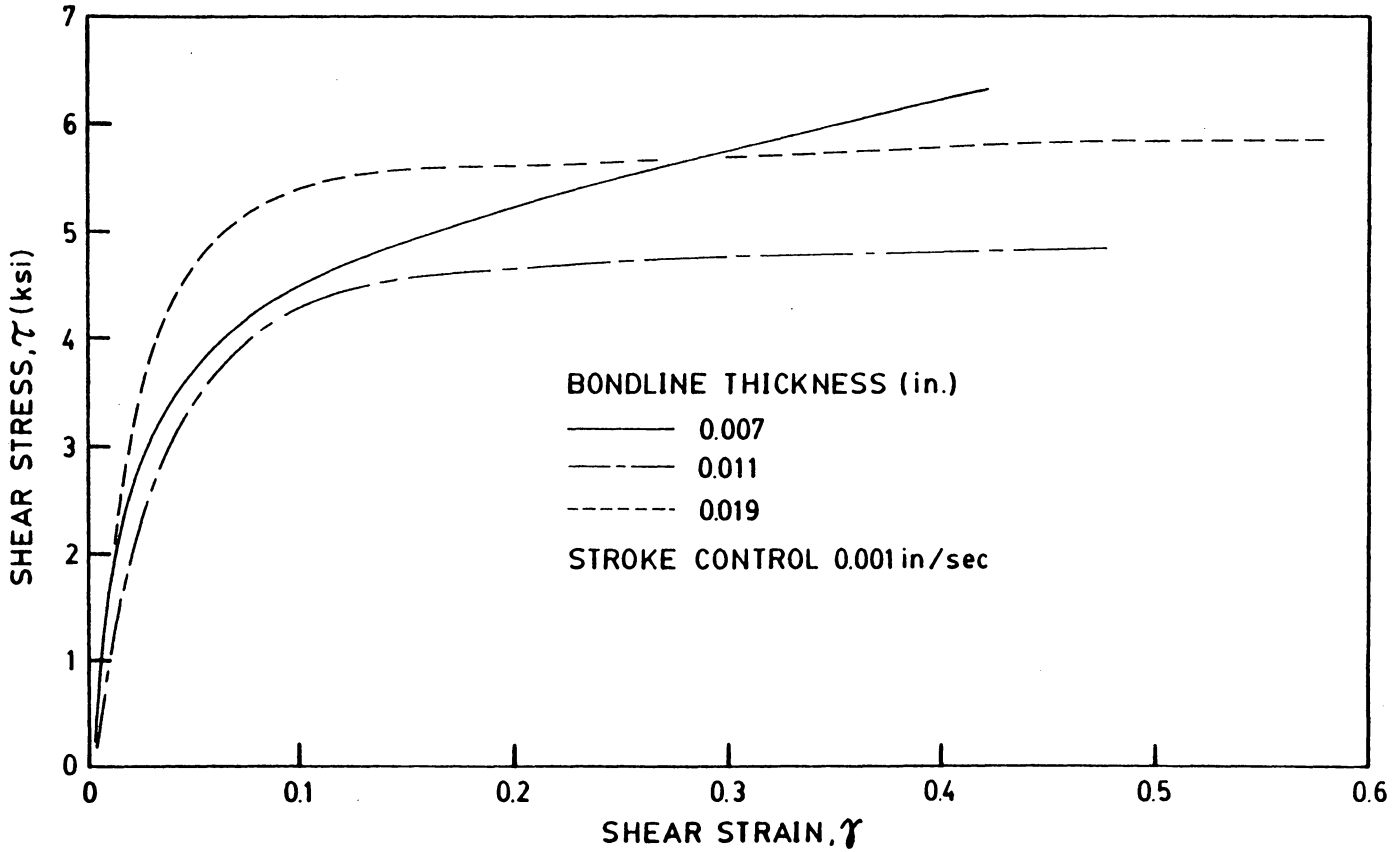

Figure 46. Representative shear stress-strain curves for several bondline thickness.

Using the measurement uncertainties and the tolerance values, the uncertainty in the measured shear modulus was determined using Eq. 18. Table 4 lists the uncertainty as a function of the specimen bondline thickness. According to the table, a substantial uncertainty exists in the measured shear modulus values at 0.003 and 0.007 in. adhesive bondline thicknesses. From the experimental data, the 0.007 in. bondline specimen had less scatter than large bondline specimens. In fact, the data scatter band for the larger bondlines (0.011 - 0.019 inches) was much larger than the uncertainty band. This suggests that systematic errors play no role in the experimental scatter associated with the measurement of the adhesive shear modulus.

Discussion

The Arcan, or stiff adherend specimen, provides the most desirable shear stress state in the test adhesive of any test geometry studied here. In addition, an important design feature of the load fixture is its ability to produce mixed stress states in the adhesive by varying the applied load axis. Furthermore, the specimen offers the added versatility of fracture mechanics studies of adhesively bonded joints.

The extensive experimental work reported in this chapter has confirmed the usefulness of the Arcan specimen in adhesive shear characterizion. Adhesive deformation measurement problems due to adherend bending were easily accounted for using a dummy specimen. Future work with the specimen might be directed at improving the deformation measurement technique. An error analysis has revealed that the large scatter in the measured shear modulus is not attributable to systematic measurement errors.

Table 4. Shear modulus uncertainty as a function of the bondline thickness.

$t_a(in)$	$\frac{u_G}{G}$
0.003	16.9
0.007	8.1
0.011	5.3
0.015	4.3
0.019	3.8

IV

Viscoelastic stress analysis

In the previous two Chapters, the adhesive behavior in several test geometries was studied assuming linear elastic behavior. Adhesives are polymers, and by their morphology, are viscoelastic. Thus, any stress analysis of adhesives in structural bonds using elastic or elastic-plastic material assumptions is not justified in terms of predicting long term behavior. Contrary to the behavior of metals which retain their elastic modulus when plastically deformed, polymers exhibit damage mechanisms which significantly alter material behavior following yielding. Furthermore, the elastic properties of adhesives determined from mechanical testing are strongly dependent on the loading rate and test temperature.

The damping characteristics of adhesive bonds are directly attributed to the viscous mechanisms present in the adhesive. In addition, stress concentrations are relieved due to the flow of the long, intertwined molecular chains. However, the viscoelastic nature of the adhesive permits large displacements due to creep behavior. Thus, the complete viscoelastic response of the adhesive plays a vital role in terms of the bonded joints ability to transmit structural loads.

Modern structural adhesives are often a blend of high molecular weight epoxy with small elastomer particles which act as adhesive toughening agents. Furthermore, scrim clothes are also embedded into epoxy films to strengthen the material. In essence, a structural adhesive is a composite material. The mechanical interactions between the bulk adhesive and toughening agents essentially make the cured adhesive an nonlinear viscoelastic material even at small deformations.

Nonlinear viscoelastic constitutive relations have been developed by a number of investigators. The first approach was developed by Green and Rivlin [31]. Their approach represented the stress as a polynomial expansion in linear functionals of the strain history. As noted by Christensen [32], the number of material functions in this multiple integral representation limits its applicability to engineering analysis. For this reason, Pipkin and Rogers [33] introduced an alternative to the Green-Rivlin theory in the form of a Boltzmann superposition integral which allows for nonlinear effects; this modified superposition approach was originally proposed by Leaderman [34]. The nonlinear superposition integral is the basis for current nonlinear viscoelastic theories.

Two separate and distinct nonlinear superposition theories have been incorporated into finite element programs. Schapery [5] developed a nonlinear superposition integral on the basis of irreversible thermodynamics. Henriksen [35] formulated a nonlinear viscoelastic finite element program using the Schapery constitutive model. The program was validated by comparison with the experimental data of Peretz and Weitsman [4]. Similarly, Knauss and Emri [36] proposed an intrinsically nonlinear model of viscoelastic behavior based on free volume. Subsequently, Becker et al. [17] incorporated this model into VISTA, a two dimensional finite element program designed specifically for analysis of adhesively bonded joints.

Nonlinear behavior, when modelled by a single integral or multiple integral theory, often limits analysis to the special load or strain histories used to establish the theory. In contrast to the well-defined relationship between the creep compliance and relaxation modulus for linear viscoelastic behavior, no simple relation exists between material properties for creep and relaxation in nonlinear behavior. According to Sternstein [37], the inversion of material properties is based on the exper-

imental observation that materials which exhibit nonlinear creep also have well-defined stress relaxation behavior. Experimental validation of nonlinear theories for histories other than loading and unloading are necessary in light of the complexities of viscoelastic response.

Christensen [32] also recognizes that in the nonlinear range of deformation, the lack of interchangeable properties limits the application of nonlinear theories to the test method used to fit the nonlinear properties. Also, displacement control of material deformation can produce different types of nonlinear behavior than load control. In effect, the type and degree of nonlinearity depends not only on the current value of stress and deformation but also on the entire past history, as a consequence of fading memory.

The nonlinear theory presented by Knauss and Emri [36] unifies experimental observations that pressure and temperature cause similar shifts in material behavior, as noted by Ferry [3]. Free volume determines segmental mobility of the polymer chains and, hence, the viscoelastic response. The dependence of the free volume on temperature is widely used to construct master curves from experimentally accessible time frames. Unlike the change in volume with temperature, the change due to pressure changes is notably nonlinear for a wide range of polymers as noted by Ferry. Knauss and Emri deduced that for small to moderate strains, the free volume of a polymer is a linear function of the dilatational strain. Moisture swelling affects the free volume in a similar fashion. In their theory, the shift function for the representative master curve is a function of temperature, T, moisture, c, and dilatational strain, θ, in the form

$$\log a(\mathrm{T,c},\theta) = \frac{-B}{2.303 f_0}\left(\frac{\alpha_t(T - T_0) + \alpha_m c + \delta\theta}{f_0 + \alpha_t(T - T_0) + \alpha_m c + \delta\theta}\right) \qquad [17]$$

where α_T is the coefficient of thermal expansion, α_m is the coefficient of moisture expansion, and δ is the parameter which relates the dilatational strain to the free volume. B and f_0 are material constants. The incorporation of a strain dependent parameter into the shift function causes an intrinsic nonlinear material response of the linear behavior. In this regard, the free volume theory avoids numerous parameters or functions which must be adjusted to fit data. The underlying theory is

sound from a physical point of view since it relates the macroscopic (continuum) behavior to microscopic processes.

For adhesive systems, the relation between the free volume and the dilatational strains is clouded by the presence of modifiers and possibly scrim cloth in the adhesive. Consider a homogeneous adhesive under the action of an applied dilatational stress. If the stress state is compressive, the free volume will collapse and restrict segmental motion. On the other hand, a tensile stress state will increase the free volume allowing greater segmental motion and an increased material response. In either case of compression or tension, the free volume changes should correspond directly to the dilatational strain state as long as no material damage has occurred or no compressibilty affects become important. At the onset of damage, the material response becomes a function of stress and linearity is never recovered.

For a two phase material, such as rubber modified epoxy, thermorheological simplicity may not be applicable. In such a material, a sufficient change of temperature may cause one phase (i.e. the bulk adhesive) to change modulus relative to the second phase (i.e. elastomer modifier); thus, significant changes in the internal stress distribution may occur. Kenner et al. [6] found that for a two phase adhesive, FM-73U, thermorheological simplicity is well-preserved at least in the linear viscoelastic region.

In two phase solids, various damage mechanisms may destroy the thermorheological simplicity of the material even at moderate strains. Under a tensile stress state, damage may occur at the interface of the bulk adhesive and modifier or in the adhesive itself due to stress concentrations. Furthermore, a tensile strain in such a material may not affect the free volume directly as in the case of a homogeneous polymer. Under a compressive strain, possibly due to residual thermal stresses, the free volume dependence on dilatation may be well-preserved up to a compressibility limit determined by the stress interaction between the constituents.

To gain insight into the viscoelastic stress analysis of adhesively bonded joints, three steps were performed. Based on the results of the first two chapters, an attempt was made to measure the linear viscoelastic properties of AF 163-2U *in-situ* using the Arcan specimen. Secondly, the actual time dependent adhesive deformations were measured for the same adhesive in the thick adherend joint using the modified Krieger extensometer for various types of loading. Lastly, predictions of adhesive behavior using VISTA were compared to the actual deformations in the thick adherend joint. From this endeavor, conclusions were drawn concerning the free volume model and mechanical property determination of adhesives *in-situ.*

Linear viscoelastic properties

The procedures for determining linear viscoelastic properties are well established experimentally. Under the assumption of thermorheological simplicity, creep or relaxation data at short times and at various temperatures are shifted to obtain the master creep or relaxation curve for the material. Thus, the complete linear viscoelastic response is determined solely from the master curve and the experimentally determined shift factor. By separating the material deformation response into shear and bulk behavior, two separate master curves are necessary with the shift factor applying to both curves. In most applications, the bulk modulus is assumed to be constant since it varies by several orders of magnitude less than the shear modulus over the entire time scale. The definition of linearity implies that the creep response may be obtained from a knowledge of the relaxation response and vice versa.

Creep tests are more experimentally advantageous than relaxation tests especially in the Arcan fixture where deformations are measured in the adherends. Kenner et al.[6] determined the linear shear creep compliance of FM-73U using a creep torsiometer as noted earlier. The creep torsiometer is a rather sophisticated instrument because it uses air bearings to minimize friction; therefore, small

deformations are easily obtained insuring linearity. Liechti and coworkers [38] modified the creep torsiometer concept to utilize a razor edge bearing. They obtained the master shear creep compliance of the same adhesive. The attempt at measuring linear viscoelastic properties *in-situ* reported here was the first such try .

The Arcan specimen was chosen to measure the shear creep compliance of AF 163-2U due to the uniform shear stress produced by mechanical loading. Since the results of the static testing showed the 0.007 in. bondline specimen to have the least amount of scatter, it was chosen as the representative test specimen. The creep tests were conducted at various temperatures in an MTS load frame. A Thermotron temperature/humidity cabinet provided a constant temperature for each test.

The creep tests were conducted at temperatures ranging from 27 °C to 94 °C. The applied load ranged from 2000 lb for the lowest temperature to 500 lb for the highest. After a creep test was conducted at a given temperature, the specimen was unloaded to allow stress relaxation overnight. This was necessary to prevent cumulative creep strains from arbitrarily shifting the experimental time scale of subsequent tests. The relatively large magnitude of the applied load was deemed necessary due to the limitations of measuring the creep strains to a large degree of accuracy. It was later found that the specimen underwent large strains at the higher temperatures.

The individual creep curves are shown in Figure 47. To obtain the master curve, the creep curves were shifted vertically by the factor

$$b = \frac{T}{T_0}$$

where T is the absolute test temperature and T_0 is the reference temperature of 300 K (27 °C). The vertically shifted curves were then shifted horizontally in an attempt to obtain the master creep compliance at the reference temperature.

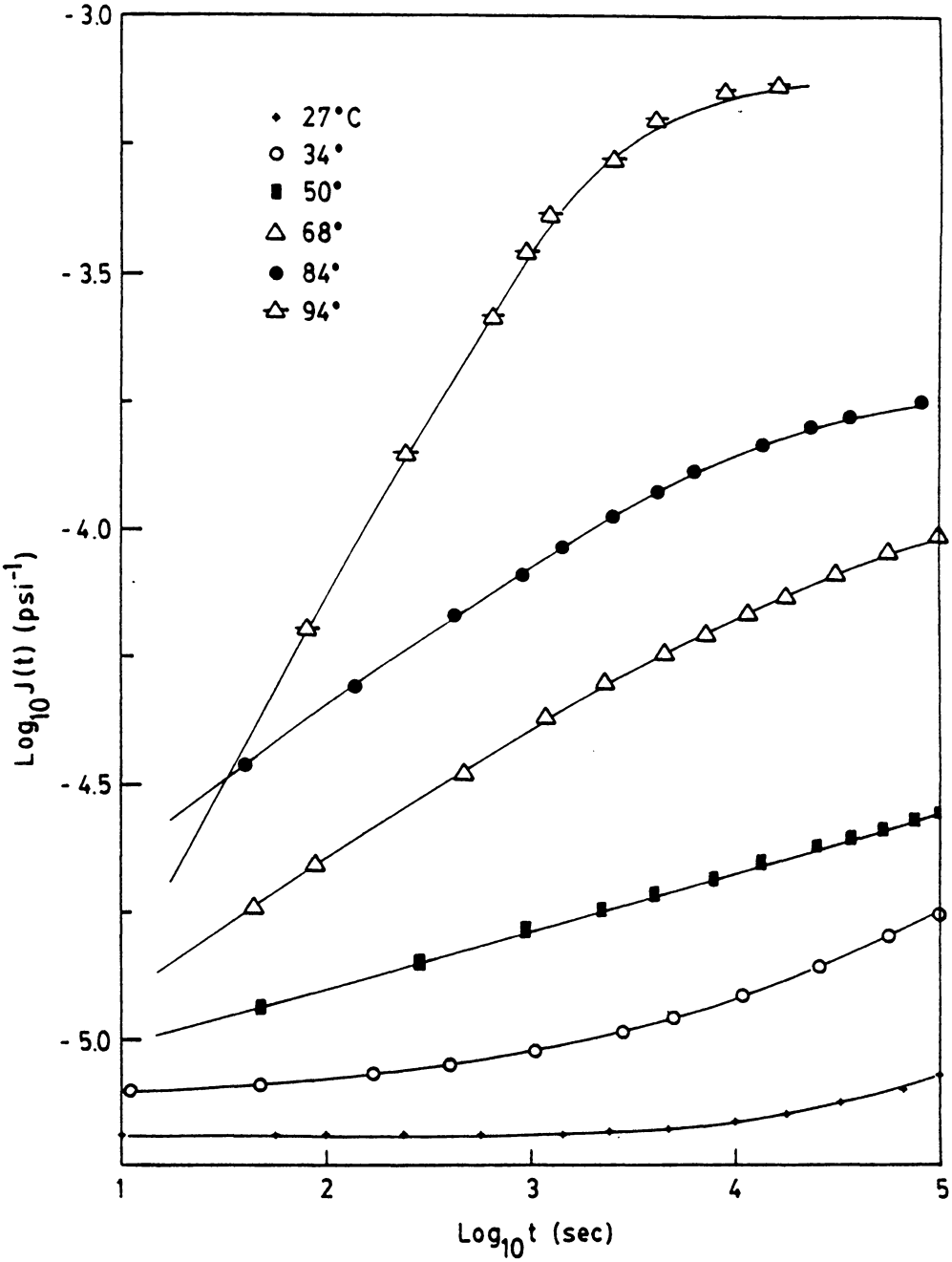

Figure 47. Shear creep compliance curves for AF 163-2U in-situ for various temperatures.

The master curve shown in Figure 48 shows that the individual creep curves did not shift well. At low temperatures, the shifting procedure produced a relatively smooth curve. As the test temperature increased, large discrepancies in the time temperature superposition, or thermorheological simplicity, became apparent. To further demonstrate the shifting problems, the experimental shift factors are shown in Figure 49.

The problems encountered in producing the master curve were attributed to several causes. First, overnight relaxation of the specimen at higher temperatures may not have been sufficient to assure a stress free reference state for the succeeding test. The curve for the highest test temperature, in which the material shear strains were highest, indicates that the material response was approaching the rubbery plateau region. This effectively means that no damage has occured at any point in the testing; however, linearity of the material response is not necessarily preserved due to the extensional strains arising from the large shear deformations as noted in Chapter 2. The main concern over the lack of thermorheological simplicity is attributed to the residual thermal stress state in the adhesive.

For most polymers, the volume expansion behavior has a sharp discontinuity at the glass transition temperature. The coefficient of thermal expansion increases almost 3 times as the temperature passes through the glass transition region. The residual stress state in the adhesive is highest at the lowest test temperature. As the test temperature increases, the thermal stress state decreases in magnitude at every point in the adhesive. At or beyond the glass transition temperature, the residual stress state decreases more rapidly for smaller differences in temperature between the stress free and current temperatures. Furthermore, the viscoelastic nature of the adhesive causes the residual stress state to depend on time as well as temperature.

Although adequate stress relaxation and smaller deformations would ensure the measurement of the true linear viscoelastic properties *in-situ*, the residual stress state present in the adhesive make these measurements difficult to relate to the true linear behavior. The residual stress state creates a tensile strain field in the adhesive compared to the bulk. Under the free volume theory, the positive

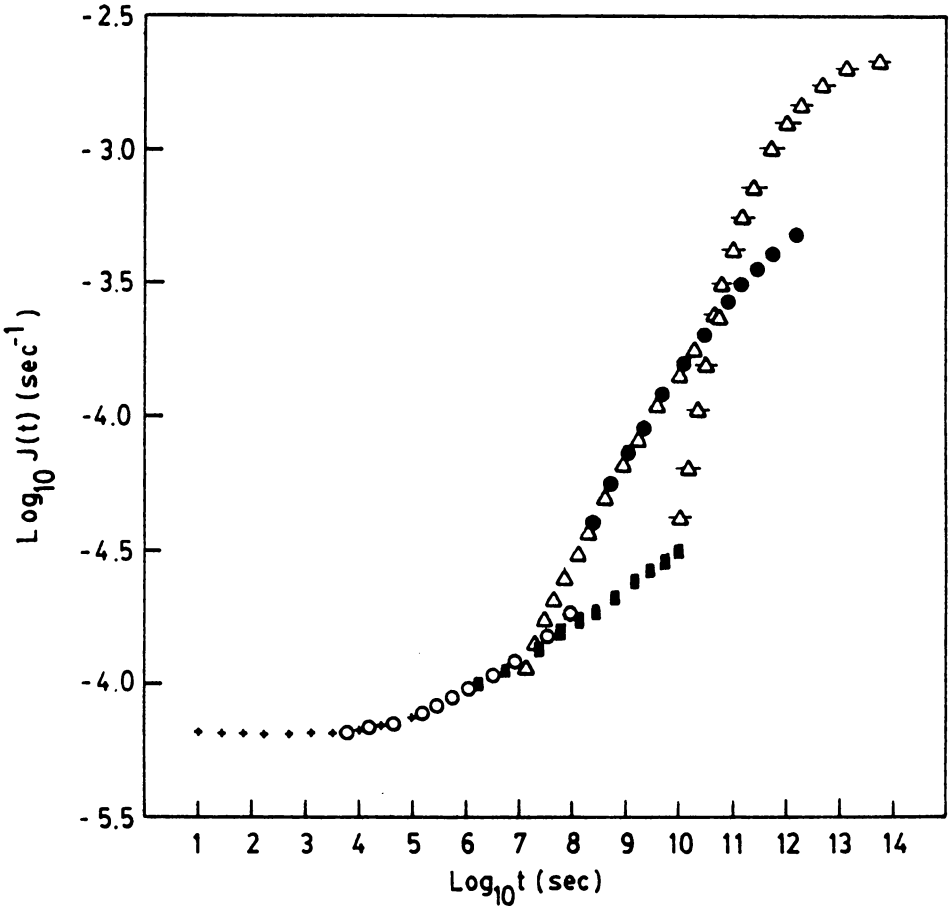

Figure 48. Master shear creep compliance curve for AF 163-2U in-situ: 27°C taken as the reference temperature T_0 .

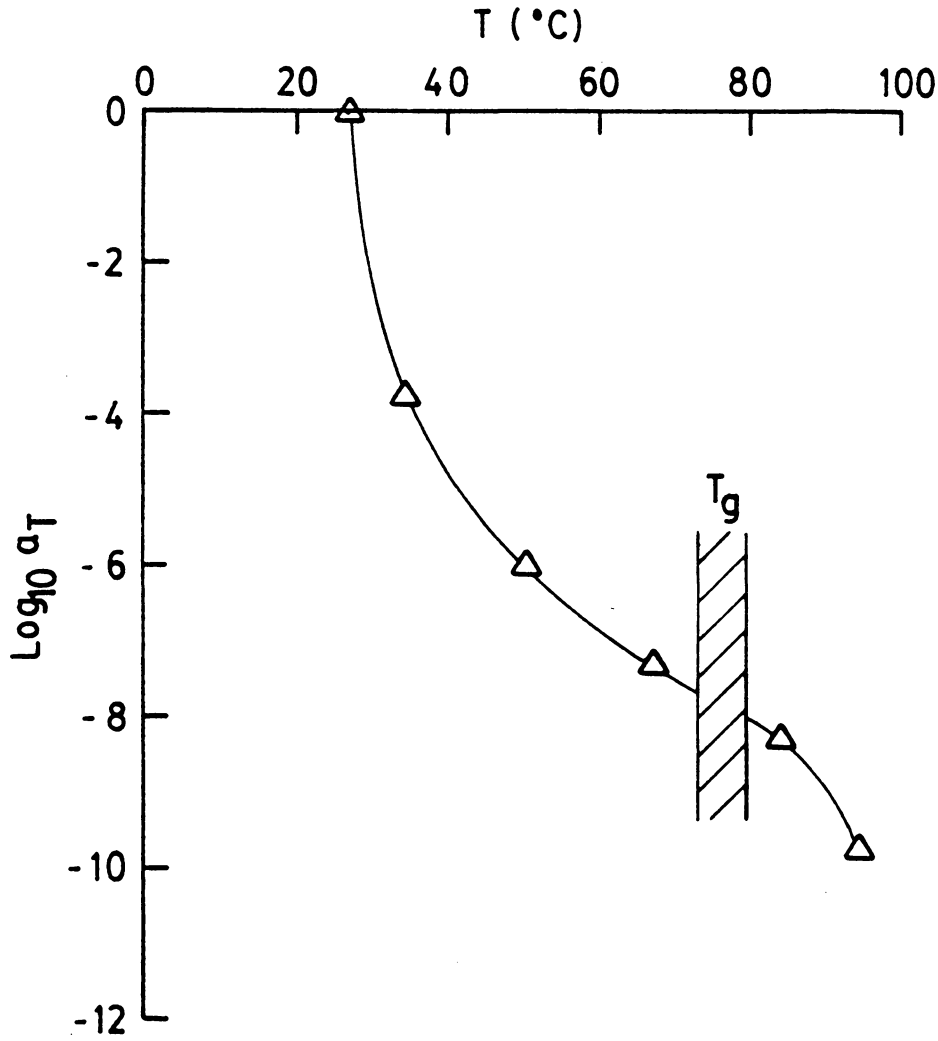

Figure 49. Experimentally determined shift factors.

dilatation associated with the residual stress state shifts the material response forward on the time scale. In this context, linear viscoleastic measurements of an adhesive *in-situ* are not feasible since the material is already in a history dependent state due to residual thermal stresses.

Time-dependent measurements

Experimental tests of thick adherend joints at various temperatures and load histories were conducted. These tests were to serve as comparison to finite element results using the measured linear viscoelastic properties of the test adhesive. Despite the problems encountered in the determination of the linear viscoelastic properties, the test results could serve as a guide for future analytical development and finite element analysis.

Thick adherend joints were fabricated using AF 163-2U adhesive as reported earlier. The modified Krieger extensometer was used to measure the deformation as a function of time for two load cases: (a) ramp loads at 27 $^{\circ}C$ and 75 $^{\circ}C$ and (b) step loads at 75 $^{\circ}C$ and 90 $^{\circ}C$. For the ramp load, 1000 lbs. was the maximum load obtained in 90 seconds; 1000 lbs was the value of the step load. All tests took place in a Thermotron temperature cabinet under the action of a MTS load frame. The extensometer output was recorded on a strip chart recorder.

The test data was transformed into shear strain versus time curves. The shear strain was calculated from Eq. 4 as done previously for static tests of the thick adherend joint. Figures 50 and 51 show the measured adhesive shear strain values as a function of time for under ramp loading for the test temperatures of 27 $^{\circ}C$ and 75 $^{\circ}C$ respectively. Figure 52 shows the results of the step loading histories.

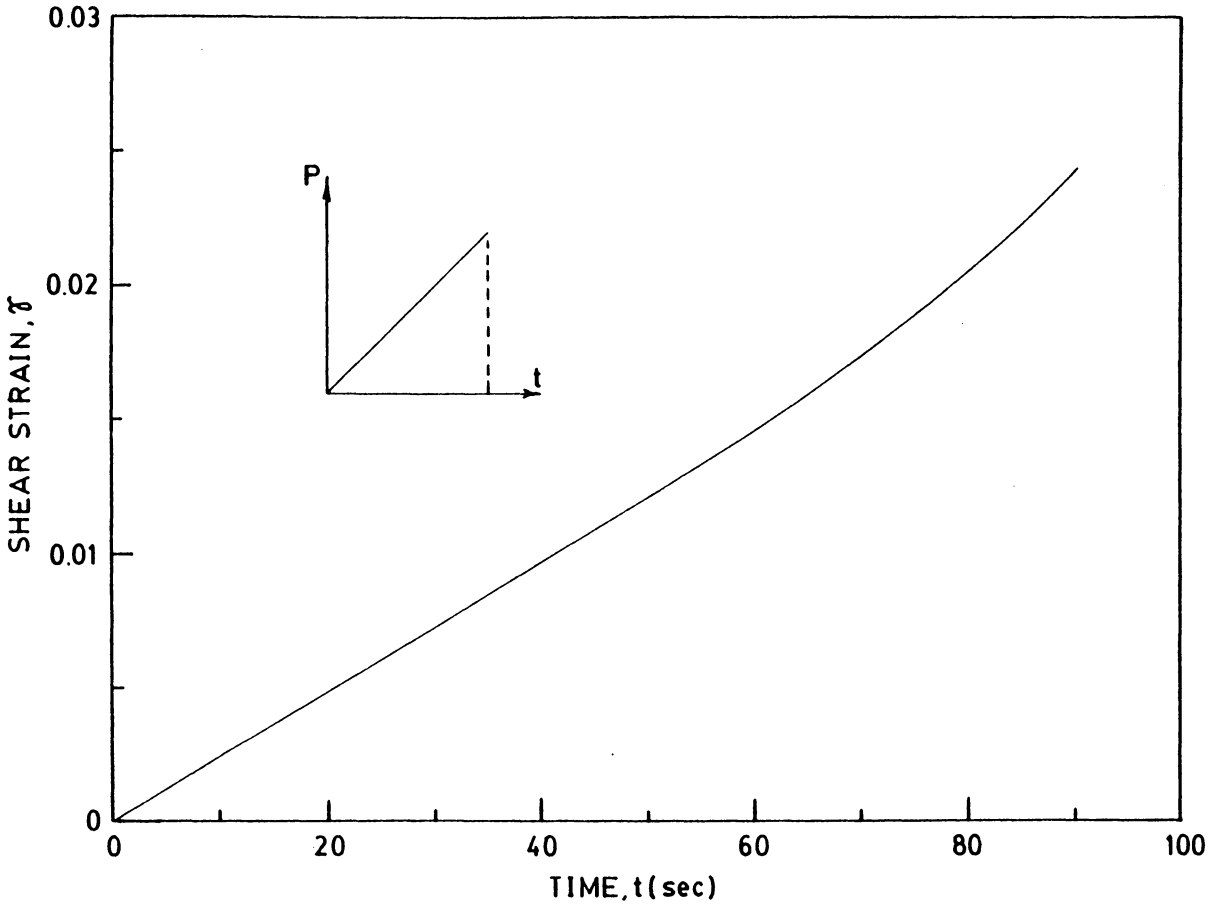

Figure 50. Shear strain versus time for AF 163-2U in thick adherend joint for a ramp load at room temperature: $T = 27°C$.

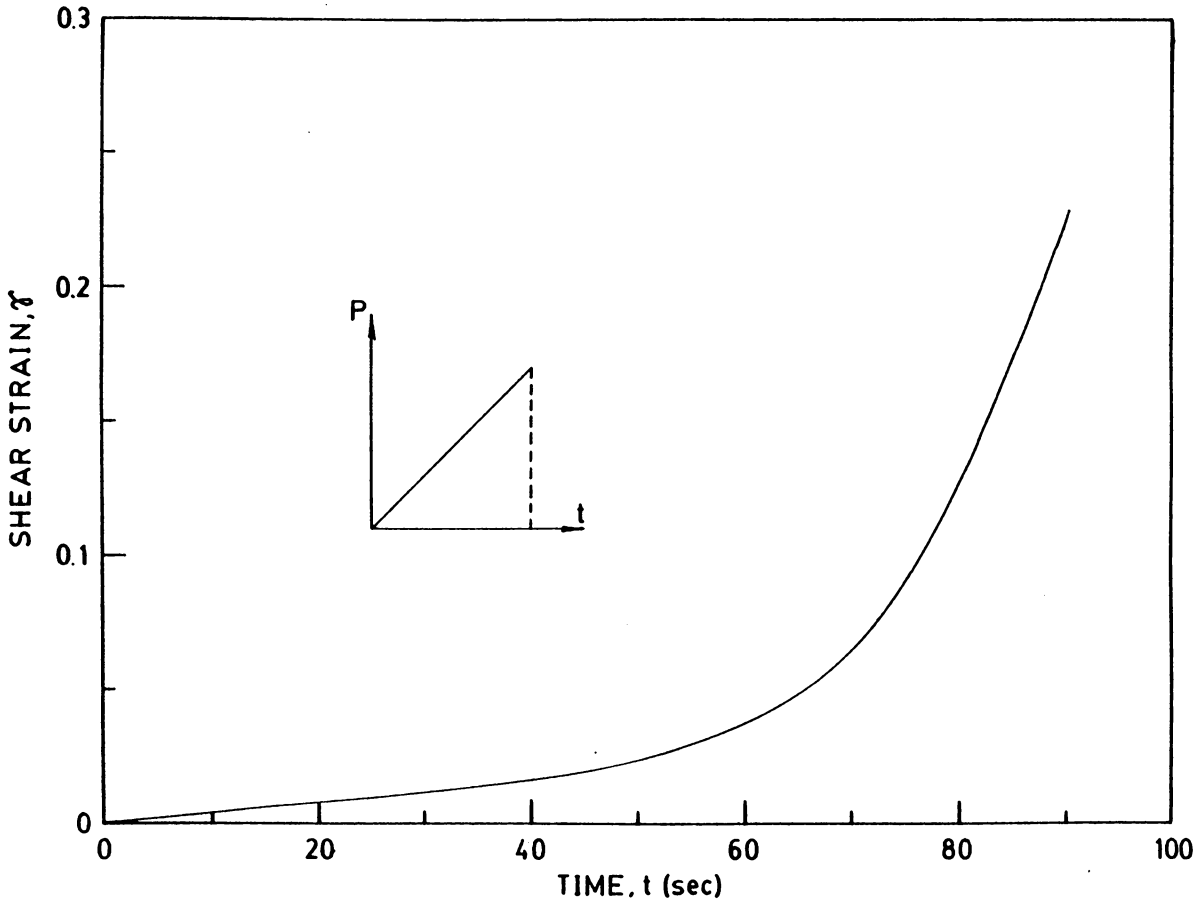

Figure 51. Shear strain versus time for AF 163-2U in thick adherend joint for a ramp load at elevated temperature: $T = 75°C$.

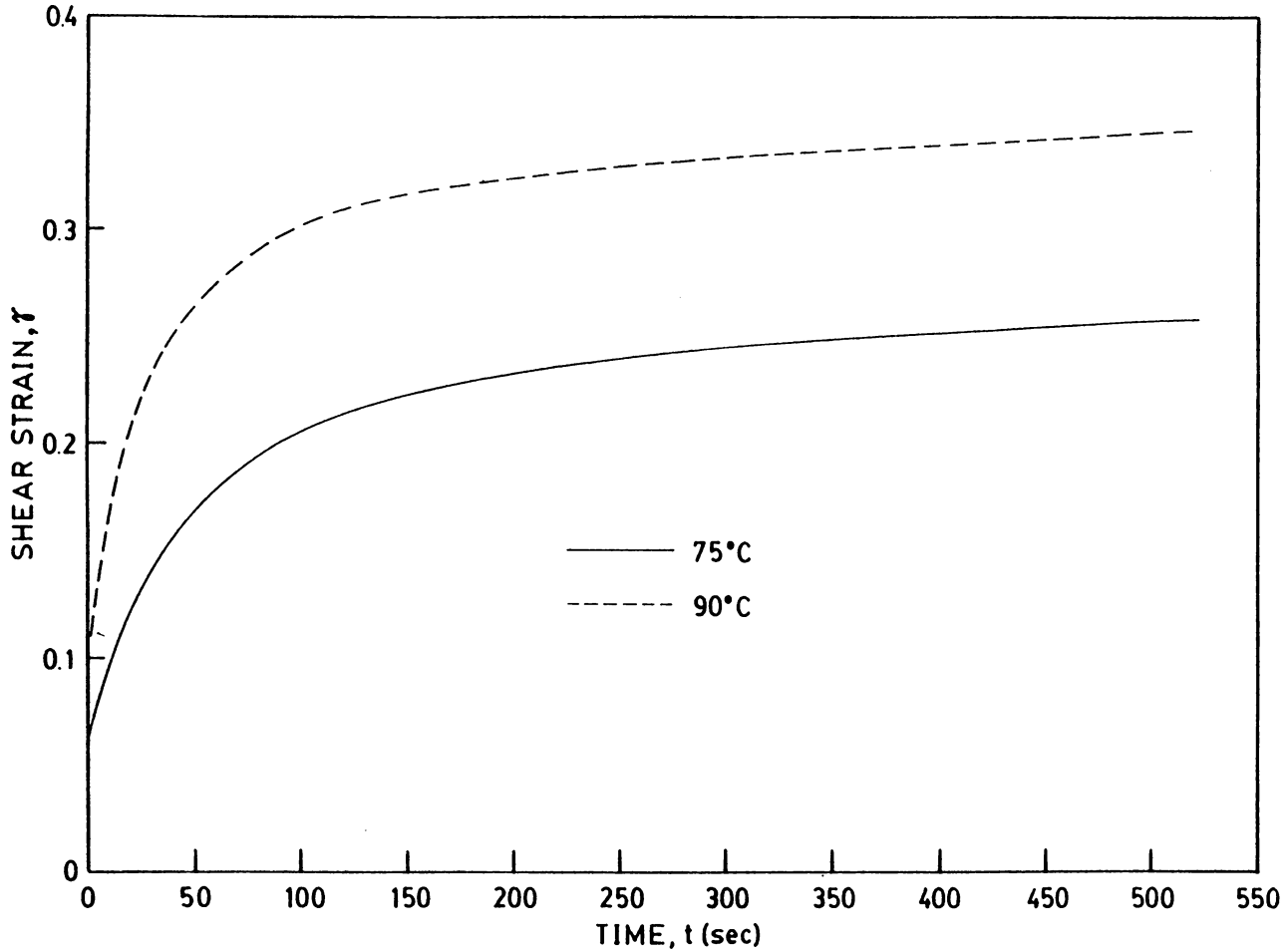

Figure 52. Shear strain versus time for AF 163-2U in thick adherend joint for a step load at two temperatures: 75°C and 90°C.

Viscoelastic behavior of the adhesive is clearly demonstrated by the measured shear strain versus time plots. Interestingly, the initial portion of both the ramp load cases indicate a linear dependence of the shear strain on time; hence, the initial behavior appears linear viscoelastic. Material nonlinearity appears, however, in the 75 $°C$ case at large values of shear strain.

Nonlinear viscoelastic finite element analysis

Comparisons between the experimental results and finite element analysis were performed using the nonlinear capabilities of VISTA. Although the linear viscoelastic properties of the test adhesive, AF 163-2U, were not found as discussed, available creep data for a similar adhesive, FM-73U [6], was used in a comparative sense. With the available Prony series representation of the linear viscoelastic creep compliance, the relaxation behavior needed as input into the program was determined using a collocation scheme similar to the one presented by Schapery [39].

For linear viscoelastic behavior, the relationship in the Laplace domain between the shear relaxation and creep compliance is given by

$$G(s) = \frac{1}{s^2 J(s)} \qquad [18]$$

With the creep compliance in the form

$$J(t) = J_0 + \sum_{i=1}^{n} J_i(1 - e^{-\frac{t}{\tau_i}}) \qquad [19]$$

and the relaxation modulus represented by

$$G(t) = G_\infty + \sum_{i=1}^{n} G_i e^{-\frac{t}{\tau_i}} \qquad [20]$$

Eq. 18 becomes

$$\sum_{j=1}^{n} \frac{G_j s_i}{s_i + \frac{1}{\tau_j}} = \left[\frac{1}{J_0 - \sum_{j=1}^{n} J_j \left(1 - \frac{s_i}{s_i + \frac{1}{\tau_j}}\right)} \right] \qquad [21]$$

The solution of the set of equations defined by Eq. 21 was accomplished numerically in the following manner. First, the final value theorem of the Laplace transform says that the long term modulus is related to the creep compliance by

$$G_\infty = \frac{1}{J(\infty)} \qquad [22]$$

or in terms of Eq. 19

$$G_\infty = \frac{1}{J_0 + \sum_{i=1}^{n} J_i}$$

To obtain the series coefficients ,G_j, the Laplace transform variable s_i was collocated to the relaxation times such that

$$s_i = \frac{\lambda}{\tau_i}$$

where λ is a factor used to obtain the best fit of the inverted data. Thus, linear equations of G_j result. A computer program, named Prony, was written to to solve the set of equations defined by Eq. 21. The program appears in Appendix B.

Representations of viscoelastic properties in Prony series entails approximations of the true stress-strain response. Although the inversion procedure outlined above did not use the initial value theorem, it was found that the initial value of the relaxation response was within 4% of the inverse of the intial creep compliance. Comparison of the relaxation behavior with a reported curve for the same material [17] derived numerically showed good agreement as indicated in Figure 53. Ap-

proximations arise naturally in the shifting procedure to obtain master curves from short term test [3]. Furthermore, the numerically obtained relaxation behavior is obviously an approximation to the real behavior of the adhesive since the creep compliance master curve reported was not obtained fully to the rubbery plateau.

Problems encountered with storage requirements in VISTA required approximations in the discretization of the thick adherend joint. Because the computational aspects of a viscoelastic analysis require large material data storage in defined arrays, the mesh was limited to a small number of elements. Figure 54 shows the mesh used to model the thick adherend specimen. The adhesive layer was two elements thick and eight elements along the bondline. This was a rather coarse mesh of the adhesive compared to earlier meshs used for elastic analysis. Small changes in the program via array dimensioning would allow finer meshes of viscoelastic adhesive layers.

The definition of the stress free reference temperature as the reference temperature of the free volume shift factor (Eq. 17) in the program also required program revisions. In VISTA, the intrinsically nonlinear shift factor is defined as

$$\log a = \frac{-B}{2.303 f_0}\left(\frac{3\alpha_T(T - T_{ref}) + 3\alpha_m c + \delta\theta}{f_0 + 3\alpha_T(T - T_{ref}) + 3\alpha_m c + \delta\theta}\right) \qquad [23]$$

where T_{ref} is the stress free reference temperature of the material. According to the implications of the free volume theory, linear behavior results when the moisture content and dilatational strain are zero. Hence, the shift factor becomes a function of temperature only such that

$$\log a_T = \frac{-B}{2.303 f_0}\left(\frac{3\alpha_T(T - T_{ref})}{f_0 + 3\alpha_T(T - T_{ref})}\right) \qquad [24]$$

The shift factor is often reported in the WLF equation form

$$\log a_T = \frac{-C_1(T - T_0)}{C_2 + (T - T_0)} \qquad [25]$$

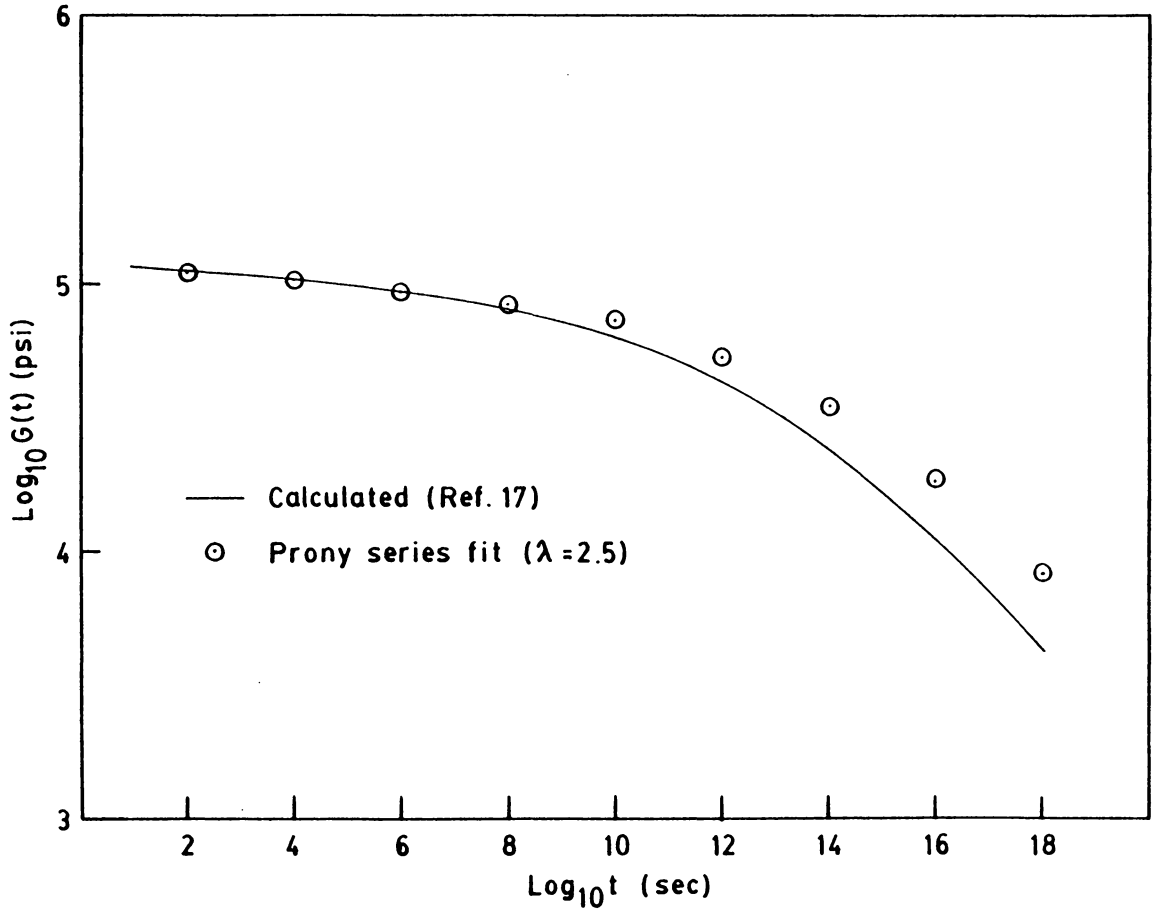

Figure 53. Comparison of the inverted Prony series creep compliance with the calculated relaxation modulus.

where T_0 is usually defined as the glass transition temperature. When $T_{ref} = T_0$ then

$$f_0 = \frac{C_2}{3\alpha_T}$$

and

$$B = 2.303\, C_1 f_0$$

For the analysis of the adhesive joint considered here, the stress free temperature is the cure temperature of 121 $°C$ which is roughly the cure temperature of most structural adhesives. The discrepancy between the stress free temperature and the WLF reference temperature for FM-73U required evaluating C_1 and C_2 for $T_0 = T_{ref}$. However, this resulted in negative values of the constants B and f_0. A negative value of f_0 indicates negative free volume, which is physically unrealistic and causes an error message in VISTA. To overcome this shortcoming, the reference temperature for the intrinsic shift factor was redefined in the subroutines LBOUND and INTSHF as the WLF reference temperature.

The nonlinear viscoelastic analysis was performed using the cure temperature as the strain-free reference temperature for the adhesive. The results of the finite element analysis predicted that the free volume shifting caused the material to stiffen under the thermal strain conditions. However this is not feasible since the adherends produce a net tensile strain in the adhesive compared to the bulk reference (linear behavior). As noted in Chapter 2 in the thermal analysis of the single lap joint, the mechanical strains in the adhesive are compressive with respect to the strain-free temperature. Thus, the current value of the dilatation did not account for the thermal strain state in terms of the bulk reference. Changes to the subroutine DILATE were made to calculate the dilatation in reference to the bulk strain-free state at the current temperature. With this modification, the analysis of the viscoelastic response was resumed.

The finite element results indicate that the residual stress state influences the adhesive material behavior according to the free volume nonlinear model. Figure 55 shows a comparison of the linear

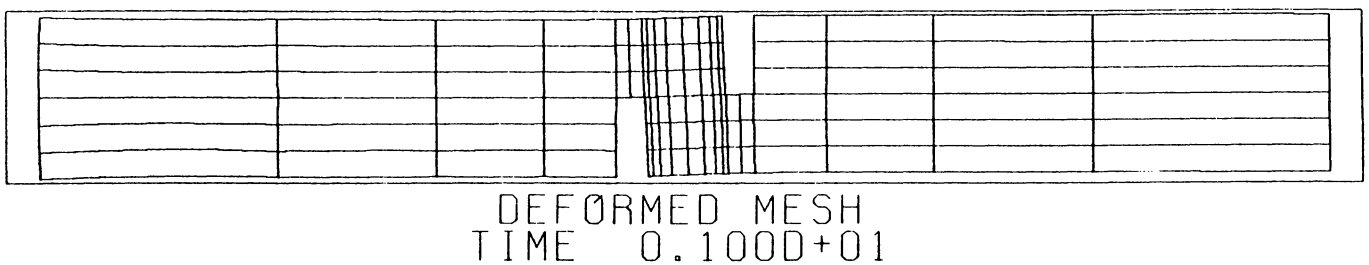

Figure 54. Reduced finite element mesh used in the viscoelastic analysis of the thick adherend joint.

and nonlinear shear strains versus time for a ramp load at room temperature. For comparison, the strain-free temperature, T_r, was defined at both the cure temperature ($T_r = 121°C$) and the glass transition temperature ($T_r = 83°C$). The presence of residual strains shifts the material response forward in time accordng to the free volume model. Note that the shift from the linear response is dependent on the definition of the strain-free reference temperature.

A similar analysis was conducted for a ramp load history at $T = 75°C$. Figure 56 shows the comparison of the linear and nonlinear response under the thermal strain state. Again the free volume model predicts that the *in-situ* adhesive behavior should be less rigid than the corresponding bulk behavior at the same temperature.

Discussion

Studies of an adhesive bond that undergoes elevated temperature curing indicate that the residual thermal stress state affects the viscoelastic response due to free volume changes. This implies that the linear viscoelastic properties cannot be obtained *in-situ* using the thermorheological simplicity assumption. Furthermore, the nonlinear finite element analysis has revealed that the residual stress state makes the adhesive response softer than the corresponding linear viscoelastic response under the free volume model.

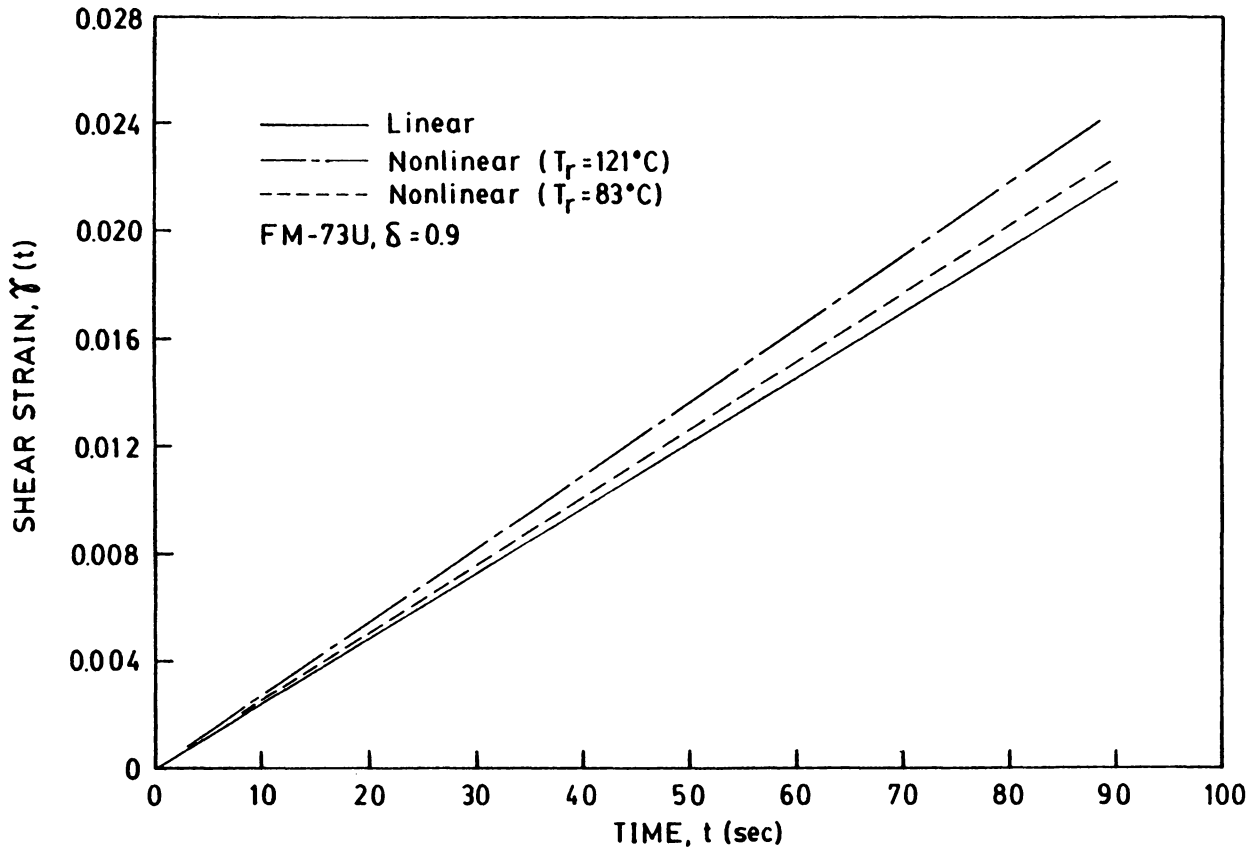

Figure 55. Finite element results of a thick adherend joint under ramp loading at room temperature: comparison of linear and nonlinear response at 27°C.

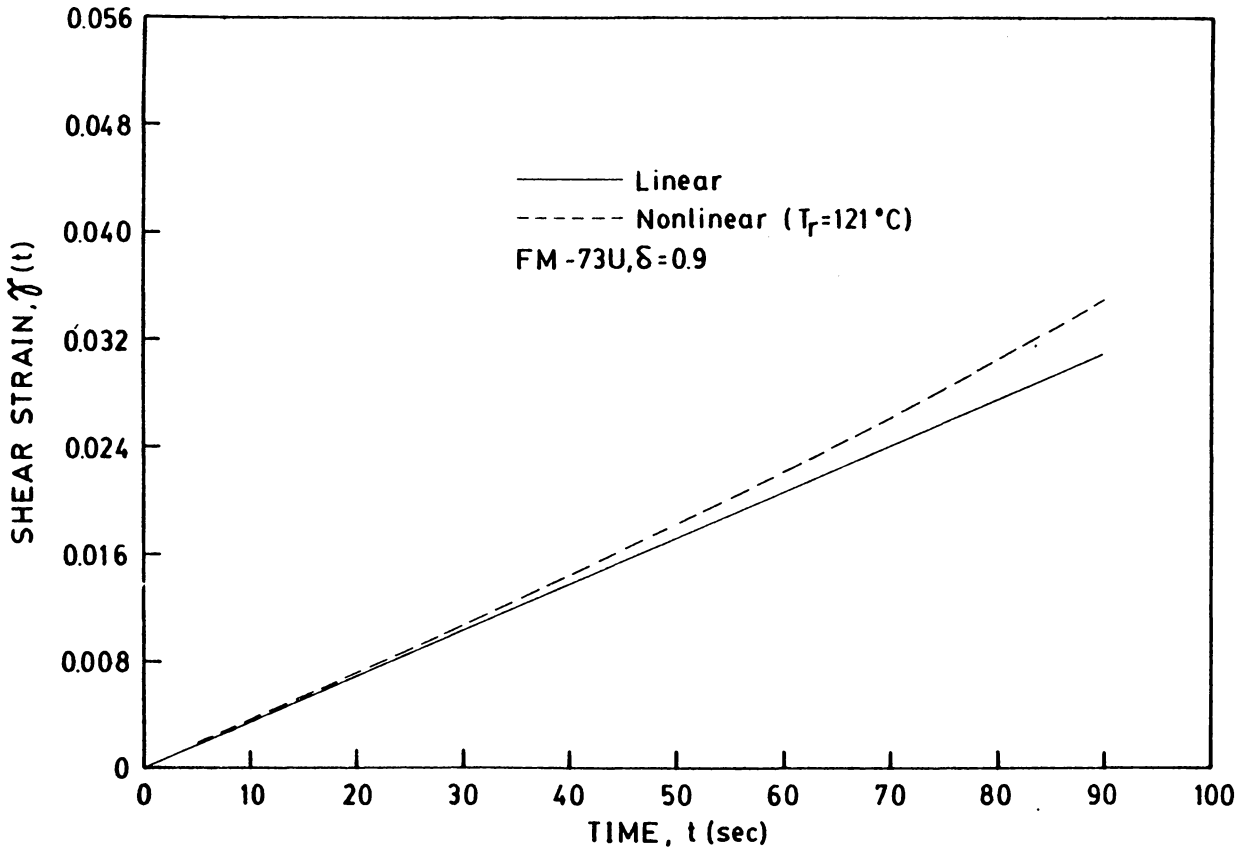

Figure 56. Finite element results of a thick adherend joint under ramp loading at elevated temperature: comparison of linear and nonlinear response at 75°C.

V

Conclusions and Recommendations

The free volume theory may adequately account for differences between the bulk adhesive and *in-situ* mechanical properties for use in finite element stress analyses provided the linear reference of the *in-situ* adhesive is known. Residual thermal stresses, created by elevated temperature cure conditions, change the free volume of the *in-situ* adhesive compared to a neat resin sample. In terms of viscoelastic response, the change in free volume causes shifting of the adhesive behavior in time due to changes in chain mobility. Other polymer variables, such as molecular weight distribution, percent crystallinity, etc. may affect the mechanical properties of the adhesive at the material interfaces in the weak boundary layer. However, these variables do not account for the measurable property differences of the *in-situ* adhesive reported here.

Significant differences between *in-situ* and bulk shear modulus values were found in static tests of various adhesive test geometries. Static tests involving the Arcan specimen indicated that the measured shear modulus is a function of the bondline thickness. An error analysis showed that the data scatter of the experimentally measured shear modulus was not due to measurement errors arising from systematic sources.

No correlation between the bulk and *in-situ* mechanical response was found. The free volume nonlinear theory predicts that the viscoelastic response of the *in-situ* adhesive is not as stiff as the linear bulk reference due to residual thermal strains. However, experimental evidence suggests that the *in-situ* adhesive is actually stiffer than the bulk material. This implies that the presence of the adherends during cure strongly influences polymerization of the adhesive.

Because the adhesive is viscoelastic, the residual thermal stresses will be relieved following adhesive cure. The material viscoelastic response is both a function of time and the current dilatational state according to the free volume theory. Before the adhesive joint is ever loaded mechanically, the adhesive modulus is changing with time due to the residual thermal stress state. Thus, the measured mechanical properties, such as the shear modulus, would be both a function of the residual stress state and the elapsed time following cure. Tests of the Arcan specimen, as well as the other test geometries studied, involved specimens cured over a period of a week; however, all static tests were conducted within several hours time. Consequently, the viscoelastic response of the adhesive due to the thermal residual stress state caused differences in the measured shear modulus of the adhesive tests undertaken.

The effect of the thermal residual stress state on the adhesive viscoelastic behavior requires further experimental investigation. Experimental techniques to quantify the residual stress state following cure are needed. Several of the adhesive test specimens studied would provide adequate data on adhesive shear response to mechanical loading. Perhaps the Arcan specimen is the most advantageous test geometry due to its versatility in producing mixed states of stress in the adhesive.

Experimental validation of the finite element stress analysis requires further work. The limitations of the free volume theory in predicting adhesive response, specifically modified adhesives, need to be fully defined. Because of the complexity of the mechanical response of a two-phase adhesive, modifications to the linear dependence of the free volume on the dilatational strain may be in order.

References

1. Alfrey, T., in **Treatise on Adhesion and Adhesives**,Vol. 1, R.L. Patrick (ed.),New York: Marcel Dekker,1961,p.151.

2. Hertzberg, R. W.,**Deformation and Fracture Mechanics of Engineering Materials**,2nd edition,New York: John Wiley, 1983,pp.193-200.

3. Ferry, J. D., **Viscoelastic Properties of Polymers**, 3rd edition,New York: John Wiley,1980.

4. Peretz, D. and Y. Weitsman, "The Non-linear thermo- viscoelastic characterization of FM 73 adhesive", **J. Rheology**,Vol. 26,1983,pp.245-261.

5. Schapery, R. A.,"Further development of a thermodynamic constitutive theory: stress formulation",Purdue Research Foundation,Project no. 4958,1969.

6. Kenner, V. H., W. G. Knauss, and H. Chai, " A Simple Creep Torsiometer and its Use in the Thermorheological Characterization of a Structural Adhesive",**Experimental Mechanics**,Vol. 22,1982,pp. 75-80.

7. Lefebvre, D. R. and H. F. Brinson, "Characterization of Structural Adhesives, FM 73 and FM 300",Oct. 1985, VPI-CAS/ESM-85-3.

8. Dolev, G. and O. Ishai, "Mechanical Charaterization of Adhesive Layers in-situ and as Bulk Material", **J. Adhesion**,Vol. 12,1981,pp.283-294.

9. **Structural Adhesives**,Vol. 3,National Materials Advisory Board,Marcel Dekker,1976.

10. Stringer, L. G.,"Comparison of the Shear Stress-Strain Behaviour of Some Structural Adhesives",**J. Adhesion**, Vol. 18,1985,pp 185-196.

11. Knollman, G. C. and J. J. Hartog,"Experimental Determination of the Variation in Shear Modulus Through the Interfacial Zone of an Adhesive," **J. Adhesion**,Vol.17,1983,pp.251-272.

12. Hahn, H. T.,"Residual stress in the Interfacial Bond Zone of Curing adhesives by a Sensitive Strain Mesaurement Technique",**J. Adhesion**,Vol.17,1984,pp.21-32.

13. Portelli, G. B.,in **Structural Adhesives- Chemistry and Technology**, S.R. Hartshorn (ed.),New York: Plenum Press,1986, pp. 407-446.

14. Volkersen, O., "Die nielkraftverteelung in zunbeanspruchten metverbindungen mit knostante laschenquerschnitten",**Luftfahrtforschung**,Vol.15,1938,pp. 4-47.

15. Goland, M. and E. Reissner, "The Stresses in Cemented Joints", **J. Applied Mechanics**,Vol. 11,1944,pp. a17-a27.

16. Botha, L. R., R. M. Jones, and H. F. Brinson, "Viscoelastic Analysis of Adhesive Stresses in Bonded Joints",May 1983,VPI-E-83-17.

17. Becker, E. B., R. S. Chambers, K. M. Liechti , and W. G. Knauss, "Viscoelastic Stress Analysis Including Moisture Diffusion For Adhesively Bonded Joints",Semi-annual Progress Report no. 1,General Dynamics Fort Worth Division FZM-6964,March 1981. (five semi-annual reports).

18. Tuttle, M. E., B. M. Barthelemy, and H. F. Brinson, "Strain Measurement Within a Single Lap Joint using Embedded Strain Gages",Experimental Techniques,

19. Frazier, T. B., " A computer assisted thick adherend test to characterize the mechanical properties of adhesives", Bell Helicopter Company paper presented at the National SAMPE Technical Conference on Aerospace Adhesives and Elastomers,Dallas,Texas,Oct.1970.

20. Hart-Smith, L. J.,"Design Criteria for Advanced Composite Joints",NASA CR 2218,1973.

21. Frazier, T. B.,"Durability of Adhesive Bonded Joints", Air Force Contract F33615-71-C1668,monthly reports.

22. Krieger, R. B.,"Stiffness Characteristics of Structural Adhesives for Stress Analysis in Hostile Environments", American Cyanamid Company Report,1973.

23. Krieger,R. B.,"Fatigue Testing of Structural Adhesives", Presented at the 24th National SAMPE Symposium and Exhibition,San Francisco,May 1979.

24. Dattaguru, B., R. A. Everett Jr., J. D. Whitcomb, and W. S. Johnson,"Geometrically Nonlinear Analysis of Adhesively Bonded Joints",**J. of Engineering Materials and Technology**,Vol.106,1984,pp. 59-65.

25. Post, D., R. Czarnek, J. Wood, D. Joh, and S. Lubowinski, "Deformations in Adhesive Joints by Moire Interferometry", NASA Contractor Report 172474,Oct.1984.

26. Grant, J.W. and J.N. Cooper,"Cone-and-Plate Shear Stress Adhesive Test',**J. Adhesion**,Vol.21, 1987,pp. 155-167.

27. Zienkiewicz, O.C.,**The Finite Element Method**,3rd edition, London: McGraw-Hill,1977,pp. 279-284.

28. Banks-Sills, L., M. Arcan, and Y. Bortman,"A Mixed Mode Fracture Specimen For Mode II Dominant Deformation",**Eng. Fract. Mechanics**,Vol. 20,1984,pp. 145-157.

29. Weissberg, V. and M. Arcan, "A Uniform Pure Shear Testing Specimen for Adhesive Characterization",Presented at the ASTM Symposium on Adhesively Bonded Joints,Baltimore,1986.

30. Arcan, M.,"The Iosipescu Shear Test Applied to Composite Materials",discussion in **Experimental Mechanics**,March 1984, pp. 66-67.

31. Green, A. E., and R. S. Rivlin,"The Mechanics on Non-Linear Materials with Memory: Part I",**Arch. Ration. Mech. and Anal.**, Vol. 1,1957,p.1.

32. Christensen, R. M.,**Theory of Viscoelasticity an Introduction**,2nd edition,New York: Academic Press,1982, pp. 332-334.

33. Pipkin, A. C., and T. G. Rogers, " A Non-linear Integral Representation for Viscoelastic Behavior",**J. Mech. Phys. Solids.**,Vol. 16,1968,pp. 59-73.

34. Leaderman, H.,**Elastic and Creep Properties of Filmentous Materials**,Textile Foundation, Washington, D.C.,1943.

35. Henriksen, M.,"Nonlinear Viscoelastic Stress Analysis - A Finite Element Approach",**Computers & Structures**, Vol. 18,1984,pp. 133-139.

36. Knauss, W. G. and I. J. Emri ,"Non-linear Viscoelasticity Based on Free Volume Consideration",**Computers & Structures**,Vol. 13,1981,pp. 123-128.

37. Sternstein, S. S., in **Treatise on Materials Science and Technology**,Vol. 10,J. M. Shultz (ed.), New York: Academic Press,1977,pp. 541-598.

38. Liechti, K. M. private communication.

39. Schapery, R. A., "A Simple Collocation Method for Fitting Viscoelastic Models to Experimental Data",GALCIT Report SM 61-23A,Nov. 1961.

Appendix A

Boeing Aircraft Company Process Specification

BAC-5555

1. Vapor degrease for 30 minutes in 1,1,1-trichloroethane.
2. Rinse surface with deionized water.
3. Alkaline clean with 5% NaOH solution at 70 °*C* for 7 minutes.
4. Rinse surface with deionized water.
5. Deoxidize with sodium dichromate solution at 70 °*C* for 10 minutes.
6. Rinse surface with deionized water.
7. Anodize in 10% weight phosphoric acid at a current density of 6 amp/ft ^{2} for 20 minutes.
8. Rinse surface with deionized water and promptly dry anodized part in oven or with nitrogen gas.

Appendix B
FORTRAN Program Prony

```
C-----------------------------------------------------------------------
C      PROGRAM PRONY
C      WRITTEN BY JAMES COOPER
C      10 MAY 87
C
C  THIS PROGRAM DETERMINES AN N-PARAMETER PRONY (DIRICHLET)
C  SERIES REPRESENTATION OF A CREEP COMPLIANCE MASTER CURVE
C  USING A TIME COLLOCATION SCHEME.  THE CREEP COMPLIANCE DATA
C  IS USED TO DETERMINE THE SHEAR RELAXATION MODULUS MASTER
C  CURVE USING THE RELATIONSHIP BETWEEN THE LAPLACE TRANSFORMED
C  COMPLIANCE AND MODULUS FOR LINEAR VISCOELASTIC BEHAVIOR.
C  THE PROGRAM ACCEPTS TWO CASES OF INPUT DATA. FOR THE FIRST
C  CASE, THE PRONY SERIES REPRESENTATION OF THE CREEP
C  COMPLIANCE IS INPUT AS DATA (IND=0).
C  IN THE SECOND CASE, THE PRONY SERIES REPRESENTATION IS
C  DETERMINED FROM THE EXPERIMENTAL MASTER CURVE (IND=1) USING
C  THE INITIAL CREEP COMPLIANCE, THE DESIRED COMPLIANCE TIMES,
C  AND THE APPROPRIATE COLLOCATION TIMES WITH THE VALUE OF THE
C  CREEP COMPLIANCE AT THAT TIME.
C  THE INPUT IS READ IN AS FREE-FORMAT.
C
C VARIABLE DECLARATION:
C
C  N=NUMBER OF TERMS IN SERIES (NUMBER OF SPECTRAL VALUES)
C  IND=INDICATOR FOR INPUT DATA CASE
C  LAMBDA=FITTING PARAMETER FOR LAPLACE INVERSION
C  J0=  INITIAL SHEAR CREEP COMPLIANCE
C  TAU(I)=  COMPLIANCE TIME SPECTRAL VALUES
C  T(I)=  COLLOCATION TIME VALUES
C  JEXP(I)=  MASTER CURVE CREEP COMPLIANCE VALUE AT TIME T(I)
C  B(I)=COMPLIANCE SERIES TERMS
C  MUINF=  EQUILIBRIUM SHEAR RELAXATION MODULUS
C  MU(I)=  SPECTRAL SHEAR RELAXATION MODULUS VALUES
C  S(I)=LAPLACE PARAMETER
C  A(I,J),D(I,J)=COEFFICIENT MATRICES
C  C(I),F(I)=STORAGE VECTORS
C-----------------------------------------------------------------------
      IMPLICIT REAL*4(A-H,O-Z),INTEGER*4(I-N)
      DIMENSION A(21,21),B(20),T(20),TAU(20),JT(20),G(20)
```

```
      DIMENSION S(20),D(21,21),MU(20),JEXP(20),Z(4,4),Y(4)
      REAL*4 J0,JEXP,MUINF,JT,MU,LAMBDA
C
C -READ THE NUMBER OF SPECTRAL TERMS AND THE INDICATOR
      READ(5,*) N,IND,LAMBDA
      NMAX = N + 1
C
C -READ THE INITIAL COMPLIANCE VALUE
      READ(5,*) J0
C
      IF(IND.EQ.0)GOTO 9
C -READ SPECTRUM TIME VALUES , COLLOCATION TIME VALUES, AND THE
C -VALUES OF THE COMPLIANCE AT THE COLLOCATION TIMES
      READ(5,*)(TAU(I),T(I),JEXP(I),I = 1,N)
      GOTO 8
 9    CONTINUE
      READ(5,*)(TAU(I),B(I),I = 1,N)
      GOTO 35
C
C - SETUP THE COEFFICIENT MATRIX (A MATRIX)
 8    CONTINUE
      DO 10 I = 1,N
       DO 20 J = 1,N
       DEL = T(I)/TAU(J)
       IF(DEL.LT.1.0E-7)DEL = 0.0
       IF(DEL.GT.1.0E02)DEL = 1.0E02
       A(I,J) = 1.0-EXP(-DEL)
 20    CONTINUE
 10   CONTINUE
C
C - COMPUTE THE C VECTOR VALUES
      DO 30 IA = 1,N
 30   A(IA,NMAX) = JEXP(IA)-J0
C
C -SOLVE THE SET OF EQUATIONS USING SIMUL
      CALL SIMUL(N,A,B,1.0E-20,1,21,DETER)
C
C - THE NEXT SECTION INVERTS THE CREEP COMPLIANCE TO THE
C - RELAXATION MODULUS USING THE LAPLACE TRANSFORM
C - RELATIONSHIP BETWEEN THE SHEAR RELAXATION MODULUS AND
C - THE SHEAR CREEP COMPLIANCE
 35   CONTINUE
      SUM = 0.0
      DO 40 I = 1,N
        S(I) = LAMBDA/TAU(I)
        SUM = SUM  +  B(I)
 40   CONTINUE
C
C - CALCULATE THE INFINITE VALUE OF THE RELAXATION MODULUS
      MUINF = 1.0/(J0 + SUM)
C
C -DETERMINATION OF THE COEFFICIENT D MATRIX
      DO 50 I = 1,N
       DO 55 J = 1,N
        D(I,J) = S(I)/(S(I) + 1.0/TAU(J))
 55    CONTINUE
```

```
 50   CONTINUE
C
C -DETERMINATION OF THE F VECTOR
      DO 60 I = 1,N
      SUM = 0.0
       DO 65 J = 1,N
      SUM = SUM  +  (B(J)*(1.0-D(I,J)))
 65    CONTINUE
C
      D(I,NMAX) = 1.0/(J0 + SUM)-MUINF
 60   CONTINUE
C
C -INVERSION OF THE D MATRIX
      CALL SIMUL(N,D,MU,1.0E-20,1,21,DETER2)
C - CALCULATE CREEP COMPLIANCE AND RELAXATION MODULUS AT
C - VARIOUS TIMES
      DO 70 I = 1,N
       SUM1 = J0
       SUM2 = MUINF
        DO 75 J = 1,N
         T(I) = 10.0**I
         DEL = T(I)/TAU(J)
         IF(DEL.LT.1.0E-07)DEL = 0.0
         IF(DEL.GT.1.0E02)DEL = 1.0E02
         SUM1 = SUM1 + (B(J)*(1.0-EXP(-DEL)))
         SUM2 = SUM2 + (MU(J)*EXP(-DEL))
 75     CONTINUE
       JT(I) = SUM1
       G(I) = SUM2
 70   CONTINUE
C - OUTPUT THE RESULTS
      WRITE(6,100)
 100  FORMAT(//,14X,'PRONY SERIES REPRESENTATION OF',/,10X,
     2 'A SHEAR CREEP COMPLIANCE MASTER CURVE',//,5X,
     3 'FOLLOWED BY THE INVERTED SHEAR RELAXATION BEHAVIOR')
      WRITE(6,105)N,FIT,J0
105   FORMAT(/,5X,'NUMBER OF DATA POINTS (SPECTRAL TERMS):',I2
     2  /,5X,'FIT PARAMETER FOR INVERSION:',E9.4,
     3  /,5X,'INITIAL SHEAR CREEP COMPLIANCE:',E9.4)
      IF(IND.EQ.1)THEN
      WRITE(6,106)
      WRITE(6,107)(I,T(I),TAU(I),JEXP(I),I = 1,N)
      ELSE
      WRITE(6,206)
      WRITE(6,207)(I,TAU(I),B(I),I = 1,N)
      ENDIF
 106  FORMAT(/,22X,'INPUT DATA',//,10X,'I',7X,'T(I)',7X,'TAU(I)',7X,
     2   'J(I)',/)
 107  FORMAT(5X,I2,5X,E9.4,5X,E9.4,5X,E9.4)
 206  FORMAT(/,22X,'INPUT DATA',//,15X,'I',9X,'TAU(I)',9X,'J(I)',/)
 207  FORMAT(14X,I2,7X,E9.4,5X,E9.4)
      IF(IND.EQ.0)GOTO 119
      WRITE(6,108)
 108  FORMAT(/,10X,'COEFFICIENTS OF THE DISCRETE SPECTRAL'
     2 ,/,7X,'REPRESENTATION OF THE SHEAR CREEP COMPLIANCE',/)
      WRITE(6,109)
```

```
 109  FORMAT(10X,'I',7X,'TAU(I)',7X,'JI(I)',/)
      WRITE(6,110)(I,TAU(I),B(I),I = 1,N)
 110  FORMAT(7X,I2,7X,E12.5,7X,E12.5)
 119  CONTINUE
      WRITE(6,120)
 120  FORMAT(//,15X,'COEFFICIENTS OF THE DISCRETE SPECTRAL'
     2 ,/,10X,'REPRESENTATION OF THE SHEAR RELAXATION MODULUS',/)
      WRITE(6,121) MUINF
 121  FORMAT(/,20X,'MUINF = ',E12.5,/)
      WRITE(6,122)
 122  FORMAT(10X,'I',12X,'TAU(I)',16X,'MU(I)',/)
      WRITE(6,125)(I,TAU(I),MU(I),I = 1,N)
 125  FORMAT(9X,I2,9X,E12.5,9X,E12.5)
      WRITE(6,130)
 130  FORMAT(//,15X,'COMPLIANCE AND MODULUS VALUES',/,22X,
     2 'AT SELECTED TIMES',/)
      WRITE(6,135)
 135  FORMAT(/,15X,'T',16X,'J(T)',15X,'G(T)',/)
      WRITE(6,140)(T(I),JT(I),G(I),I = 1,N)
 140  FORMAT(8X,E12.5,7X,E12.5,7X,E12.5)
      STOP
      END
C
C
      SUBROUTINE SIMUL(N,A,X,EPS,INDIC,NRC,DETER)
C --- THIS SUBROUTINE SOLVES A SET OF LINEAR EQUATIONS.
C     THIS SUBROUTINE IS A TAKEN FROM:
C     CARNAHAN, B., H. A. LUTHER, AND J. O. WILKES,
C     APPLIED NUMERICAL METHODS,NEW YORK: JOHN WILEY,1969.
C
      IMPLICIT REAL*4(A-H,O-Z)
      REAL*4 A,X,EPS,DETER
      DIMENSION IROW(50),JCOL(50),JORD(50),Y(50),A(NRC,NRC),X(N)
C
      MAX = N
      IF(INDIC.GE.0) MAX = N + 1
C
C --- BEGIN ELIMINATION PROCEDURE
      DETER = 1.0
      DO 18 K = 1,N
      KM1 = K-1
C
C --- SEARCH FOR THE PIVOT ELEMENT
      PIVOT = 0.0
      DO 11 I = 1,N
      DO 11 J = 1,N
C --- SCAN IROW AND JCOL ARRAYS FOR INVALID PIVOT SUBSCRIPTS
      IF(K.EQ.1) GOTO 9
      DO 8 ISCAN = 1,KM1
      DO 8 JSCAN = 1,KM1
      IF(I.EQ.IROW(ISCAN)) GOTO 11
      IF(J.EQ.JCOL(JSCAN)) GOTO 11
 8    CONTINUE
 9    IF(ABS(A(I,J)).LE.ABS(PIVOT)) GOTO 11
      PIVOT = A(I,J)
      IROW(K) = I
```

```
      JCOL(K)=J
   11 CONTINUE
C
C --- INSURE THAT SELECTED PIVOT IS LARGER THAN EPS
      IF(ABS(PIVOT).GT.EPS) GOTO 13
      DETER=0.0
      RETURN
C
C --- UPDATE THE DETERMINANT VALUE
   13 IROWK=IROW(K)
      JCOLK=JCOL(K)
      DETER=DETER*PIVOT
C
C --- NORMALIZE PIVOT ROW ELEMENTS
      DO 14 J=1,MAX
   14 A(IROWK,J)=A(IROWK,J)/PIVOT
C
C --- CARRY OUT ELIMIANTION AND DEVELOP THE INVERSE
      A(IROWK,JCOLK)=1.0/PIVOT
      DO 18 I=1,N
      AIJCK=A(I,JCOLK)
      IF(I.EQ.IROWK) GOTO 18
      A(I,JCOLK)=-AIJCK/PIVOT
      DO 17 J=1,MAX
   17 IF (J.NE.JCOLK) A(I,J)=A(I,J)-AIJCK*A(IROWK,J)
   18 CONTINUE
C
C --- ORDER SOLUTION VALUES (IF ANY ) AND CREATE JORD ARRAY
      DO 20 I=1,N
      IROWI=IROW(I)
      JCOLI=JCOL(I)
      JORD(IROWI)=JCOLI
   20 IF(INDIC.GE.0) X(JCOLI)=A(IROWI,MAX)
C
C --- ADJUST SIGN OF DETERMINANT
      INTCH=0
      NM1=N-1
      DO 22 I=1,NM1
      IP1=I+1
      DO 22 J=IP1,N
      IF(JORD(J).GE.JORD(I)) GOTO 22
      JTEMP=JORD(J)
      JORD(J)=JORD(I)
      JORD(I)=JTEMP
      INTCH=INTCH+1
   22 CONTINUE
      IF(INTCH/2*2.NE.INTCH) DETER=-DETER
C
C -- IF INDIC IS POSITIVE RETURN WITH RESULTS
      IF (INDIC.LE.0) GOTO 26
      RETURN
C
C --- IF INDIC IS NEGATIVE OR ZERO, UNSCRAMBLE THE INVERSE
C  FIRST BY ROWS
   26 DO 28 J=1,N
      DO 27 I=1,N
```

```
      IROWI = IROW(I)
      JCOLI = JCOL(I)
   27  Y(JCOLI) = A(IROWI,J)
      DO 28 I = 1,N
   28  A(I,J) = Y(I)
C -- THEN BY COLUMNS
      DO 30 I = 1,N
      DO 29 J = 1,N
      IROWJ = IROW(J)
      JCOLJ = JCOL(J)
   29  Y(IROWJ) = A(I,JCOLJ)
      DO 30 J = 1,N
   30  A(I,J) = Y(J)
C
      RETURN
      END
```

Appendix C
Sample input data

```
18 0 1.5
8.715E-06
6.0E01 2.80E-07
6.0E02 2.99E-07
6.0E03 3.20E-07
6.0E04 3.50E-07
6.0E05 3.90E-07
6.0E06 4.50E-07
6.0E07 5.20E-07
6.0E08 6.00E-07
6.0E09 7.99E-07
6.0E10 1.10E-06
6.0E11 1.70E-06
6.0E12 2.55E-06
6.0E13 3.75E-06
6.0E14 5.58E-06
6.0E15 9.17E-06
6.0E16 2.60E-05
6.0E17 4.58E-05
6.0E18 4.59E-05
```

Appendix D
Program output

PRONY SERIES REPRESENTATION OF
A SHEAR CREEP COMPLIANCE MASTER CURVE

FOLLOWED BY THE INVERTED SHEAR RELAXATION BEHAVIOR

NUMBER OF DATA POINTS (NUMBER OF SPECTRAL TERMS):18
FIT PARAMETER FOR INVERSION:.1500E+01
INITIAL SHEAR CREEP COMPLIANCE:.8715E-05

INPUT DATA

I	TAU(I)	J(I)
1	.6000E+02	.2800E-06
2	.6000E+03	.2990E-06
3	.6000E+04	.3200E-06
4	.6000E+05	.3500E-06
5	.6000E+06	.3900E-06
6	.6000E+07	.4500E-06
7	.6000E+08	.5200E-06
8	.6000E+09	.6000E-06
9	.6000E+10	.7990E-06
10	.6000E+11	.1100E-05
11	.6000E+12	.1700E-05
12	.6000E+13	.2550E-05
13	.6000E+14	.3750E-05
14	.6000E+15	.5580E-05
15	.6000E+16	.9170E-05
16	.6000E+17	.2600E-04
17	.6000E+18	.4580E-04
18	.6000E+19	.4590E-04

COEFFICIENTS OF THE DISCRETE SPECTRAL REPRESENTATION
OF THE SHEAR RELAXATION MODULUS

MUINF= 0.64820E+04

I	TAU(I)	MU(I)
1	0.60000E + 02	0.36342E + 04
2	0.60000E + 03	0.35719E + 04
3	0.60000E + 04	0.35949E + 04
4	0.60000E + 05	0.36502E + 04
5	0.60000E + 06	0.38119E + 04
6	0.60000E + 07	0.40178E + 04
7	0.60000E + 08	0.43087E + 04
8	0.60000E + 09	0.44274E + 04
9	0.60000E + 10	0.54756E + 04
10	0.60000E + 11	0.62884E + 04
11	0.60000E + 12	0.85355E + 04
12	0.60000E + 13	0.90004E + 04
13	0.60000E + 14	0.10433E + 05
14	0.60000E + 15	0.87746E + 04
15	0.60000E + 16	0.12067E + 05
16	0.60000E + 17	0.10189E + 05
17	0.60000E + 18	0.47268E + 04
18	0.60000E + 19	0.17328E + 04

COMPLIANCE AND MODULUS VALUES AT SELECTED TIMES

T	J(T)	G(T)
0.10000E + 02	0.87635E-05	0.11410E + 06
0.10000E + 03	0.89940E-05	0.11116E + 06
0.10000E + 04	0.92932E-05	0.10757E + 06
0.10000E + 05	0.96146E-05	0.10397E + 06
0.10000E + 06	0.99662E-05	0.10030E + 06
0.10000E + 07	0.10359E-04	0.96483E + 05
0.10000E + 08	0.10810E-04	0.92455E + 05
0.10000E + 09	0.11333E-04	0.88164E + 05
0.10000E + 10	0.11955E-04	0.83581E + 05
0.10000E + 11	0.12774E-04	0.78140E + 05
0.10000E + 12	0.13926E-04	0.71651E + 05
0.10000E + 13	0.15667E-04	0.63447E + 05
0.10000E + 14	0.18280E-04	0.54337E + 05
0.10000E + 15	0.22175E-04	0.44378E + 05
0.10000E + 16	0.28270E-04	0.34826E + 05
0.10000E + 17	0.39666E-04	0.23764E + 05
0.10000E + 18	0.65452E-04	0.14112E + 05
0.10000E + 19	0.10677E-03	0.88416E + 04

The vita has been removed from the scanned document